STUDY ON THE INFLUENCE OF SCAFFOLD INNER ORGANIZATION ON THE TREATMENT OF SPINAL CORD INJURY

A THESIS SUBMITTED TO
THE GRADUATE SCHOOL OF NATURAL AND APPLIED SCIENCES
OF
MIDDLE EAST TECHNICAL UNIVERSITY

BY

TUĞBA DURSUN

IN PARTIAL FULFILLMENT OF THE REQUIREMENTS
FOR
THE DEGREE OF MASTER OF SCIENCE
IN
BIOTECHNOLOGY

SEPTEMBER 2013

Approval of the thesis:

STUDY ON THE INFLUENCE OF SCAFFOLD INNER ORGANIZATION ON THE TREATMENT OF SPINAL CORD INJURY

submitted by **TUĞBA DURSUN** in partial fulfillment of the requirements for the degree of **Master of Science in Biotechnology Department, Middle East Technical University** by,

Prof. Dr. Canan Özgen _____

Dean, Graduate School of **Natural and Applied Sciences**

Prof. Dr. Nesrin Hasırcı _____

Head of Department, **Biotechnology**

Prof. Dr. Vasıf Hasırcı _____

Supervisor, **Biological Sciences Dept., METU**

Assist. Prof. Dr. Deniz Yücel _____

Co-Supervisor, **Histology Embryology Dept., Acıbadem U.**

Examining Committee Members:

Prof. Dr. İnci Eroğlu _____

Chemical Engineering Dept., METU

Prof. Dr. Vasıf Hasırcı _____

Biological Sciences Dept., METU

Prof. Dr. Kezban Ulubayram _____

Pharmacy Dept., Fac. Med., Hacettepe University

Assoc. Prof. Dr. Can Özen _____

Biotechnology Dept., METU

Assoc. Prof. Dr. Mayda Gürsel _____

Biological Sciences Dept., METU

Date: 04.09.2013

I hereby declare that all information in this document has been obtained and presented in accordance with academic rules and ethical conduct. I also declare that, as required by these rules and conduct, I have fully cited and referenced all material and results that are not original to this work.

Name, Last Name: Tuğba Dursun

Signature :

ABSTRACT

STUDY ON THE INFLUENCE OF SCAFFOLD INNER ORGANIZATION ON THE TREATMENT OF SPINAL CORD INJURY

Dursun, Tuğba
M.Sc., Department of Biotechnology
Supervisor: Prof. Dr. Vasıf Hasırcı
Co-Supervisor: Assist. Prof. Dr. Deniz Yücel

September 2013, 78 pages

Permanent loss of neurologic function occurs when the central nervous system (CNS) is injured. Nerve regeneration is extremely limited because of dense scar tissue formation at the lesion site, especially in the spinal cord. For the treatment of this type of injury, different strategies are needed. The emerging approach to solve these problems is to provide a physical support via tubular bridging devices such as "nerve guides". They are used to bridge the neural gaps in the treatment of spinal cord injury, and therefore, the design of its inner architecture is very important to provide desired guidance. To test this, the effectiveness of the aligned and random media within tubular nerve guides were compared. Although ultimately a tubular construct is used, planar, composite structures were used for convenient monitoring and analysis.

The bottom layer or the main bulk of the nerve guide was a PHBV foam that was prepared by lyophilization. Aligned and randomly oriented PHBV/collagen (2:1) fiber mats, to be placed on this bottom layer were made by electrospinning directly on the PHBV foam. PHBV/collagen (2:1) foam to serve as a 3D disorganized medium was also made by lyophilization. Crosslinking of the bilayer guides was made by dehydrothermal treatment (DHT) at 150℃ for 24 h. Mercury porosimetry showed that porosity of the PHBV foam was 85%, and the pore size was between 5 and 200 μm. Diameter of the fibers were measured by scanning electron microscope and found to be in between 200-900 nm. In situ biodegradation test revealed that weight loss of uncrosslinked guides (no DHT) were less than the crosslinked ones (15% after 28 days), and therefore, crosslinking of the scaffolds with DHT was abandoned.

Aligned fiber-foam (AF-Fo) and random fiber-foam (RF-Fo) nerve guides were seeded with rat bone marrow stromal cells (rBMSCs) and cultured for 7 days. Cell behavior and differentiation to neural cells on these constructs was examined. Cell attachment and proliferation were found to be better on the RF-Fo construct. The neural differentiation level of the cells were same on both bilayer. No conclusive evidence for the positive contribution of an aligned interior could be observed.

It was concluded that the nerve guides prepared had proper porosity, pore size and degradation rate which would allow cell growth at the spinal cord injury site.

Keywords: Nerve Tissue Engineering, Rat Bone Marrow Stromal Cell, Nano/Microfiber

ÖZ

HÜCRE TAŞIYICILARIN İÇ DÜZENİNİN OMURİLİK ZEDELENMELERİNİN TEDAVİSİ ÜZERİNE ETKİSİ

Dursun, Tuğba
Yüksek Lisans, Biyoteknoloji Bölümü
Tez Yöneticisi: Prof. Dr. Vasıf Hasırcı
Ortak Tez Yöneticisi: Yrd. Doç. Dr. Deniz Yücel

Eylül 2013, 78 sayfa

Merkezi sinir sistemi (MSS) yaralanmalarında kalıcı nörolojik fonksiyon kaybı ortaya çıkmaktadır. Lezyon yerinde yoğun yara dokusu oluşumu nedeniyle özellikle omurilikte sinir yenilenmesi çok sınırlıdır. Bu tip yaralanmaların tedavisi için farklı stratejiler gerekmektedir. Bu sorunları çözmek için yeni geliştirilen yaklaşım, boru biçimli "sinir yönlendiricileri" gibi bağlayıcı aygıtlarla fiziksel destek sağlamaktır. Omurilik zedelenmesinin tedavisinde sinirler arası açıklıkları bağlamakta kullanılırlar ve bu yüzden iç mimarilerinin tasarımı yönlenme sağlanabilmesi için çok önemlidir. Bunu test etmek adına, boru biçimli sinir yönlendiricileri arasından yönlü ve yönlü olmayan ortamların etkinliği karşılaştırılmıştır. Gözlem ve değerlendirmeyi kolaylaştırmak adına, boru biçimli bir yapı kullanılmasına karşın, testlerde düz ve kompozit yapılar kullanılmıştır.

Sinir kılıfının en alt katmanı veya ana kısmı olan PHBV sünger, liyofilizasyon yöntemiyle hazırlanmıştır. Temele konulacak olan yönlü ve yönlü olmayan PHBV/kollajen (2:1) lif yapılar, PHBV köpüğü üzerinde doğrudan elektroeğirme uygulanarak yapılmıştır. Rastgele bir 3 boyutlu aracı işlevi gören PHBV/kollajen (2:1) liyofilizasyon yöntemiyle yapılmıştır. Çift katmanlı yönlendiricilerin 24 saat boyunca 150℃ sıcaklıkta dehidrotermal işlemlerle çapraz bağlanmaları sağlanmıştır. Cıva porozimetresi incelemesi, PHBV süngerin porozitesinin %85 olduğunu ve gözenek çaplarının 5 ile 200 μm arası olduğunu göstermiştir. Liflerin çapları tarama elektron mikroskopisi ile ölçülmüştür ve 200-900 nm arasında bulunmuştur. In situ biyobozunma testi, çapraz bağlanmamış (DHT kullanılmamış) örneklerde ağırlık kaybının çapraz bağlanmış (28 gün sonunda %15) olanlara göre daha az olduğunu göstermiştir ve bu nedenle iskelelerin çapraz bağlanması yöntemi uygulanmamıştır.

Yönlü lif sünger (AF-Fo) ve yönlü olmayan lif sünger (RF-Fo) sinir yönlendiricilerine sıçan kemik iliği stroma hücreleri (rBMSCs) ekilmiştir ve 7 gün kültür edilmişlerdir. Yapılardaki hücre davranışı ve sinir hücresine farklılaşma incelenmiştir. Hücre tutunması ve çoğalmasının RF-Fo yapılarda daha iyi olduğu bulunmuştur. İki yapıda da stroma hücrelerinin sinir hücrelerine farklılaşması aynı düzeydedir.

Sonuç olarak, sinir yönlendiricileri, omurilik zedelenmesi alanında hücre büyümesine ve farklılaşmasına izin verecek uygun gözenekliliğe, gözenek büyüklüğüne ve bozunma hızına sahiptir. Yönlü iç mimarinin olumlu etkisine yönelik herhangi bir kanıt gözlemlenmemiştir.

Anahtar Kelimeler: Sinir Doku Mühendisliği, Sıçan Kemik İliği Stroma Hücresi, Nano/Mikrofiber

Dedicated to my lovely family…

ACKNOWLEDGEMENTS

I would like to express my deepest gratitude to my supervisor Prof. Dr. Vasıf HASIRCI for his continuous guidance, advice, support, encouragement and insight throughout the research.

I am also grateful to my co-supervisor Assist. Prof. Dr. Deniz YÜCEL for her support, and guidance.

I would like to thank my friend Arda BÜYÜKSUNGUR for his help and support in the confocal microscopy.

I would also grateful to Menekşe ERMİŞ, Cemile KILIÇ, and Selcen ALAGÖZ for their help with the flow cytometry.

I am grateful to my special friends Ayşegül Özgür GEZER, Şafak CHASAN, Gizem KURT, Aktan ALPSOY, and İrem KAYMAK for their continuous support and sincere friendship.

I would like to thank all the members of METU-BIOMATEN Center of Excellence in Biomaterials and Tissue Engineering. Thanks to all my labmates, especially my roommates Damla ARSLANTUNALI, Aysu KÜÇÜKTURHAN, Deniz SEZLEV, and my friends Senem HEPER, Gökhan BAHÇECİOĞLU, Ezgi ANTMEN, Bilgenur KANDEMİR, Gözde EKE, Sepren ÖNCÜ, Aylin KÖMEZ, Büşra AYGÜN, Esen SAYIN, our postdoctoral fellow, Dr. Türker BARAN, our technician Zeynel AKIN for their support in this study.

I would also like to thank my best friend Kerem Alp USAL for everthing that he made. Without his continuous support, love, and patience, this study would not be completed.

Finally, I would like to express my deepest gratitudes to my family: my parents Ayşe and Osman DURSUN, and my dear sister Tuğçe DURSUN for their endless patience and unique support. Without them, this study would not mean so much to me. I thank each of them for their flawless tenderness.

I would like to acknowledge to TÜBİTAK for their support through BİDEP 2210 Scholarship.

TABLE OF CONTENTS

ABSTRACT v

ÖZ vi

ACKNOWLEDGEMENTS viii

TABLE OF CONTENTS ix

LIST OF TABLES xii

LIST OF FIGURES xiii

LIST OF ABBREVIATIONS xviii

CHAPTERS .....

1. INTRODUCTION 1
    1.1. The Nervous System 1
        1.1.1. Anatomy of the Nervous System 1
            1.1.1.1. Central Nervous System (CNS) 1
            1.1.1.2. Peripheral Nervous System (PNS) 2
        1.1.2. Histology of the Nervous System 2
            1.1.2.1. Neurons 2
                1.1.2.1.1. The Classification of Neurons 3
                    1.1.2.1.1.1. Structural Classification of Neurons 3
                    1.1.2.1.1.2. Functional Classification of Neurons 4
            1.1.2.2. Glial Cells 4
        1.1.3. Synaptic Activity 5
            1.1.3.1. Signal Transduction 6
    1.2. Neuronal Injury 7
        1.2.1. Cellular Response to Nerve Injuries 7
            1.2.1.1. CNS Injury 8
                1.2.1.1.1. Spinal Cord Injury 9
            1.2.1.2. PNS Injury 10
    1.3. Tissue Engineering and Regenerative Medicine 10
        1.3.1. Cell Sources in Tissue Engineering 11

1.3.2. Scaffolds in Tissue Engineering 12
1.3.2.1. Scaffold Production Methods 13
1.3.2.2. Biomaterials Used in Scaffold Production 15
1.3.2.3. Nerve Tissue Engineering Approaches 16
1.3.2.3.1. CNS 16
1.3.2.3.1.1. Embryonic Stem Cells 16
1.3.2.3.1.2. Synthetic Nerve Conduits 17
1.3.2.3.1.2.1. Physical Modifications 17
1.3.2.3.1.2.2. Bio-chemical Modifications 18
1.3.2.3.1.2.3. Supporting Cells 20
1.3.2.3.2. PNS 21
1.3.2.3.2.1. Autologous Nerve Grafts 22
1.3.2.3.2.2. Allografts and Acellular Nerve Matrices 22
1.3.2.3.2.3. Nerve Guides 23
1.4. The Aim of the Study 24
1.5. Novelty of the Study 24

2. MATERIALS AND METHODS 25
2.1. Materials 25
2.2. Methods 26
2.2.1. Collagen Type I Isolation from Rat Tails 26
2.2.1.1. Collagen Type I Characterization 26
2.2.2. Preparation of Scaffolds 27
2.2.2.1. Preparation of PHBV5 Foam 27
2.2.2.2. Preparation of Foams with Aligned and Random PHBV5/Collagen (2:1) Fibers 27
2.2.2.3. Preparation of PHBV5/Collagen (2:1) Foam 28
2.2.2.4. Stabilization of the Scaffolds with Dehydrothermal (DHT) Treatment 28
2.2.3. Scaffold Characterization 28
2.2.3.1. Measurement of Thickness 28
2.2.3.2. Measurement of Porosity 28
2.2.3.3. Pore Size Distribution 28
2.2.3.4. Scanning Electron Microscopy (SEM) Analysis 28
2.2.3.5. Degradation of the Foams 29
2.2.3.5.1. Degradation with Collagenase 29
2.2.3.5.2. Degradation In PBS 29
2.2.4. *In Vitro* Studies 29
2.2.4.1. Cell Culture 29
2.2.4.1.1. Isolation and culture of rat bone marrow stromal cells (rBMSCs) 29
2.2.4.1.2. Characterization of rBMSC 29
2.2.4.2. Sterilization 30

2.2.4.3. Cell Seeding……..... 30
2.2.4.4. Differentiation Medium …….……. 30
2.2.4.5. Cell Viability with Alamar Blue Assay……..... 30
2.2.4.6. Microscopy of the Tissue Engineered Construct..... 31
2.2.4.6.1. Fluorescence Microscopy..... 31
2.2.4.6.2. SEM..... 32
2.2.5. Differentiation Studies……...…… 32
2.2.5.1. Flow Cytometry…….. 32
2.2.5.2. Neuron Specific Enolase (NSE) Kit…….... 32
2.2.5.3. Immunohistochemistry……... 33
2.3. Statistical Analysis..... 33
3. RESULTS AND DISCUSSION 34
3.1. Collagen Type I Characterization..... 34
3.2. Characterization of Scaffolds..... 34
3.2.1. Characterization of PHBV5 Foam……..…….. 34
3.2.1.1 Porosity and Pore Size Distribution of the PHBV5 Foam……. 36
3.2.2. Characterization of PHBV5/Collagen (2:1) Aligned and Random Fibers……...……36
3.2.3. Characterization of PHBV5/Collagen (2:1) Foam…….... 38
3.2.4. Examination of 3D Scaffolds……..... 39
3.2.4.1. Thickness of Scaffolds..... 39
3.2.4.2. Degradation of Scaffolds..... 40
3.2.4.2.1. Degradation with Collagenase..... 41
3.2.4.2.2. Degradation in PBS..... 42
3.3. *In vitro* Studies..... 42
3.3.1. Rat Bone Marrow Stromal Cell (rBMSC) Characterization……. 42
3.3.2. Cell Attachment and Proliferation on Scaffolds..... 45
3.3.3. Microscopy of Tissue Engineered Construct..... 46
3.3.3.1. Fluorescence Microscopy..... 46
3.3.3.2. SEM..... 48
3.3.4. Differentiation Studies..... 51
3.3.4.1. Flow Cytometry…… 52
3.3.4.2. Neuron Specific Enolase (NSE) Kit……..... 59
3.3.4.3. Immunohistochemistry……. 60
4. CONCLUSION AND FUTURE STUDIES 66

REFERENCES 67

APPENDICES 73
A. ALAMAR BLUE CALIBRATION CURVE 73

B. NEURONAL SPECIFIC ENOLASE CALIBRATION .CURVE……..74

LIST OF TABLES

TABLES

Table 2.1. Composition of SDS-PAGE Gel Solutions ……..…… 28

Table 3.1. Pore size of PHBV5 foam by Image J analysis …….…….. 39

Table 3.2. Thickness of Scaffolds ……..……... 44

Table 3.3. Degradation of the fibers, foams and 3D construct in collagenase type II (at 37^{0}C, 2h) and in PBS (pH 7.4, 10 mM) ..……..... 45

Table 3.4. Scaffold degradation in PBS (pH 7.4, 10 mM) …….. 46

Table 3.5. Expression of nestin and beta III-tubulin with different differentiation procedures and quantified with flow cytometry….…….... 62

Table 3.6. NSE expression in undifferentiated and differentiated cells……... 63

LIST OF FIGURES

FIGURES

Figure 1. 1. Anatomy of the Nervous System ……..……...…… 1

Figure 1. 2. The anatomy of a multipolar neuron. (A) Regions of a neuron, (B) Structural components of a neuron ……..…… 3

Figure 1. 2. Structural classifications of neurons ……..…..... 4

Figure 1. 3. The principal types of glial cells in the central nervous system ……..….... 5

Figure 1. 4. Physiology of the synapse ……...…….……... 6

Figure 1. 5. On a myelinated axon, a nerve impulse appears to jump from node to node 7

Figure 1. 6. Regeneration of axons in PNS ……...…….... 8

Figure 1. 7. Schematic representation of the CNS injury site ……..... 9

Figure 1. 8. Flowchart of tissue engineering ……...……..… 11
.
Figure 1. 9. Main parts of an electrospinning set up ……...….…. 13

Figure 1. 10. Novel approaches to spinal cord repair using ES cells ……..... 17

Figure 1. 11. End-to-end suturing of peripheral nerves. Alignment of the fascicles is critical in successful regeneration and microsurgical techniques have been developed to optimize this surgery ……...……...…… 23

Figure 1. 12. Sequence of events in empty silicone nerve guides ..…….. 24

Figure 2.1. Preparation of a bilayer construct. (A) Aligned PHBV5/Collagen fibers on PHBV5 foam, (B) Random PHBV5/Collagen fibers on PHBV5 foam …….……..….. 28

Figure 2.2. Schematic presentation of PHBV/Collagen (2:1) foam placed over PHBV foam 30

Figure 3.1. SDS-PAGE for comparison of collagen isolated from Sprague-Dawley rat tails and the commercial Type I collagen. Lanes represent: (I) isolated collagen (0.5%, w/v), (II) isolated collagen (0.75%, w/v), (III) protein ladder (Fermentas), (IV) commercial type I collagen (Sigma-Aldrich) …….…….. 37

Figure 3.2. SEM of PHBV5 foam. (A) surface (x1000), (B) horizontal section (x1000), and (C) cross section (x1000). (inset: x5000 of (A), (B), and (C))..……..... 38

Figure 3.3. Pore size distribution of PHBV5 foam …….. 39

Figure 3.4. Scanning electron micrographs of aligned fibers (A) x1000, (B) x10000. Arrow shows the alignment direction ……...…….. 40

Figure 3.5. SEM of random fibers (x200) ……..... 41

Figure 3.6. SEM of the upper part (A) x50, (B) x150, and the bottom part (C) x50 of PHBV5/Collagen (2:1) foam ……... 42

Figure 3.7. Schematic presentation of the three types of 3D scaffolds (A) Aligned PHBV5/Collagen fibers on PHBV5 foam, (B) Random PHBV5/Collagen fibers on PHBV5 foam, (C) PHBV/Collagen (2:1) over PHBV foam ……..... 43

Figure 3.8. SEM of the scaffolds after dehydrothermal treatment (A) Before DHT (x200), (B) After DHT (x150) ……..... 44

Figure 3.9. Flow cytometry analysis of rBMSC P2 after incubation in DMEM-high glucose tissue culture medium containing penicillin (100 U/mL), streptomycin (100 µg/mL). (A) Fluorescence intensity of controls, and (B) the samples, CD90, CD45, and CD11b ……. 47

Figure 3.10. Dot plots of different types of antibodies in rBMSCs Passage 2 culture. (A) Anti-CD90/Anti-CD11b mix, (B) Anti-CD90/Anti-CD45 mix ……... 48

Figure 3.11. Cell proliferation profile of rat bone marrow stromal cells (rBMSCs) on bilayer AF-Fo, and RF-Fo scaffolds …….….. 49

Figure 3.12. Fluorescence microscopy on aligned fiber-foam (AF-Fo) constructs of after (A) Day 1, (B) Day 4, and (C) Day 7 of cell culture, Alexa Fluor® 532-Phalloidin for cytoskeleton and DAPI for the nucleus, x40…….....50

Figure 3.13. Fluorescence microscopy on random fiber-foam (RF-Fo) constructs of after (A) Day 1, (B) Day 4, and (C) Day 7 of cell culture, Alexa Fluor® 532-Phalloidin for cytoskeleton and DAPI for the nucleus, x40…….…… 51

Figure 3.14. SEM of cell seeded AF-Fo after Day 1 of cell culture in differentiation medium. (A) x500, (B) x1000…….….. 52

Figure 3.15. SEM of cell seeded AF-Fo after Day 4 of cell culture in differentiation medium. (A) x500, (B) x1000…..... 52

Figure 3.16. SEM of cell seeded AF-Fo after Day 7 of cell culture in differentiation medium. (A) x500, (B) x1000…..... 53

Figure 3.17. SEM of cell seeded RF-Fo after Day 1 of cell culture in differentiation medium. (A) x500, (B) x1000…..... 53

Figure 3.18. SEM of cell seeded RF-Fo after Day 4 of cell culture in differentiation medium. (A) x500, (B) x1000……..... 54

Figure 3.19. SEM of cell seeded RF-Fo after Day 7 of cell culture in differentiation medium. (A) x500, (B) x1000……..... 54

Figure 3.20. SEM of cell seeded AF-Fo after Day 7 of cell culture in differentiation medium, x500 ……..…. 55

Figure 3.21. Flow cytometry results of (A) Nestin, (B) Beta III-tubulin expression of undifferentiated rBMSCs Passage 2.……..…….. 56

Figure 3.22. Flow cytometry results of (A) Nestin, CD-90, beta III-tubulin, (B) Controls, nestin and beta III-tubulin expression of undifferentiated rBMSCs.…… 57

Figure 3.23. Flow cytometry results of (A) Nestin, (B) Beta III-tubulin expression of Passage 2 rBMSCs after application of Differentiation Procedure 1 ……..…..... 58

Figure 3.24. Flow cytometry results of controls, nestin and beta III-tubulin expression of Passage 2 rBMSCs after application of Differentiation Procedure 1 ……..…... 59

Figure 3.25. Flow cytometry results of (A) Nestin, (B) Beta III-tubulin expression of Passage 2 rBMSCs after application of Differentiation Procedure 2 ……..…… 60

Figure 3.26. Flow cytometry results of controls, nestin and beta III-tubulin expression of Passage 2 rBMSCs after application of Differentiation Procedure 2 ……..…….. 60

Figure 3.27. Flow cytometry results of (A) Nestin, (B) Beta III-tubulin expression of Passage 2 rBMSCs after application of Differentiation Procedure 3 61

Figure 3.28. Flow cytometry results of controls, nestin and beta III-tubulin expression of Passage 2 rBMSCs after application of Differentiation Procedure 3 62

Figure 3.29. Immunohistochemistry results of AF-Fo in terms of nestin (green) and tyrosine hydroxylase (blue) expression after Day 4 of cell culture. (A) Normal medium, (B) Neurogenic Differentiation medium (Differentiation Procedure 1) 64

Figure 3.30. Immunohistochemistry results of AF-Fo in terms of beta III-tubulin (green) and synaptophysin (blue) expression after Day 4 of cell culture. (A) Normal medium, (B) Neurogenic Differentiation medium (Differentiation Procedure 1)..... 64

Figure 3.31. Immunohistochemistry results of AF-Fo in terms of nestin (green) and tyrosine hydroxylase (blue) expression afer Day 7 of cell culture. (A) Normal medium, (B) Neurogenic Differentiation medium (Differentiation Procedure 1) 65

Figure 3.32. Immunohistochemistry results of AF-Fo in terms of beta III-tubulin (green) and synaptophysin (blue) expression after Day 7 of cell culture. (A) Normal medium, (B) Neurogenic Differentiation medium (Differentiation Procedure 1) 65

Figure 3.33. Immunohistochemistry results of RF-Fo in terms of nestin (green) and tyrosine hydroxylase (blue) expression after Day 4 of cell culture. (A) Normal medium, (B) Neurogenic Differentiation medium (Differentiation Procedure 1) 66

Figure 3.34. Immunohistochemistry results of RF-Fo in terms of beta III-tubulin (green) and synaptophysin (blue) expression after Day 4 of cell culture. (A) Normal medium, (B) Neurogenic Differentiation medium (Differentiation Procedure 1) 66

Figure 3.35. Immuhistochemistry results of RF-Fo in terms of nestin (green) expression after Day 7 of cell culture. (A) Normal medium, (B) Neurogenic Differentiation medium (Differentiation Procedure 1) 67

Figure 3.36. Immunohistochemistry results of RF-Fo in terms of beta III-tubulin (green) after Day 7 of cell culture. (A) Normal medium, (B) Neurogenic Differentiation medium (Differentiation Procedure 1) 67

Figure 3.37. Negative control of immunostaining 68

LIST OF ABBREVIATIONS

µm	micrometer
2D	Two Dimensional
3D	Three Dimensional
AF-Fo	Aligned Fiber-Foam
APS	Ammonium persulfate
BBB	Blood-brain Barrier
BDNF	Brain-derived Neurotrophic Factor
b-FGF	Basic Fibroblast Growth Factor
BMSC	Bone Marrow Stem Cell
BSA	Bovine Serum Albumin
BSCB	Blood-spinal Cord Barrier
Ca	Calcium
cAMP	Cyclic Adenosine Monophosphate
cm	centimeter
CNS	Central Nervous System
CNTF	Ciliary Neurotrophic Factor
CO_2	Carbon Dioxide
Col	Collagen
Da	Dalton
DAPI	4', 6-diamidino-2-phenylindole
DHT	Dehydrothermal
DMEM	Dulbecco's Modified Eagle Medium
DMSO	Dimethyl Sulfoxide
ECM	Extracellular Matrix
EDTA	Ethylenediaminetetraacetic Acid
ELISA	Enzyme-linked Immunosorbent Assay
ESC	Embryonic Stem Cell
FADH	Flavin Adenine Dinucleotide
FBS	Fetal Bovine Serum
FITC	Fluorescein Isothiocyanate
FL	Fluorescence Laser
Fo-Fi	Foam-Fiber
Fo-Fo	Foam-Foam
FSC	Forward Scatter Channel
g	gram
GABA	Gamma-aminobutyric Acid
GDNF	Glial Cell-derived Neurotrophic Factor
GFAP	Glial Fibrillary Acidic Protein

GFP	Green Fluorescent Protein
h	hour
HA	Hyaluronic Acid
HAc	Acetic Acid
HFIP	1,1,1,3,3,3-hexafluoroisopropanol
HLF	Human Ligament Fibroblast
IGF1	Insulin-like Growth Factor 1
IgG	Immunoglobulin G
kDa	kilo Dalton
L	Liter
M	Molarity
mA	milliampere
MAG	Myelin-associated Glycoprotein
mg	milligram
min	minute
mL	milliliter
mm	millimeter
mM	millimolar
MSC	Mesenchymal Stem Cell
MW	Molecular Weight
Na	Sodium
Na_2HPO_4	Disodium Hydrogen Phosphate
NaCl	Sodium Chloride
NADH	Nicotinamide Adenine Dinucleotide
NADPH	Nicotinamide Adenine Dinucleotide Phosphate
NaH_2PO_4	Sodium Dihydrogen Phosphate
ng	nanogram
NGC	Nerve Guide Channel
NGF	Nerve Growth Factor
NI	Neural Induction
nm	nanometer
NSC	Neural Stem Cell
NSE	Neuron-specific Enolase
NT	Neurotrophin
NT3	Neurothrophin-3
OEC	Olfactory Ensheathing Cells
OEG	Olfactory Ensheathing Glia
PBS	Phosphate Buffer Saline
PCL	Poly(ε-caprolactone)
PDMS	Poly(dimethylsiloxane)
PDO	Polydioxanone
PDT	Population Doubling Time

PE	Polyethylene
PEG	Polyethylene Glycol
Pen/Strep	Penicillin/Streptomycin
PGA	Poly(glycolic acid)
PHB	Poly(3-hydroxybutyrate)
PHBV	Poly(3-hydroxybutyrate-co-3-hydroxyvalerate)
PHEMA	Poly(2-hydroxyethyl methacrylate)
PI	Preinduction
PLA	Poly(lactic acid)
PLGA	Poly(Lactic Acid-co-Glycolic Acid)
PLLA	Poly(L-Lactic Acid)
PMMA	Poly(methyl methacrylate)
PNI	Peripheral Nerve Injury
PNS	Peripheral Nervous System
PU	Polyurethane
RF-Fo	Random Fiber-Foam
rpm	Rotation per minute
s.d.m	Standard Deviation of the Mean
SC	Stem Cell
SCI	Spinal Cord Injury
SDS-PAGE	Sodium Dodecyl Sulphate- Polyacrylamide Gel Electrophoresis
SEM	Scanning Electron Microscopy
SF	Silk Fibroin
SSC	Side Scatter Channel
T_c	Critical Temperature
TEMED	N,N,N′,N′-Tetramethylethane-1,2-diamine
T_g	Glass Transition Temperature
T_m	Melting Temperature
UL	Upper Left
UV	Ultra Violet
UV-Vis	UV-visible
v/v	volume/volume
VA	Valproic Acid
w/v	weight/volume

CHAPTER 1

INTRODUCTION

1.1. The Nervous System

The nervous system is most significant and complex system in the body since it controls the basic functions of an human being. Behavioral functions of the nervous systems are: 1) receipt and processing of sensory information, 2) programming and realization of motor and emotional responses, 3) storing information (Kandel et al., 2000).

1.1.1. Anatomy of the Nervous System

The nervous system is anatomically divided into two systems: central nervous system (CNS), and peripheral nervous system (PNS) (Figure 1.1).

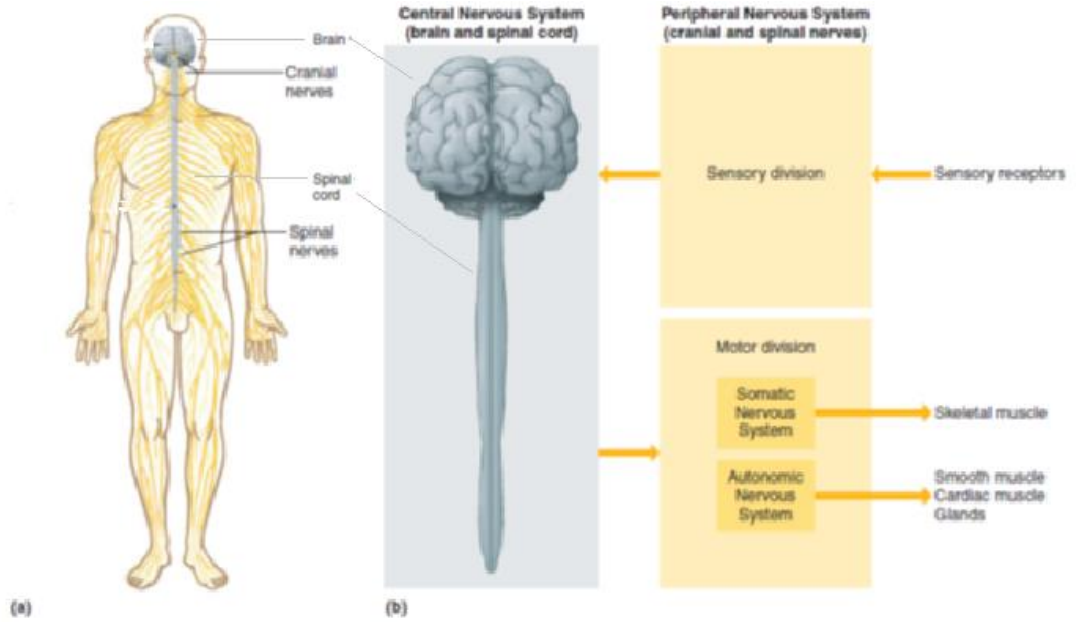

Figure 1.1. Anatomy of the Nervous System. Adapted from Shier, 2010.

1.1.1.1. Central Nervous System (CNS)

The CNS includes the brain, and the spinal cord. Besides the neural tissue, these complex organs include blood vessels and the various connective tissues which provide physical support and protection. Roles of CNS in the body are to integrate, process, store and program and coordinate sensory data and motor commands (Martini et al., 2006).

1.1.1.2. Peripheral Nervous System (PNS)

The PNS consists of all the neural tissue outside the CNS. These are cranial nerves, sensory nerve bundles and the spinal nerves, first two of which arise from the brain and the last one originates from the spinal cord. The peripheral nervous system is anatomically but not functionally distinct from the CNS. The PNS delivers sensory information to the CNS and carries motor commands from the CNS to peripheral tissues and systems. PNS has a sensory division which receives signals from sensory receptors, and a motor division which performs the motor activities and is divided into two as autonomic and somatic nervous system (Shier et al., 2010).

1.1.2. Histology of the Nervous System

The nervous system has two main classes of cells: nerve cells (neurons) and glial cells (glia). Neurons have a role in the generation of signals and the communication of signals between nerve cells. Glial cells surround the nerve cell bodies, axons, and dendrites. They also produce the growth factors (e.g. NGF, BDNF) and neurotransmitters (e.g. acetylcholine, GABA, dopamine). In cell culture experiments, certain types of neuroglia (astrocytes) signal neurons to form and maintain synapses (Kandel et al., 2000).

1.1.2.1. Neurons

Nerve cells are the main signaling units of the nervous system. A typical neuron has four morphologically defined regions: the cell body, dendrites, the axon, and presynaptic terminals (Figure 1.2A). The cell body, or soma, contains a large round nucleus. Perikaryon is the cytoplasm surrounding the nucleus. There are neurofilaments and neurotubules, which are similiar to microfilaments and microtubules of other types of cells, in the perikaryon. Neurofibrils, bundles of neurofilaments, extend into the dendrites and axon to provide internal support for them. Dentrites, which extend from the cell body, are highly branched, and each of them has dendritic spines. In CNS, a neuron receives information primarily at these sites. An axon is long cytoplasmic process capable of propagating an electrical impulse known as action potential. Cytoplasm in an axon is called axoplasm, and contains neurofibrils, neurotubules, small vesicles, lysosomes, mitochondria and various enzymes. Axoplasm is surrounded by a specialized portion of cell membrane, called axolemma. Axon hillock is the thickened region where initial segment of the axon in a multipolar neuron is attached to cell body (Figure 1.2B). All the behavioral functions of the brain are carried out by specific sets of interconnected neurons (Martini et al., 2006).

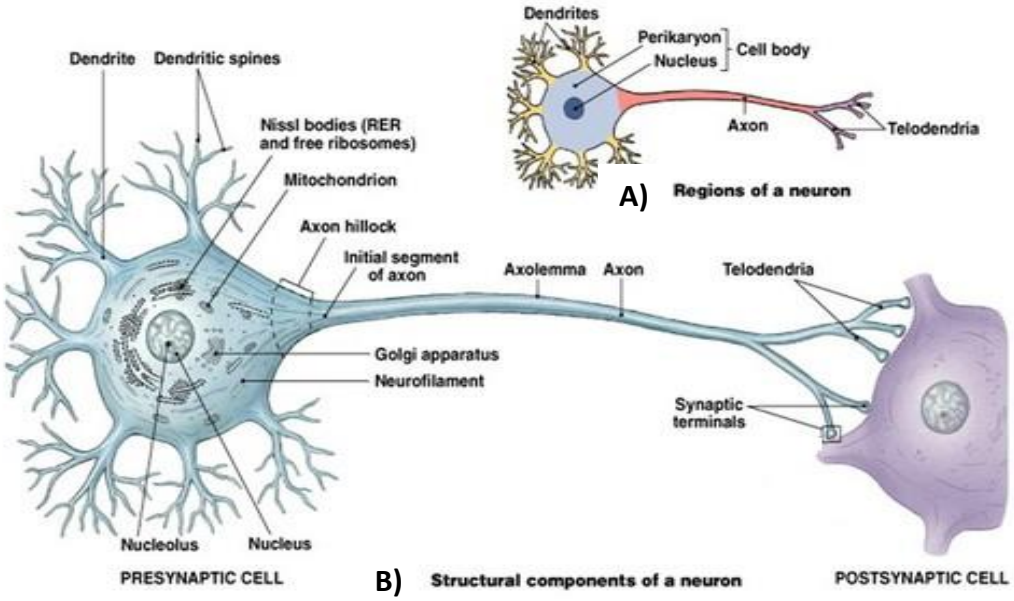

Figure 1.2. The anatomy of a multipolar neuron. (A) Regions of a neuron, (B) Structural components of a neuron. Adapted from Martini, 2006.

1.1.2.1.1. The Classification of Neurons

Neurons can be classified according to their structure and function.

1.1.2.1.1.1. Structural Classification of Neurons

Neurons are categorized as anaxonic, bipolar, unipolar, and multipolar on the basis of relationship between the dentrites and the cell body and the axon (Figure 1.3). Anaxonic neurons have no anatomical features that distinguish dentrites from axons. They are located in the brain and their functions are poorly understood. Bipolar neurons have two processes: an axon and a dendrite. They are rare in adults and are only found in some special sense organs such as the eye or nose. They act as receptor cells in sensory processing. Unipolar neurons have a single process emerging from the cell body. They are very short and divide almost immediately into proximal (central) and distal (peripheral) processes. Multipolar neurons have several processes extending from the cell body. They are the most common structural type in the body since all motor and association neurons are multipolar (Marieb and Hoehn, 2006).

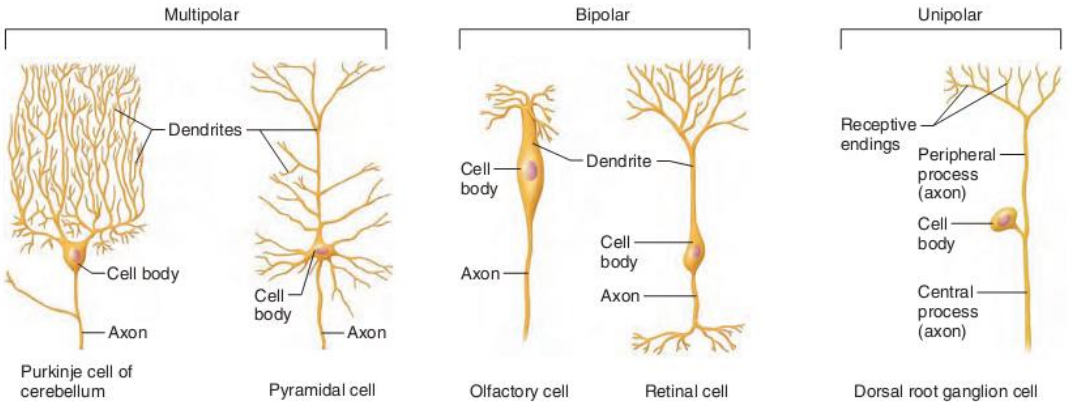

Figure 1.3. Structural classifications of neurons. Adapted from Marieb and Hoehn, 2006.

1.1.2.1.1.2. Functional Classification of Neurons

Neurons are grouped as sensory neurons, motor neurons, and interneurons according to their function. Sensory neurons are also called afferent neurons and they deliver the signals from the sensory receptors to the central nervous system. They are generally unipolar neurons which collect information concerning the external or internal environment. Motor neurons are also called efferent neurons and are found in the peripheral nervous system. They carry messages from CNS to PNS. The axons from CNS are called efferent fibers. There are two efferent nervous systems: (i) somatic nervous system including all the somatic motor neurons that innervate skeletal muscles and (ii) autonomic nervous system innervating smooth muscles, cardiac muscle, glands and adipose tissue. Interneurons are also called association neurons and are the highest number of neurons in the body (20 billion). Most of them are located in the brain and the spinal cord, but some of them are found in autonomic ganglia. Distribution of sensory information and the coordination of motor activity are done by interneurons. They also have role in memory, learning, and planning (Martini, 2006).

1.1.2.2. Glial Cells

Glial cells are the second type of cell in the nervous system, and their number is higher than neurons. As shown in Figure 1.4., neuroglial cells are astrocytes, oligodendrocytes, microglia, and ependyma (Kandell, 2000). Astrocytes are star-shaped cells, and commonly found between neurons and blood vessels. They provide support and hold structures together with abundant cellular processes. When brain tissue is injured, astrocytes form a special type of scar tissue (glial scar), which fills spaces and closes gaps in the CNS. They also have role in the blood-brain barrier, which restricts movement of substances between the blood and the CNS. Another type of glial cells are oligodendrocytes. They resemble astrocytes but are smaller and have fewer processes. Along myelinated axons, they are found in a row form and produce myelin in the brain and spinal cord. Microglial cells are small, and they have fewer processes than other types of glial cells. They help support neurons and phagocytize bacterial cells and cellular debris in the CNS. Final type of glial cells are ependymal cells. They are cuboidal or columnar in shape and may have cilia. The inner lining of the central canal that extends downward through the spinal cord were formed by ependymal cells. They also form

a one-cell thick epithelial-like membrane that covers the inside of spaces in the brain called ventricles (Marieb and Hoehn, 2007).

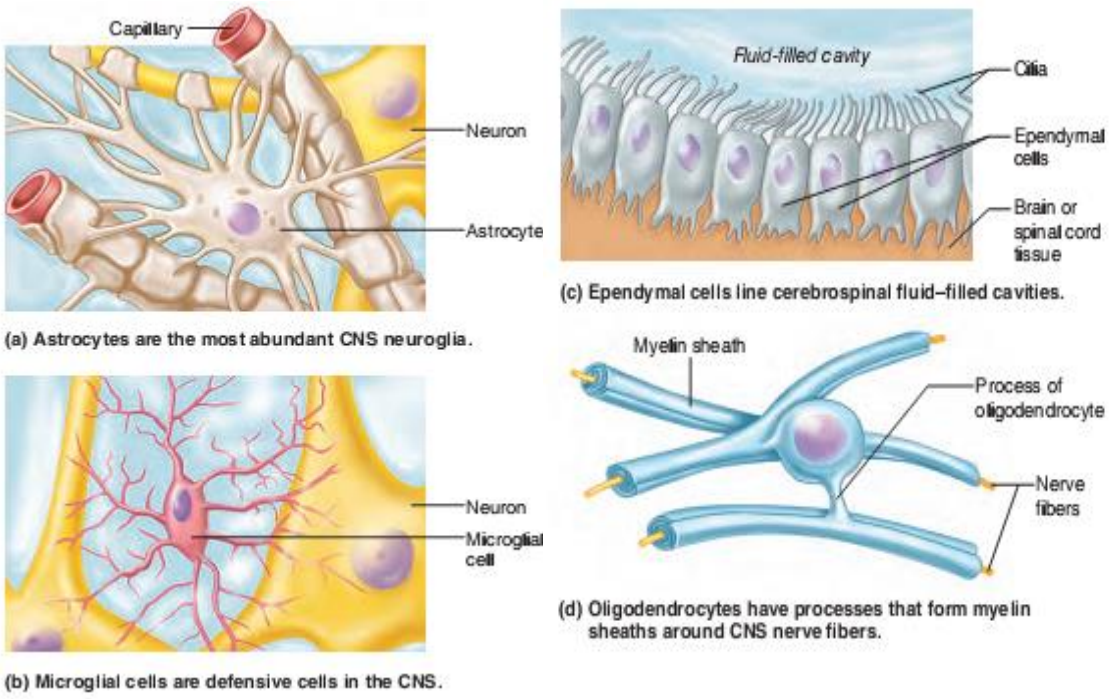

Figure 1.4. The principal types of glial cells in the central nervous system. Adapted from Marieb and Hoehn, 2007.

1.1.3. Synaptic Activity

A synapse is defined as the junction between two cells. The gap between parts of two cells at a synapse is called a synaptic cleft. In the synaptic transmission process, the impulse in the presynaptic neuron signals the postsynaptic cell. At first, a nerve impulse travels along the axon to a synapse. Then, axons secrete neurotransmitters from synaptic knobs at their distal ends. When a nerve impulse reaches the end of an axon, the neurotransmitter which diffuses across the synaptic cleft is released (Figure 1.5). Finally, depending on the neurotransmitter reaching a postsynaptic neuron or other cell, signal may be excitatory or inhibitory (Guyton and Hall, 2006).

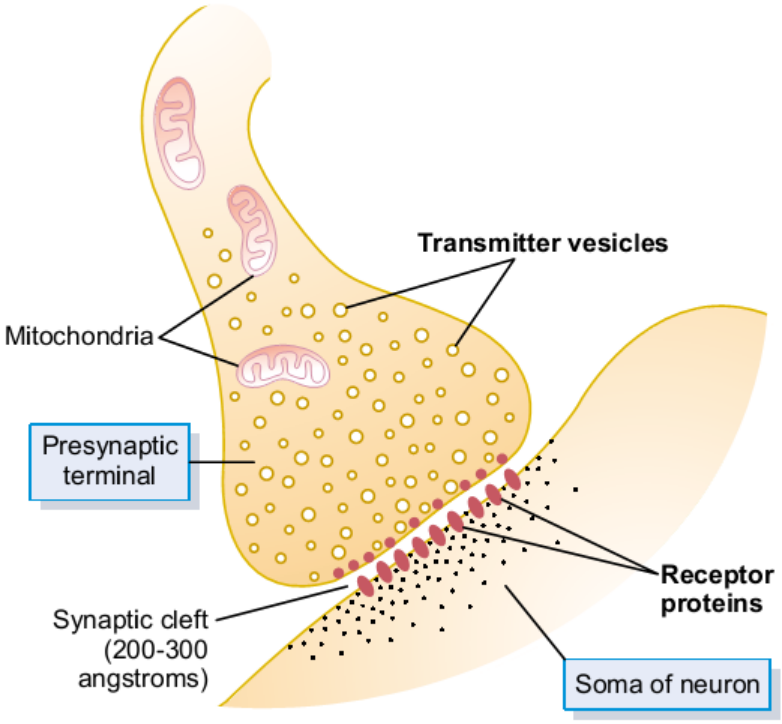

Figure 1.5. Physiology of the synapse. Adapted from Guyton and Hall, 2006.

1.1.3.1. Signal Transduction

Signal transduction occurs through nerve impulses which pass from neuron to neuron at synapses. A presynaptic neuron brings the impulse to the synapse, and stimulates or inhibits a postsynaptic neuron by being excitatory or inhibitory. Direction of a nerve impulse is the axon to the axon terminal (Figure 1.6). Axons have several rounded synaptic knobs at their terminals, which are called synaptic vesicles. These knobs contain neurotransmitter molecules in their structures. Voltage-sensitive calcium channels open and calcium diffuses inward from the extracellular fluid, when a nerve impulse reaches a synaptic knob. The increased level of calcium concentration inside the cell causes a series of events. Firstly, the synaptic vesicles are fused with the cell membrane, where they release their neurotransmitter by exocytosis. When the neurotransmitter binds to receptors on a post-synaptic cell, the action of neurotransmitter on the post-synaptic cell is either excitatory or inhibitory. The combined effect of the excitatory and inhibitory inputs from as few as 1 to 100,000 or more presynaptic neurons determines the net effect on the post-synaptic cell (Shier et al., 2010).

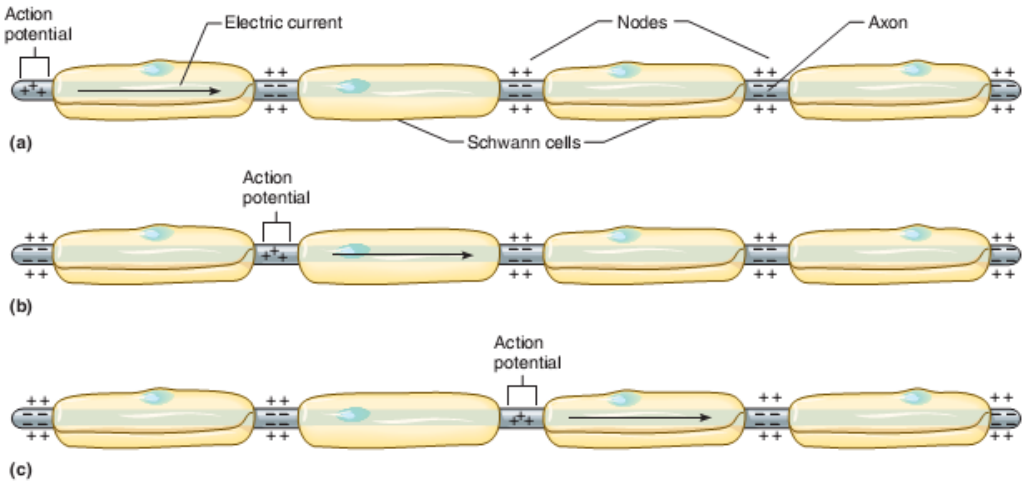

Figure 1.6. On a myelinated axon, a nerve impulse appears to jump from node to node. Adapted from Shier, 2010.

1.2. Neuronal Injury

The nervous system can be damaged by mechanical, thermal, chemical, or ischemic factors. These damages cause problems in various nervous system functions such as memory, cognition, language, and voluntary movement. Damage to nervous system results in the interruption of communication between nerve cells and their targets. Of all the types of injury, the most prominent one is to the CNS since it is most likely to result in death or permanent disability (Zhang et al, 2005).

1.2.1. Cellular Response to Nerve Injuries

When the PNS is injured, the injured axons are capable of regenerating long segments. They also have the capacity to establish connections with their targets. Although growth of a regenerating axon is slow (3-4 mm/day), the new axon may eventually reestablish the former connection. When a myelinated axon is injured, several events occur over the following several weeks and months (Figure 1.7). When the damage occurs, the portion of the axon disconnected from the cell body is called the distal segment. The portion still connected to the cell body is the proximal segment. The proximal segment may survive, but the distal portion does not. In time, the proximal portion may develop extensions that grow into the tube of the basement membrane. Connective tissue cells possibly reestablish the former connection. Neuroglia secrete nerve growth factors that assist the regeneration process. These nerve growth factors help direct the growing axon. However, the regenerating axon may still end up in the wrong place, so full function often is not recovered (Martini, 2006).

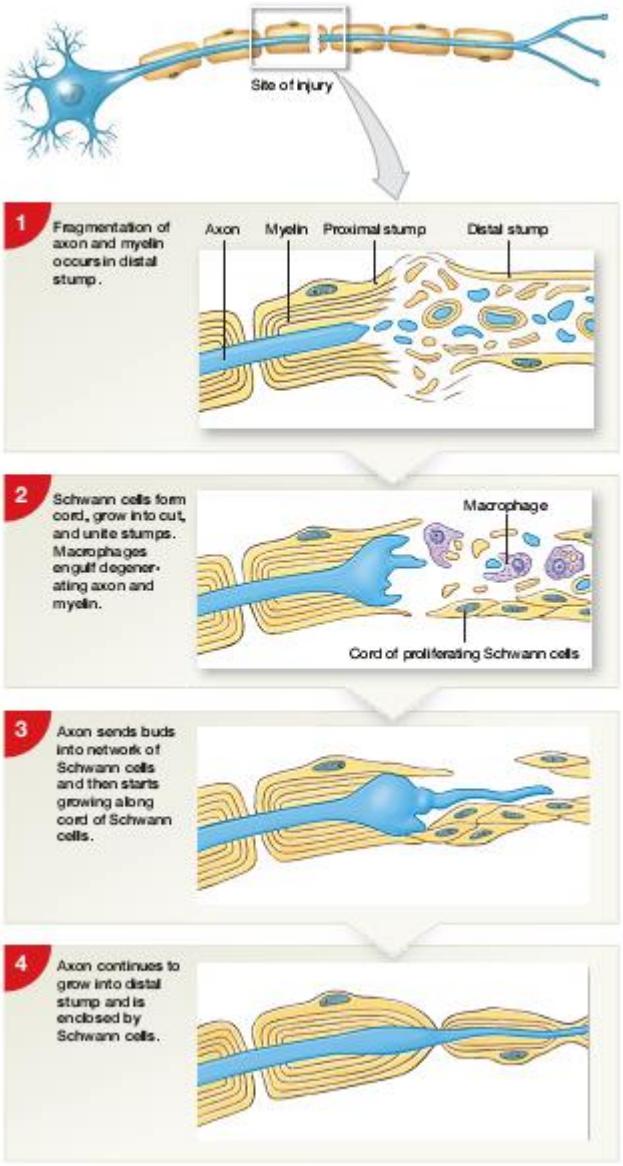

Figure 1.7. Regeneration of axons in PNS. Adapted from Martini, 2006.

1.2.1.1. CNS Injury

Axonal regeneration in the CNS is limited due to inhibitory influences of the glial and extracellular environment (Bahr and Bonhoeffer, 1994). Upon injury, myelin-associated inhibitors of neurite growth, astrocytes, oligodendrocytes, and microglia migrate to the injury site, and make the environment unsuitable for axonal growth. In the CNS, degeneration is slower compared to the PNS because the inhibitory myelin and axonal debris are not cleared away as quickly. The axons that survive axotomy are surrounded by the glial scar. Axonal outgrowth is stopped, because neurons cannot regenerate beyond the glial scar (Silver and Miller, 2004). Although proximal

axons initially attempt to regenerate, the surrounding environment prevents this (Tatagiba et al., 1997). Therefore, regenerating axons in the CNS cannot reach synaptic targets and reestablish their original connections (Figure 1.8). There is no natural mechanism to remove or neutralize the inhibitory components of cellular debris in the CNS. However, severed CNS axons may regrow in more permissive environments. They are able to recognize target areas and to reestablish functional synapses with target neurons (Bray et al., 1987). There has been much recent evidence that suggests that the mature CNS is a less hostile environment for regeneration than was previously thought. There is possibility of regrowth and functional recovery in the unscarred areas, if the axons can transverse the injury site (Teng et al., 2002). Different strategies such as the use of tissue engineering, cell implantation and replacement therapies involving neural stem, Schwann and olfactory ensheathing cells, and provision of growth factors have shown potential for production of new neurons and the repair of injured CNS regions (Recknor and Mallapragada, 2007).

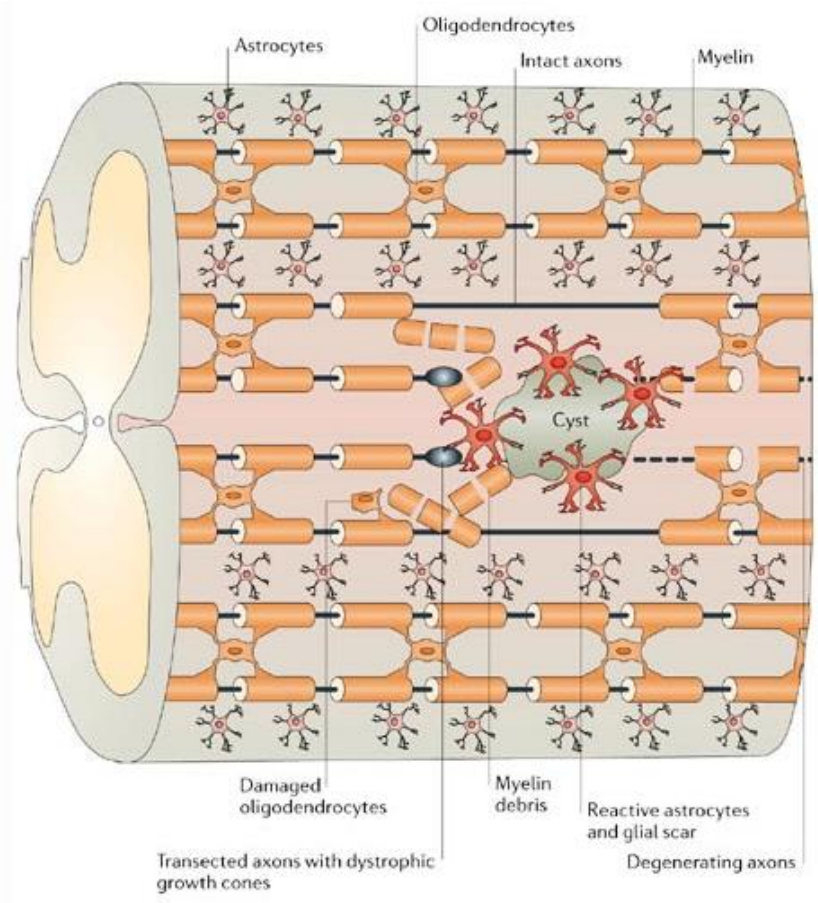

Figure 1.8. Schematic representation of the CNS injury site. Adapted from Yiu and He, 2006.

1.2.1.1.1. Spinal Cord Injury

It is estimated that the annual incidence of spinal cord injury (SCI), not including those involving death, is ca. 40 cases per million in the U.S. or approximately 12,000 new cases each year (National Spinal Cord Injury Database, 2013).

In case of a traumatic SCI, both sensory and motor axons are distrupted which breaks down the continuity of the spinal cord. Following the primary injury, Ca^{2+} influx, release of inflammatory cytokines, oxidative stress and fluid build up occur within the lesion site. These secondary events cause neurons (in the grey matter), and oligodendrocytes (in the white matter), to die. The speed of electrical conduction in the surviving axons are affected by the death of oligodendrocytes and subsequent loss of the myelin sheath. Therefore, a sustained and long lasting loss of function occurs (Dalton et al., 2007).

1.2.1.2. PNS Injury

Peripheral nerve injuries (PNI) can lead to dysfunction and disfigurement for a lifetime. In Europe and US, several hundred thousand such traumatic injuries occur each year. A characteristic chain of degenerative and regenerative events are triggered by PNI. The myelin and axons break up at the site of nerve damage which results in the migration of phagocytic cells, Schwann cells and macrophages into the PNS to clean up debris. A severed peripheral nerve is capable of a significant degree of regeneration. Once the defect is bridged, regenerating axons are guided for long distances along Bands of Büngner (Faweett and Keynes, 1990) that occur naturally. Implantation of artificial substitues and substrates to guide the naturally regenerating axons towards the distal segment is currently the most popular approach in peripheral nerve tissue engineering.

The proximal nerve stump swells after the initial injury but the damage is relatively small compared to the distal end. The distal portion undergoes degeneration due to the protease activity termed "Wallerian Degeneration". The axonal cytoskeleton is broken and Schwann cells shed their myelin lipids at the distal end. When macrophages clear the myelin and other debris, the potential for nerve regeneration increases. Myelin-associated glycoprotein (MAG) the myelin of PNS inhibits peripheral axon regeneration (Shen et al., 1998), and successful PNS regeneration can only occur after the myelin is cleared and myelin-specific proteins are downregulated by the Schwann cells. Peripheral nerve regeneration is prevented due to the delay of myelin clearance unless the MAG gene is disrupted (Schafer et al., 1996). Specific factors that stimulate axon regrowth are secreted by Schwann cells in the distal portion of the severed nerve. Regeneration of the nerve begins at the proximal end and continues toward the distal stump after complete clearance of the debris. It is very critical to achieve accurate alignment of the original fascicles in microsurgical repair. Bands of Büngner play a crucial role in successful peripheral nerve regeneration in the distal nerve (Scherer and Salzer, 2001). Functional reinnervation in humans occurs at a rate of about 2–5 mm/day, therefore, significant injuries can take many months to heal and full restoration of sensory or motor function is not very common.

1.3. Tissue Engineering and Regenerative Medicine

Transplantation is a very successful method, but it has its constraints. Obtaining enough tissue and organs for all the patients is the major problem. Immunological rejection is another if it is an allograft. Immunosuppressors can cause new tumor formation in the body. Tissue engineering which does not have these limitations has emerged where new and functional living tissue is fabricated in the lab using living cells, which are usually associated with a matrix or scaffold to guide tissue development. As cell source, mostly types of stem cells are used in the production of tissue engineered constructs. Regenerative medicine initially was used to explain cell therapy where no scaffold material was used but now the meaning is broadened to encompass both the tissue engineering and cell therapy. Scaffolds can be made from natural, or synthetic materials, or from a blend of both. After implantation, cells of the host can migrate into the tissue engineered implant. The cells used to populate tissue engineered constructs can be isolated from the tissues of the host as fully differentiated cells, or they can be manipulated to produce the desired function after being isolated from stem cell sources in the body of the host such as a bone marrow. Tissue engineering offers an advantage over simple cell transplantation alone because in this method organized three-dimensional functional tissue is designed and developed (Vacanti and Vacanti, 2007).

As outlined in Figure 1.9., initially cells are isolated from the tissue samples of the host and are manipulated with tissue culture techniques. Then, cells and growth factors are seeded into the scaffold, and grown in the flasks. Finally, this structure is implanted at the injured site.

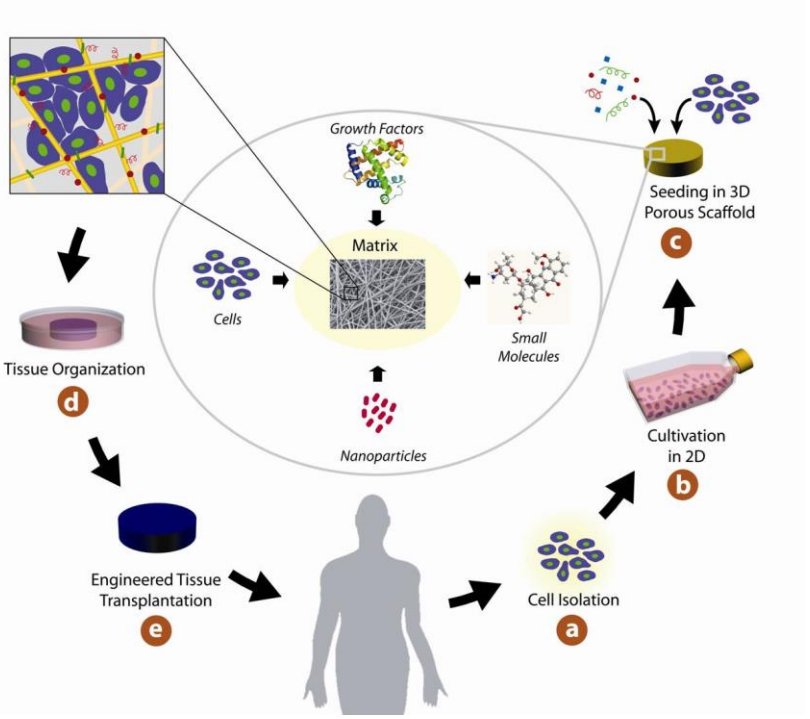

Figure 1.9. Flowchart of tissue engineering. Adapted from Dvir, 2013.

1.3.1. Cell Sources in Tissue Engineering

Different types of stem cells (SCs) are used in the tissue engineering applications. Differentiation potential of the stem cell can be defined as the potency. In terms of potency, there are different types of stem cells. Totipotent, also called omnipotent, stem cells can differentiate into embryonic and extraembryonic cell types. Such cells can construct a complete, viable organism (Shöler, 2007). These cells are produced from the fusion of an egg and sperm cell. Cells produced by the first few divisions of the fertilized egg are also totipotent (Mitalipov and Wolf, 2009). Pluripotent stem cells are the descendants of totipotent cells and can differentiate into nearly all cells, i.e. cells derived from any of the three germ layers (Hu et al., 2005). Multipotent stem cells can differentiate into a number of cells, but only those of a closely related family of cells. Oligopotent stem cells can differentiate into only a few cells, such as lymphoid or myeloid stem cells. Unipotent cells can produce only one cell type, their own, but have the property of self-renewal, which distinguishes them from non-stem cells (Shöler, 2007).

Adult SCs: Adult SCs have been derived from many animal and human tissues for use in tissue engineering such as: bone marrow, peripheral blood, brain, spinal cord, dental pulp, blood vessels, skeletal muscle, heart, epidermis, mucosa of the digestive system, cornea, liver, and pancreas (Blitterswijk, 2008). They are undifferentiated cells with a long term self renewal capacity. Adult SCs can also differentiate to mature cell types with specialized functions. Maintaining tissue homeostasis and replacing cells lost due to injury or disease are the main role of adult stem cells. Before they reach the fully differentiated state of mature cells, SCs generate intermediate cell types (progenitors and precursors). These cells are considered as cells committed toward differentiation along a specific cellular pathway.

Embryonic Stem Cells (ESCs): The inner cell mass (ICM) of the developing blastocyst stage embryos five to eight days after fertilization is the source for ESCs. With a capacity of unlimited expansion *in vitro* and being considered an immortal epiblast derivative that can be maintained at a natural checkpoint in differentiation, ESCs can be expanded as undifferentiated colonies in the presence of appropriate feeder cells.

Bone marrow derived stem cells (BMSCs): BMSCs are capable of differentiating into many types of connective tissues such as cartilage, bone, muscle, bone marrow stroma (hematopoietic support tissue), fat, and tendon. They can also differentiate into neural cells, cardiac myocytes, vascular support cells (pericytes, smooth muscle cells) (Jackson et al., 2001; Shi and Gronthos, 2003). They are considered as a valuable cell sources for various tissue engineering applications due to the multipotential of culture expanded BMSCs. Both scaffolds and various growth factors/cytokines are required in such strategies to support and guide the proliferation and differentiation of MSCs to form specific tissues. Most of the time, the tissue damage site and its microenvironment provide the required instructional support. In other cases, the instructional cues are provided with pretreatment of the cells or placing the cells within unique scaffolds with appropriate physical and chemical guidance cues (Caplan, 2003).

1.3.2. Scaffolds in Tissue Engineering

An ideal scaffold should be biocompatible and bioresorbable with a controllable degradation rate that matches the regeneration rate of the new tissue. It should also be three-dimensional and highly porous with an interconnected, sufficiently large pores to allow cell attachment and migration, new tissue ingrowth, and flow of the nutrients and waste products, and have mechanical properties matching the native tissue (Hutmacher, 2000). Different types of scaffolds can be used in tissue engineering depending on the purpose of the study. For examle, when fibrous structure of ECM is needed in the construct, electrospun fiber mats are preferred. Therefore, choice of the scaffold types depends on what tissue is needed. Mostly common tissue engineering scaffold types are foams, films, patterned films, fiber mats, and membranes. In addition, decellularized tissues are used as substrates for tissue engineering applications.

1.3.2.1. Scaffold Production Methods

There are different scaffold production methods. For fibrous scaffold production, electrospinning, wet spinning and extrusion techniques can be used. Freeze drying, solvent casting/particulate leaching, and gas foaming are used for porous scaffold production.

Fibrous Scaffolds

-Electrospinning: In this technique, a polymer solution is sprayed out of a nozzle under an electrical force. There are three main components in an electrospinning setup: (i) a high voltage power supply, (ii) an electrically conducting spinneret (i.e., a metal needle usually connected to a syringe controlled by a syringe pump), and (iii) a collector at a certain distance from the needle tip (Figure 1.10). When the syringe pump is turned on, and the electrical potential is applied, the polymer solution is ejected from the syringe towards the collector and fibers are formed on the collector as the electrical force overcomes the surface tension on the liquid droplet.

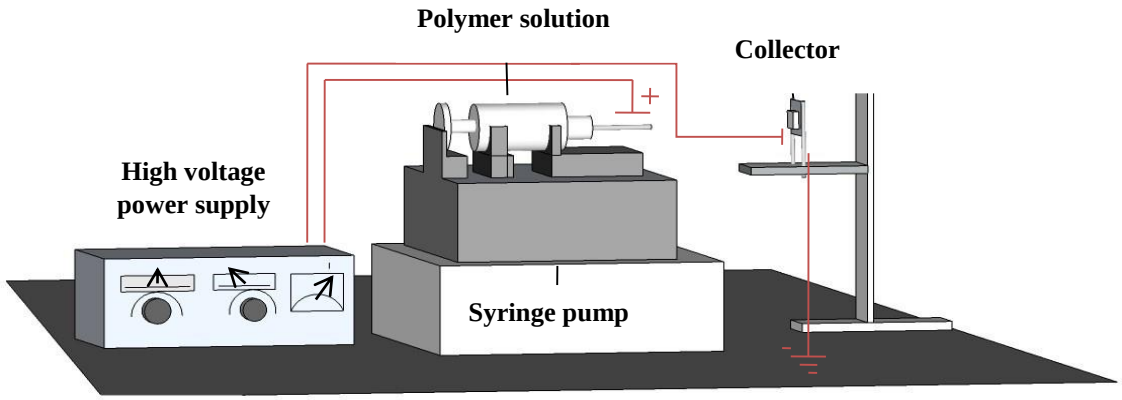

Figure 1.10. Main parts of an electrospinning set up.

The main parameters which affect the properties of the electrospun fibers are the polymer type and concentration, solvent, potential, distance between the needle tip, the material shape and the state (static or revolving) of the collector (Huang et al, 2003). The collectors used in electrospinning could be in the form of a drum, plate or disc, and they define the properties of the fibers as aligned or random, and hollow or filled solid in. Electrospinning produces micro- and nano-scale fibers which conform to the structural properties of the ECM. Parellel fiber mats can be used to align cells to construct engineered equivalents of highly anisotropic tissues such as corneal stroma, nerve, cardiac tissues and muscles.

-Wet spinning: In wet spinning, a polymer is dissolved in a good solvent and then injected by a syringe into a non-solvent that is miscible with the solvent. As soon as the polymer solution comes in contact with the non-solvent, solvent diffuses into the non-solvent and the polymer precipitates. Parameters that affect the dimensions of fibers are injection rate, concentration, and diameter of the needle. The fiber properties are also affected by the processing conditions, such as coagulation bath composition, and drying conditions (Ndreu, 2007). Proteins can also be wet spun. For example, wet spinning procedure for proteins consists of extrusion of protein solutions, formation of the protein thread, and coagulation of the protein threads into fibers (Qiu et al, 2009). Fibers with diameters in the range from 10-100 μm were reported by this method.

-Extrusion: In this thermal application, a thermoplastic polymer is forced through a small orifice after decreasing its viscosity by heating to temperatures above its T_g but below its T_m and then applying pressure. The extruded polymer takes the form and the size of the orifice through which it is extruded. Blends of polymers, drugs, inorganic or organic fillers can be processed using this approach (Mo et al, 2004).

Sponge Type of Scaffolds

-Freeze drying (Lyophilization): This technique has been used widely to make porous scaffolds for use in tissue engineering applications. This process consists of three stages: freezing, primary drying and secondary drying (Thomson et al, 1995). The sample is generally a polymer solution, and it is generally frozen at -20 °C or -80 °C, depending on the freezing point of the solvent and the available freezing system. The frozen sample is then placed in a lyophilizer to remove the frozen solvent by sublimation. Rapid cooling in the primary drying is used to cause thermodynamic instability and phase separation or small crystallites. The solvent is then removed by sublimation under vacuum leaving behind a porous structure (Tang and Pikal, 2004). The frozen sample is kept below the glass transition temperature or the melting point at all times. The primary drying step is energy intensive and requires a relatively long processing time, which is directly related to the ice sublimation rate and determined by factors such as the level of vacuum, shelf temperature, sample volume and exposed surface area. Secondary drying is carried out to desorb the unfrozen solvent bound to the polymer and for this process a vacuum level lower than that for primary drying is required (Qian and Zhang, 2011). Typical pore sizes produced with this

technique are in the range of 100-200 μm and the degree of porosity is around 90-99 % (Griffon et al, 2006; Qian and Zhang, 2011).

Solvent casting-particle leaching: This technique was developed for a higher control of porosity and pore size in a scaffold than could be obtained with lyophilization (Shokrolahi et al, 2011). The method mainly involves dispersion of a porogen, a particulate solid of predetermined size, shape, and amount (Annabi et al, 2010) within a polymer solution in which the particles do not dissolve. A polymer–porogen network is produced upon drying this solution the thicknesses of which determined by the porogen amount. The porogen is then leached or dissolved away by immersing the sample in a solvent for the particles leaving behind a porous sponge. The use of many different types of porogens such as salts (Mikos et al, 1994), glucose (Holy et al, 1999), gelatin microspheres (Thomson et al, 1998), paraffin microspheres as well as ice particles (Gutierrez et al, 2008) were reported.

Gas foaming: It is another technique used to make porous scaffolds. It can be carried out in two ways: conventional gas foaming and dense gas foaming.

i) Conventional gas foaming: The mechanism of pore formation in this technique involves three basic steps: (1) polymer/gas solution formation, (2) pore nucleation, and (3) pore growth and density reduction (Lips et al, 2005). The polymer/gas solution is formed by subjecting the polymer to a high pressure CO_2 (800 psi) to saturate it with gas. The gas phase separates from the polymer in the form of pores and growth of these pores is caused by diffusion of the gas in areas of the polymer adjacent to these pore nucleation sites (Harris et al, 1998). Every step of this method affects the final foam morphology. Controlling the pressure regulates the amount of gas in the polymer, and therefore, the pore volume or fraction. The rate of pressure release influences pore nucleation density, and the rate of temperature decrease governs pore growth, and therefore, pore diameter and interconnections (Hou et al, 2003).

ii) Dense gas foaming: A dense gas is a fluid above or close to its critical temperature and pressure, and demonstrates physical properties in between those of a true gas and liquid. Dense gas CO_2, which has a relatively low critical temperature (T_c 31˚C), is an attractive candidate for use in biomaterial processing because it is inert, nontoxic, and inexpensive. This gas has been widely used as a foaming agent to induce porosity in scaffolds of hydrophobic, and hydrophilic polymers, and in hydrophilic/hydrophobic blends (Quirk et al, 2005). Dense gas has often been used in the preparation of scaffolds from common hydrophobic polymers such as poly(lactic acid) (PLA), poly(lactic acid-co-glycolic acid) (PLGA), and poly(ε-caprolactone) (PCL) (Chen et al, 2006;Tai et al, 2007).

1.3.2.2. Biomaterials Used in Scaffold Production

Both biodegradable and nondegradable polymers of natural and synthetic origin are used to make scaffolds, but biodegradable ones are usually preferred. This is because in the tissue construction process, first the cells are grown on porous structures, then cells they populate the

structure and finally the polymer starts to degrade creating more space for cell growth and ECM deposition within the structure. One important requirement is that the degradation products should be biocompatible.

Synthetic polymers such as poly(glycolic acid) (PGA), poly(lactic acid) (PLA), copolymers and blends of PGA and PLA, poly(ε-caprolactone) (PCL), polydioxanone (PDO), and natural polymers such as collagen (types I–IV), gelatin, elastin, silk, fibrinogen, hemoglobin, and myoglobin can be used in making scaffolds (Huang et al, 2003). Natural polymers often lack the strength required, however, their mechanical strength and stability can be improved by crosslinking or by blending with synthetic polymers or by adding mineral components into their structures. Collagen is one of the most abundant proteins in the human body. Collagen based scaffolds have attractive biological and structural properties in addition to being natural; they carry load, hydrophilic, have low antigenicity, and good compatibility (Kolacna et al, 2007). Elastin is another important protein, which is found in the ECM of connective and elastic tissues, and is often used in tissue engineering of scaffolds. Recently, silk fibroin (SF) has gained importance as a scaffold material in the tissue engineering field. Even though it is not a natural component of human body, it is biocompatible, has significant crystallinity, high elasticity and tensile strength, and toughness. SF was at first electrospun for use in ligament tissue engineering, and has more recently been used for vascular, bone, and skin tissue engineering (Huang et al, 2003).

1.3.2.3. Nerve Tissue Engineering Approaches

Central and peripheral nervous systems have very different molecular and cellular environments, and different strategies are required in the engineering of these tissues. Scaffolds and matrices in the nervous system has to provide a surface or a support system for axonal growth. The focus of tissue engineering in the peripheral nerve has been the reconnection of severed nerves separated from their target tissues or the distal nerve segments (Dalton et al, 2008). As explained in Section 1.2.2.1. and 1.2.2.2., cellular responses to nerve injury are different in the two divisions of the nervous system, CNS and PNS. Therefore, approaches to provide nerve regeneration at these sites has to differ from each other.

1.3.2.3.1. CNS

Many destructive events, such as loss of tissue and function in motor and sensory systems, begin with spinal cord injury. The presence of a glial scar at the site of injury is one of the main obstacles for regenerating axons in the injured spinal cord. In the case of an intraspinal transplant, the glial scar is present at the "transplant–host spinal cord" interface. Compared with the use of peripheral nerve autografts and nerve bridges in PNS, there is currently no reproducible and successful clinical therapy for SCI. The predominant focus of tissue engineering strategies has been a combination of cell transplantation with supportive matrices and scaffolds or neurotrophic factors. Studies in this field have been focused 1) Increasing the number of damaged ascending and descending axons that regenerate, 2) Improving the remyelinization of these regenerating axons, 3) Guidance of regenerating axons back to their appropriate target regions in the brain or spinal cord. Therapeutic outcomes in injured patients through the use of these approaches could

further be improved with support from new techniques like gene therapy and ex vivo manipulation of cells (Blitterswijk, 2008).

1.3.2.3.1.1. Embryonic Stem Cells

Neurons, astrocytes, and oligodendrocytes could be replaced by use of ESCs, appropriate remyelination achieved, and locomotion improved as shown in early animal studies (Siegenthaler et al., 2010). Although the mechanisms underlying the functional improvement remain unclear for all transplantation studies, ES cells offer a novel tool to understand these mechanisms. It is now possible for investigators to track transplanted cells that have been transfected with genes that express green fluorescent protein. Genetic modification allows researchers to track the integration and differentiation of ES cells.

One of the most pragmatic approaches to restoring function to the damaged spinal cord is achieving remyelination. ES cell–derived precursors could be used as bridges that can support axonal regrowth. These precursors could phagocytose key inhibitory molecules in the glial scar tissue, thereby, creating an inhibitor-free bridge over which axons sprout rapidly from the transplant into the normal cord. To create bridging circuits across the injury site, newly generated neurons could be used. The injury could be limited by ES cell transplantation. ES cells can be genetically altered to deliver growth molecules, such as NT3, after transplantation in order to overcome the hostile environment of the injured nervous system. Since ES cells are embryonic in nature, the adult CNS could be reprogrammed through their progenitors to optimize spontaneous host regeneration (McDonald and Becker, 2008). To regain normal CNS function such as neovascularization, and replacing nonneural cells are also very important. Similar applications of ES cells in the peripheral nervous system are possible (Figure 1.11).

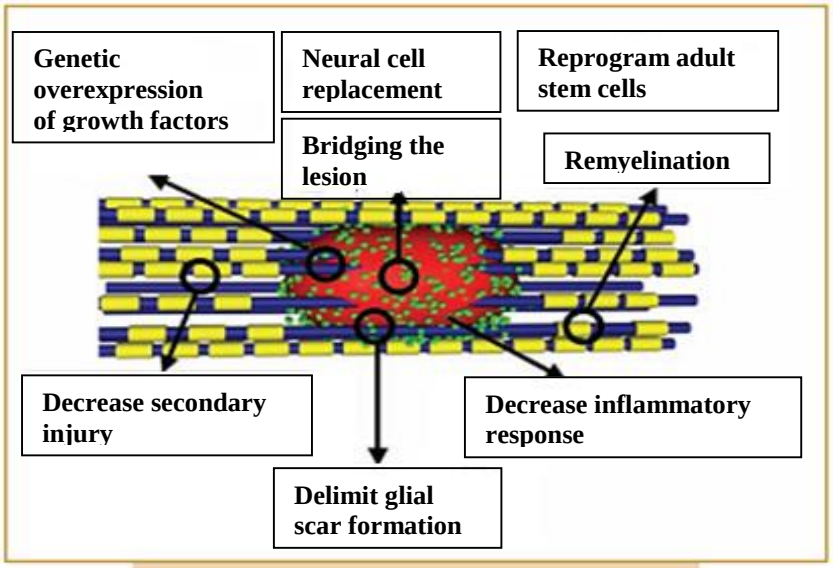

Figure 1.11. Novel approaches to spinal cord repair using ES cells. Adapted from Langer, 2008.

1.3.2.3.1.2. Synthetic Nerve Guide Conduits

Synthetic nerve guide conduits are prepared with different features. Physical, bio-chemical, and cellular modifications can be applied to improve the structure and the function of the nerve guides.

1.3.2.3.1.2.1. Physical Modifications

The following are some of the physical modifications.

Microtexturing: For many reasons, scaffolds are extremely useful for evaluating and supporting nerve regeneration processes. The outgrowth of neurons and regulation of regeneration are controlled by the changing the microtexture of the surface of the lumen of the cylindirical conduit. The formation of an organized, discrete nerve cable with myelinated axons is possible with smooth inner surfaces. On the other hand, with rough inner surfaces nerve fascicles are dispersed unorganized throughout the lumen unorganized inside which results in little regeneration. It was discovered that rougher the texture of the surface, the greater the spread of nerve fascicles in a study with expanded microfibrillar Gore–Tex® poly(tetrafluroethylene) tubes with different inter-nodal distances (1, 5, and 10 μm) (Valentini, 2000). Additionally, the stability of the wall structure (Evans et al., 1999) and channel geometry (Sundback et al., 2003) both were shown to affect the molecular and cellular makeup of the regenerating tissue.

Micropatterning: It is possible to create a specific biomaterial "inner architecture" and use it in the recovery of tissue function. The organization of the cytoskeleton, cell adhesion, and cell-to-cell interactions determine the responses of a cell to topographical structure in the enviroment and these in return determine the cell fate. Through the fabrication of microgrooves and other patterns on substrate surfaces, cell growth can be controlled at the molecular and cellular level (Clark et al., 1990). Precise design and creation of features on a surface is possible using a variety of materials and microfabrication and nanofabrication techniques including photolithography and reactive ion etching. The move from silicon wafer-based fabrication to polymer-based scaffolds in 2D and 3D was made possible by the recent developments in the nano and micro level manufacturing techniques. When the analyzing functional changes in individual cells and their relationship with their environment in culture, ability to have control over their shape and distribution on the substrate is extremely valuable. Fabrication techniques producing substrates with various feature shapes and dimensions can be used in the study of cell behavior and morphology *in vitro* before integrating similar techniques into a scaffold design.

Microfabrication and transfer patterning techniques have been used to develop micropatterned biodegradable and nonbiodegradable substrates (Recknor et al, 2004). Microcontact printing techniques involving elastomeric polydimethylsiloxane (PDMS) stamps have been used in creating adhesive islands for the control of cell shape, growth, and function, (Singhvi et al, 1994). Microfluidic patterning has also been used to develop topographical (and chemical) cues on substrates. Different substrate materials, including Perspex (polymethyl methacrylate), silicon wafers, quartz, polystyrene and biodegradable polymers, including

poly(lactide-co-glycolide) and poly(dl-lactide) have been employed in the studies on the effects of the microenvironment on cell behavior (Fisher et al., 2008).

1.3.2.3.1.2.2. Biochemical Modifications

Molecules with biological function are being employed in the creating modified surfaces.

Neurotrophic factors: After the nerve damage many molecules including cytokines start the "healing" process through scar formation which actually is not good for recovery of function. Therefore, the lumen of nerve guides should provide with cytokines and neurotrophic factors after implantation to circumvent these negative activities and to induce recovery. Neurotrophic factors which include the neurotrophins (NTs), neuropoetic cytokines and fibroblast growth factors (FGFs) (Lundborg, 2000; Scherer and Salzer, 2001). There are different methods of delivering neurotrophic factors in combination with nerve guides. To direct the release, the growth factors can be loaded homogeneously within the nerve guide bulk, or specifically at the lumen (Piotrowicz and Shoichet, 2006). Heparin-binding growth factors (e.g. NGF, NT-3) were reported to be locally delivered from matrices to help the axons regenerate. The release rate of a NGF could be controlled by the heparin-incorporated fibrin matrix (Lee et al., 2003).

Gene therapy: Genetic manipulation of neural cells is another attractive strategy because of the slow production of therapeutic proteins in their bioactive form, particularly true for more labile growth factors. This approach can be an attractive route for enhancing nerve regeneration when NGCs are introduced genes that encode proteins that function in preventing motor neuron loss, enhancing initial axonal sprouting, preserving motor endplate morphology and promoting accurate reinnervation (Harvey et al., 2006). Two common methods are directing *in vivo* gene transfer and modification, or the isolation, purification, followed by genetic modification of specific cell sex vivo prior to implantation (Jiang et al., 2010).

There is great potential in gene therapy in the treatment of many types of neurodegenerative CNS diseases, too. It has been shown by using different cell types, including Schwann cells that delivery of therapeutic molecules can stop or delay the progression of neurodegeneration (Tuszynski, 2002) and stimulate the regenerative capacity of CNS neurons. Fibroblasts, olfactory ensheathing glia (OEG) and neural progenitors were also reported in such applications (Kobayashi et al., 1997, Blits et al., 2003, 2004, Cao et al., 2004). Furthermore, neurotrophic factors could be selectively delivered to specific CNS locations by engineering the cells (Jakobsson and Lundberg, 2006). OEG that were genetically modified to secrete NTs (NT-3, BDNF, GDNF) stimulated long distance growth in certain spinal cord tracts sets an example of the potential of the system (Ruitenberg et al., 2003, 2005). NT-secreting OEG were also shown to improve spinal tissue sparing (Ruitenberg et al., 2005), and it was believed to improve behavioral outcomes (Ruitenberg et al., 2003).

Drug Delivery: Drug delivery can be used as a reparative and regenerative strategy for CNS injury was shown in animal models and in clinical test. Molecules are used in systemic deliveries and local injections to the epidural space, intrathecal space. Molecules that can cross the BBB or blood-spinal cord barrier (BSCB) are the only ones suitable for systemic delivery, but the high doses of

those which cannot easily cross can cause side effects. Limiting degeneration (providing neuroprotection) and promoting regeneration (enhancing neuroregeneration) are the main goals of drug delivery in the CNS. Even though it is strictly defined as a long lasting increase in functional ability, the term neuroprotection is also applied to indicate cases of increased axonal sparing or reduced lesion volume.

The majority of drugs delivered to the CNS have been through the systemic route. Most common agents used in these studies are the steroid methylprednisolone and GM-1 ganglioside, but their success was not found to be satisfactory in a clinical trial (Ramer et al., 2005). Methylprednisolone has strong anti-inflammatory effects (Bracken et al., 1998) and GM-1 ganglioside is effective in inhibiting apoptosis and promoting axonal sprouting (Geisler et al., 2001). A tetracycline derivative, minocycline (Stirling et al.,2005), cytokine IL-10 (Bethea et al., 1999) and erythropoietin (Eid and Brines, 2002) are other drugs that attemp to induce host inflammatory response. A variety of cellular targets, such as reduced die back of certain neuronal populations or oligodendrocytes and inhibition of microglial activation are used by these molecules (Eid and Brines, 2002; Ramer et al., 2005). Growth factors are valued for their regenerative potential and they can also be used for neuroprotection. Survival of either or both the sensory and motor neurons was enhanced by nerve growth factor (NGF), brain-derived neurotrophic growth factor (BDNF), neurotrophin-3 (NT-3) (Nakahara et al., 1996), ciliary neurotrophic factor (CNTF) (Sendtner et al., 1990), and glial cell-line-derived neurotrophic factor (GDNF) (Matheson et al., 1997).

ECM molecules: A fluid matrix that consists mostly of a fibrin clot often accumulates at the damaged nerve ends after a nerve is transected (Chen et al., 2006). In an attempt to mimic the post-injury microenvironment, such ECM molecules have been included into NGC design. This biomimetic environment was expected to enhance nerve regeneration. Dubey et al. (2001) demonstrated improved nerve regeneration using a magnetically aligned fibrin matrix used as a lumen filler of a nerve conduit designed for neuronal contact guidance. Seckel et al. (1995) showed that the presence of hyaluronic acid (HA) produced a better conduction velocity, higher axon counts and a trend towards earlier myelination as compared with saline-filled conduits when used as a luminal filler. Other NGC luminal fillers which have also been evaluated include various other ECM molecules, such as collagen, laminin and fibronectin (Jiang et al., 2010). Chen et al. (2000) used silicone conduits filled with a mixture of collagen, laminin and fibronectin to bridge a 10-mm sciatic nerve defect gap in a rat model. They recognized that the presence of the ECM protein fillers resulted in the formation of more mature myelinated axons and larger nerve cross sectional area at 6 weeks post-implantation, compared with empty silicone tubes.

1.3.2.3.1.2.3. Supporting Cells

To encourage injured axons to grow through areas of damage towards and into their target areas, transplant of other cells into the spinal cord are used as a “bridge”. Most recently stem cells derived from either embryonic or adult tissue have been investigated for this goal.

Schwann cells: These are the myelin-forming cells of the PNS. Repair of PNI is faciliated by these cells through expression of axonal growth-promoting molecules, including neurotrophic

factors, surface cell adhesion molecules and extracellular matrix. The Schwann cell is a good candidate for providing a growth related compound for injured CNS axons because of its ability to produce a variety of growth-promoting molecules. Schwann cells can be isolated and cultured from peripheral nerves and elicit an axonal regeneration and myelination response in the CNS. This was demonstrated by Xu et al. (1997), who transplanted a P(AN-VC) nerve guide seeded with Schwann cells and Matrigel™ into the completely transected adult rat thoracic spinal cord. Several weeks after transplantation, myelinated and unmyelinated axons were present within the Schwann cell cable that connected the opposing cord stumps. These and other experiments demonstrated the potential of the Schwann cell for spinal cord repair approaches. They also form myelin sheaths around CNS axons that allow signal conduction when the axons were regenerated (Imaizumi et al., 2000). An intraspinal Schwann cell graft showed a neuroprotective effect in addition to axon regeneration, reducing the secondary injury (Takami et al., 2002). Schwann cells were injected by Pearse et al. (2004) into the cystic cavity while maintaining an increased level of cyclic adenosine monophosphate (cAMP) which resulted in improved functional recovery.

Olfactory Ensheathing Cells: Olfactory bulb ensheathing cells (OECs) are the primary glial cells found in both the PNS and CNS of the olfactory system. Since axons continue to grow throughout adulthood, this system differs from other CNS tissues. Astrocytes of the CNS and Schwann cells from the PNS have similar characteristics with OECs. OECs express glial fibrillary acidic protein (GFAP) like astrocytes even though they ensheath and myelinate axons and support axonal regrowth, which are features of Schwann cells. OEC transplantations promoted myelination of demyelinated rat spinal cord axons (Franklin et al., 1996) and fostered regeneration of damaged axons in mature CNS (Navarro et al., 1999) form the basis of most work in this area. Axonal regeneration was enhanced by incorporating OECs into conduits in both the PNS (Verdu et al., 1999) and CNS (Ramon-Cueto et al., 1998) where Schwann cell-filled guidance tubes were used. These results demonstrated a distinct advantage of OECs over Schwann cells.

Bone marrow stromal cells (BMSC) (or mesenchymal stem cells, MSCs): MSCs are multipotent stem cells derived from the bone marrow and was shown to be able to transdifferentiate into neural cells (Yim et al., 2007). MSCs can serve as the an alternative to Schwann cells since they are easy to obtain via bone marrow aspirates and expand in culture (Fickert et al., 2003). Zhang et al. (2005) seeded, GFP-labeled undifferentiated MSCs in a Matrigel-containing chitosan nerve guide to bridge a 5 mm gap in the rat sciatic nerve. In the presence of MSCs, nerve conduction velocity and sciatic functional index were significantly improved after 6 weeks. Nerve regeneration was also comparable to the case of Schwann cell transplantation. It is possible that undifferentiated MSCs may also contribute to nerve regeneration by secreting growth factors and depositing basal lamina components even though the exact mechanisms behind the enhanced nerve regeneration with MSCs is not established yet (Chen et al., 2007).

Neural stem cells (NSCs): There are NSCs present in the mammalian CNS that have the potential to produce new neurons and glia. Although neurogenesis no longer occurs in most areas after birth, these cells can remain in certain regions of the adult CNS after development. Neural progenitors have been known to proliferate throughout life in a variety of mammalian species, including

humans but they have limited capacities in terms of growth and differentiation (Temple, 2001). In one study, NSCs were seeded into a dual scaffold structure made of biodegradable polymers for therapy of spinal cord injury. The general design of the scaffold mimicked the spinal cord with an outer section that mimics the white matter with long axial pores to achieve axonal guidance. The inner section was seeded with neural stem cells and therefore mimicked the gray matter (Lavik et al., 2001). Compared to cells alone, the seeded scaffold improved functional recovery following spinal cord injury. Long-term improvement in function was achieved through use of the neural stem cell seeded scaffolds in an adult rat hemisection model of spinal cord injury. The improvement was persistent for up to one year in some animals.

1.3.2.3.2. PNS

The death of damaged axons must be prevented for successful regeneration and the sprouting axons from the proximal nerve stump must extend into the distal nerve stump and make synaptic connections to the correct target regions. Grafting of natural tissue and entubulization using nerve conduits or scaffolds are the most common repair techniques in the attemp to achieve regeneration. Proximal and distal nerve stumps are connected using a synthetic or biologically derived conduit in these methods. By allowing for both physical and chemical guidance and reducing cellular invasion and scarring of the nerve, regeneration is optimized. Unregulated axonal growth at the site of injury is minimized by entubulization which provides a distinct, controlled environment. Entubulization also allows for diffusion of trophic factors emitted from the distal stump to reach the proximal segment, therefore, enhancing the physiological conditions for nerve regeneration. Nerve regeneration is promoted and difficulties associated with grafting are minimized by the transplantation of tissue engineered nerve conduits based on polymers and by alternative methods where an artificial environment is created to mimic the natural physical and chemical stimulus (Recknor and Mallapragada, 2008).

1.3.2.3.2.1. Autologous Nerve Grafts

Blunt trauma or penetrating missiles such as bullets are the most common reasons of PNI, but fractures and fracture-dislocations can cause PNI as well. Crush injuries happen more frequently than nerve transections. A bridging section of nerve is used and two end-to-end sutures are performed when nerve endings are unable to be rejoined without tension. The crushed section of nerve is cut, removed and replaced by a nerve taken from a less important site in the body (Figure 1.12). Typically the sural nerve which is taken from the back of the leg is used (Evans, 2001). Although the autograft works relatively well in practice and is the gold standard upon which all alternative therapies are judged, a surgery is required to obtain the graft and there is loss of function at the donor site. This often leads to detrimental changes such as scarring and the possible formation of painful neuromas. The limited number of donor nerves is another problem, so studies to provide a viable tissue engineering alternative to this treatment continues (Dalton et al., 2008).

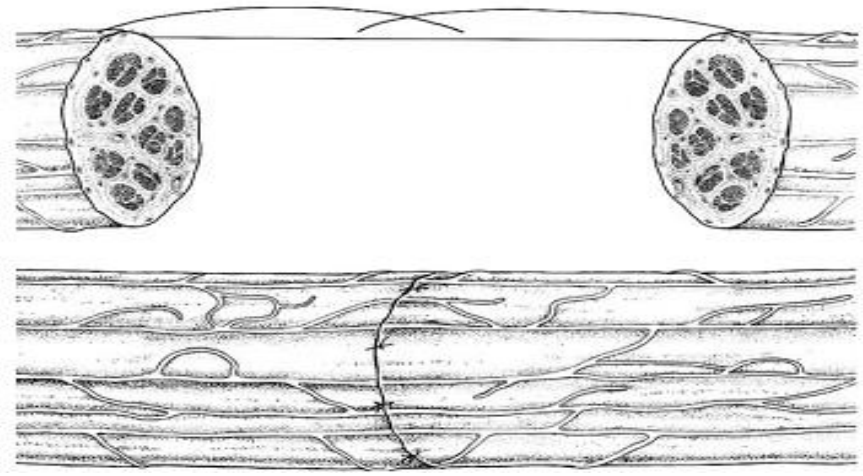

Figure 1.12. End-to-end suturing of peripheral nerves. Alignment of the fascicles is critical in successful regeneration and microsurgical techniques have been developed to optimize this surgery. Adapted from Blitterswijk, 2008.

1.3.2.3.2.2. Allografts and Acellular Nerve Matrices

Nerve allografts are nerve tissue transferred from a donor to the patient to replace lost function. Although, allografts eliminate the need for harvesting the graft from the patient tissue, rejection and lack of donor tissue are two major disadvantages. Another risk is disease transmission. Even though using allografts with immunosuppression has been considered, results have not matched the performance observed with autografts (Evans, 2000).

Other biomaterials which have also been observed useful for nerve regeneration are acellular nerve matrix allografts (Kim and Atala, 2002). By preserving the extracellular matrix components, these allografts mimic the ECM of peripheral nerves mechanically and physically. The ECM structure can, however, be damaged during the decellularization techniques used, such as thermal decellularization, and extraction of all cellular components can fail, and lead to inflammation upon implantation (Frerichs et al., 2002).

1.3.2.3.2.3. Nerve Guides

Nerve guides are off-the-shelf alternatives for small injury gaps (around 3–10 mm) which function by enclosing the therapy area. As shown in Figure 1.13., when an empty silicone tube is implanted at the injury site, some regenerative events occur. Firstly, fluid and cytokines fill up the nerve guide, and a fibrin matrix inside the lumen is formed. Then, Schwann cells and axons penetrate to the distal stump. The regenerated nerve usually is thinner in the middle of the bridge.

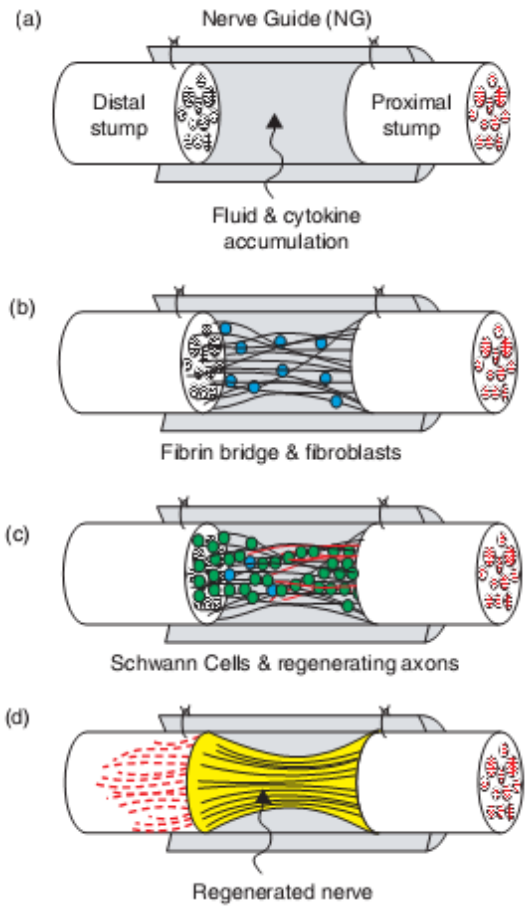

Figure 1.13. Sequence of events in empty silicone nerve guides. Adapted from Blitterswijk, 2008.

Hollow tubes (nerve guides or nerve guidance channels) have successful outcomes comparable with autograft in various animal and comparable clinical situations for nerve gaps up to 10 mm. Degradable collagen nerve guides (Neuragen™; Integra Life Sciences) which are being clinically used to treat paralysis due to PNI, have been approved for use by the Food and Drug Administration (USA). Many tissue engineering-based strategies, such as use of matrices, scaffolds, cell transplants and/or drug delivering therapies are possible (Dalton et al., 2008).

1.4. The Aim of the Study

This study aimed to create a nerve guide and to compare the effect of orientation of the nanofibrous fillers on the growth and differentiation of rat bone marrow stem cells (rBMSCs) *in vitro*. For this purpose, three different types of scaffolds (AF-Fo, RF-Fo, Fo-Fo) were prepared as bilayers.

1.5. Novelty of the Study

For spinal cord injury treatment, many types of nerve conduits are available. In 2006, a research group concluded that treatment with bone marrow cell populations had a positive effect on behavioral outcome and histopathological assessment after SCI, which was most pronounced after MSC injection (Sykova et al., 2006). Therefore, BMSCs were chosen for this study. Generally, the nerve guides are either empty in the inside or filled with some kind of a medium. To the best of our knowledge it has not been tested whether the orientation of nanofibers is important in the performance of a nerve guide. However, in this study random structures were also used to observe the effect of this in the growth and differentiation of cells. There are also studies in the literature about the effect of random and aligned media. But, most of them were focused on the cell viability. Here, effect of random and aligned structures was assessed in terms of differentiation, too.

CHAPTER 2

MATERIALS AND METHODS

2.1. Materials

Poly(3-hydroxybutyrate-*co*-3-hydroxyvalerate) (PHBV5) (with 5% HV), chloroform, 1,1,1,3,3,3-hexafluoroisopropanol (HFIP), collagen Type I, paraformaldehyde (37%), Coomassie Brilliant Blue, N,N,N′,N′-Tetramethylethane-1,2-diamine (TEMED), amphotericin B, sodium cacodylatetrihydrate, FITC-labeled phalloidin, 4,6-diamidino-2-phenylindole dihydrochloride (DAPI), mouse anti-human collagen Type I, and Alexafluor532-conjugated anti-mouse Ig antibody were purchased from Sigma (USA and Germany).

Sodium dihydrogen phosphate (NaH_2PO_4), disodium hydrogen phosphate (Na_2HPO_4), sodium chloride (NaCl), ethanol, acetic acid (HAc), acetone, 1,4-dioxane, and Tween-20 were purchased from Merck Millipore (Germany).

DMEM-High glucose, DMEM-High glucose colorless, fetal bovine serum (FBS), trypsin-EDTA (0.25 %) (HyClone), multicolor broad range protein ladder (Fermentas), and SnakeSkin pleated dialysis tubing were purchased from Thermo Scientific (USA).

Trypan blue (0.4 %) and Alamar blue were from Invitrogen Inc. (USA). New born calf serum was from Lonza (Sweden). NucleoCasette was obtained from ChemoMetec (Denmark). Mesenchymal stem cell neurogenic differentiation medium was purchased from PromoCell (Germany). Rat neuron-specific enolase (NSE) ELISA kit was obtained from Cusabio (China). Collagenase Type I was obtained from GIBCO (USA). Penicillin/streptomycin (Pen/Strep) (100 units/mL - 100 μg/mL), and bovine serum albumin (BSA) were purchased from Fluka (Switzerland). Ammonium persulfate (APS), dimethyl sulfoxide (DMSO) and Triton-X 100 were obtained from AppliChem (Germany). Anti-CD45, Anti-CD90, Anti-Synaptophysin, Anti-Neuron specific beta III tubulin antibody, Anti-Nestin, Anti-Tyrosine hydroxylase, Rabbit IgG (DyLight®488)-Isotype control, Donkey anti-Rabbit IgG H&L (DyLight®488) secondary antibody were purchased from Abcam (USA).

Male Sprague-Dawley rats for rat bone marrow cell isolation were purchased from Kobay Animal Experiments Incorporate (Turkey). Tails of Male Sprague-Dawley rat used in the isolation of collagen type I were kind gifts from GATA Animal Experiments Laboratory (Turkey).

2.2. Methods

2.2.1. Collagen Type I Isolation from Rat Tails

Isolation of type I collagen from rat tails was performed according to the procedure previously described by Kinikoglu et al., 2011. Briefly, rat tails were dissected by making a full incision along the tail skin and stripped away. Removed tendons were placed in a cold acetic acid solution (0.5 M) at 4°C by stirring until totally dissolved. Insoluble fatty tissue was removed by through glass wool. Then the collagen solution was filled into dialysis tubing (15 cm, 10,000 MW cut-off, Thermo Scientific) and dialyzed against a dialysis buffer (5 L, 12.5 mM Na_2HPO_4, 11.5 mM NaH_2PO_4, pH 7.2) at 4ºC to achieve further purification. The solution was then centrifuged (Sigma 3K30, Germany, 16,000 g, 10 min, 4^0C), the white pellet was dissolved in acetic acid (1.5 L, 0.15 M). 75 g NaCl was added to yield a final concentration of 5% (w/v) and incubated overnight at 4°C. Following a second centrifugation step, the pellet was dissolved in acetic acid solution and dialyzed under the same conditions with the first dialysis for 7 days. Second dialysis was followed by a centrifugation step and the resulting pellets were sterilized by storing in 70% (v/v) ethanol at cold room (4ºC) for 2 days, centrifuged again, the pellet was frozen at -80ºC in an Ultra Low Temperature Freezer (Sanyo MDF-U53865, Japan), lyophilized (FreeZone 6, Labconco Co., USA) and stored at 4ºC.

2.2.1.1. Collagen Type I Characterization

Purity of collagen type I was determined by sodium dodecyl sulfate (SDS)-polyacrylamide gel electrophoresis (PAGE). An aliquot (20 µL) of collagen solution (0.2%, w/v in 0.15 M acetic acid) was denatured at 95°C for 3 min in mercaptoethanol, and loaded in SDS-PAGE gels (separating gel- 12% acrylamide/bisacrylamide, and stacking gel- 4% acrylamide/bisacrylamide). Preparation conditions are shown in Table 1. Samples were run at 30 mA for 2.5 h and stained with Coomassie Brilliant Blue (0.2% (w/v)) by incubation overnight and visualized after destaining with Water:Methanol:Acetic acid (4:5:1) solution.

Table 2.1. Composition of SDS-PAGE Gel Solutions

	Separating Gel (12%)	Stacking Gel (4%)
Acrylamide/Bisacrylamide (30%)	2 mL	415 µL
Distilled H_2O	1.65 mL	1.7 mL
1.5 M Tris-HCl pH8.8	1.25 mL	-
0.5 M Tris-HCl pH6.8	-	315 µL
SDS 10 %	50 µL	10 µL
APS	35 µL	10 µL
TEMED	3.5 µL	2.5 µL

2.2.2. Preparation of Scaffolds

2.2.2.1. Preparation of PHBV5 Foams

PHBV5 powder (0.75 g) was dissolved in 6 mL chloroform by warming at 55°C for 10 min. Then 9 mL dioxane was added to obtain 5% PHBV5 (w/v) solution. The solution was poured into a Petri plate and frozen at -80°C (Sanyo MDF-U53865, Japan). The samples were lyophilized (FreeZone 6, Labconco Co., USA) for 8 h and stored in a desiccator at room temperature.

2.2.2.2. Preparation of Foams with Aligned and Random PHBV5/Collagen (2:1) Fibers

A solution of PHBV5/collagen (2:1) (5% (w/v) in HFIP) was prepared, and then transferred into a syringe with a metal needle with a blunt end (22-G x 1.2'', 0.70 mm ID x 32 mm). The syringe was placed in a syringe pump (New Era Pump Systems Inc., UK), and a positive electrode was connected to the tip of the needle (High voltage DC power, Gamma High Voltage Research, USA). The potential was set to 11 kV and the polymer solution was dispensed at a flow rate of 4 µL/min. To obtain aligned fibers, a copper plate with parallel grids and attached to a ground source was used as the collector was previously described (Yucel et al., 2010). Aligned fibers were produced on the PHBV5 foam, when the foam was attached onto the collector. To obtain random fibers, 5% PHBV5 (w/v) foams were placed onto an aluminum foil collector attached to a grounded source and the fibers were collected on the foams (Figure 2.1B). The distance between the collector and the tip of the needle was 11 cm.

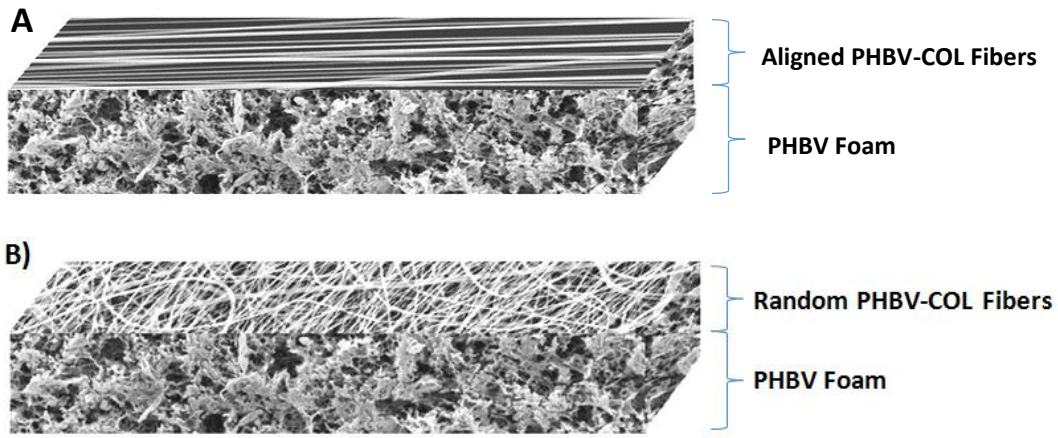

Figure 2.1. Preparation of a bilayer construct. (A) Aligned PHBV5/Collagen fibers on PHBV5 foam, (B) Random PHBV5/Collagen fibers on PHBV5 foam.

2.2.2.3. Preparation of PHBV5/Collagen Foam

A solution of PHBV5/collagen (2:1) (5%, w/v) in HFIP was prepared. The polymer solution was frozen at -80°C, and lyophilized (FreeZone 6, Labconco Co., USA) for 8 h. This foam was then placed on and adhered to a PHBV5 foam by using PHBV5 solution (10%, w/v) as the glue, yielding the foam-foam (fo-fo) construct (Figure 2.2).

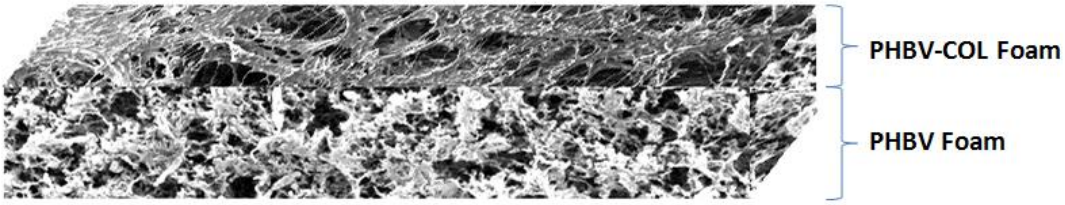

Figure 2.2. Schematic presentation of PHBV/Collagen (2:1) foam placed over PHBV foam.

2.2.2.4. Stabilization of the Scaffolds with Dehydrothermal (DHT) Treatment

Scaffolds were physically crosslinked by dehydrothermal (DHT) treatment. In order to achieve this, the scaffolds were incubated in a vacuum oven (Cole-Parmer, Model 281A, USA) at 150°C for 24 h.

2.2.3. Scaffold Characterization

2.2.3.1. Thickness Measurement

Foam thicknesses, in dry and wet states, were measured using a standard micrometer (Erste Qualitat, Germany) to a sensitivity of 0.1 μm. Five samples were used and at least 3 measurements were done on each sample, and the average was tabulated.

2.2.3.2. Porosity Measurement

Surface porosities of PHBV5 and PHBV5/Collagen (2:1) foams were determined by the NIH image J analysis program (USA) after obtaining micrographs on a stereomicroscope (Nikon SMZ 1900). Four samples were used, in the calculation for each foam type.

2.2.3.3. Pore Size Distribution

Mercury porosimetry (Quantachrome Corporation, Poremaster 60, USA) was used to determine the pore size distribution of the foams.

2.2.3.4. Scanning Electron Microscopy (SEM) Analysis

Scaffolds were coated with gold under vacuum and observed with a scanning electron microscope (SEC, Mini-SEM, South Korea). Some other samples were coated with gold-palladium (Au-Pd) under vacuum and examined with SEMs (Nova, NanoSEM, USA and Quanta 400F Field Emission SEM, Netherlands).

2.2.3.5. Degradation of the Foams

2.2.3.5.1. Degradation with Collagenase

The stability of the PHBV5 based foams against collagenase was studied by gravimetry. The samples were incubated in collagenase type I solution (0.1 mg/mL in PBS, pH 7.4) for 2 h. The samples were washed, dried by lyophilization and weighed to determine the weight loss of the samples.

2.2.3.5.2. Degradation in PBS

To study the degradation behavior in PBS, the scaffolds were weighed to a sensitivity of 0.1 mg and incubated in PBS (10mM, pH 7.4) at 37°C for 4 weeks. Weekly the samples were removed from PBS, rinsed with distilled water 3 times, lyophilized and weighed again. Weight loss was determined weekly for 4 weeks.

2.2.4. *In Vitro* Studies

2.2.4.1. Cell Culture

Rat bone marrow stromal cells (rBMSCs) (passages 1 to 3, P1-3) isolated from rat bone marrows were cultured under standard conditions (37°C, 5% CO_2) until confluency. Cells were passaged once before seeding onto the scaffolds.

2.2.4.1.1. Isolation and culture of rat bone marrow stromal cells (rBMSCs)

Six week old rat was euthanized by ether pads or cotton. Then, the rat was transferred into a betadine: 70% EtOH (1:1) solution. Femurs and tibia were excised aseptically. The bones were transferred into a 50 mL test tube containing harvest medium (DMEM-high glucose tissue culture medium containing penicillin (100 U/mL), streptomycin (100 µg/mL), and 1 µg/mL amphotericin B), the marrow was flushed out with 4 mL primary medium (DMEM-high glucose tissue culture medium). The cell suspension was centrifuged (2500 rpm, 5 min) and the supernatant containing the fatty cells was removed. Then, the pellet was resuspended in primary medium, transferred into T75 flasks, left undisturbed for 2-3 days. The medium in each flask was refreshed every 2 days.

2.2.4.1.2. Characterization of rBMSC

Rat bone marrow stromal cells (rBMSCs) were characterized by using a Flow Cytometry (BD Accuri C6). rBMSCs are positive for CD90, and negative for CD45. After culturing this cells, they were trypsinized, and centrifuged (3000 rpm, 5 min). Pellet was washed with PBS containing 1/100 BSA and 1/1000 sodium azide, centrifuged, the cells were fixed with paraformaldehyde (4%, w/v), and vortexed. After 15 min incubation at room temperature, cells were centrifuged and the pellet was resuspended with PBS. Aliquots (100 µL) of cell suspension were transferred into eppendorf tubes. Then, 2 µL of primary antibodies (1 µg/mL) were added onto each tube. After 30 min incubation at room temperature, cells were washed three times with PBS, and centrifuged (3000 rpm, 5 min). The cells were then incubated in fluorochrome-labeled secondary antibody

solutions (1 μg/mL), Donkey anti-Rabbit IgG H&L (DyLight®488) and the tubes were kept in dark for 30 min. After staining, cells were washed with 1 mL of PBS, centrifuged, and resuspended in 400 μL of PBS. The fluorescent responses were studied under a flow cytometer through three channels: 1) forward scatter channel (FSC), 2) side scatter channel (SSC), 3) fluorescence channel (FL1, emission maximum 488 nm). Data were analyzed with CFlow®Plus software (BD Biosciences, USA) and the forward and side scatter profiles were gated out of debris and dead cells. An isotype control was used in each experiment to calculate specific staining.

2.2.4.2. Sterilization

Scaffolds were sterilized with immersion in 70% (v/v) ethanol for 3 h. During the 3 h, each surface was exposed to UV for 1.5 h. Then, the scaffolds were washed with PBS three times to remove any remnants of ethanol. After washing, they were immersed in DMEM-high glucose tissue culture medium containing penicillin (100 U/mL), streptomycin (100 μg/mL), and 10% FBS overnight to check for signs of contamination of the scaffolds.

2.2.4.3. Cell Seeding

rBMSCs were suspended and diluted to a concentration of 6 x 10^5 cells/mL in DMEM-high glucose tissue culture medium containing penicillin (100 U/mL), streptomycin (100 μg/mL), and 10% FBS. Aliquots (50 μL) of the cell suspension were seeded on scaffolds (150x150x1,7 mm^3) so that a cell density of $3x10^4$ cells/scaffold was achieved. The cell seeded foams were incubated at 37°C and 5% CO_2 for 2 h to ensure attachment of the cells. Then, fresh medium (DMEM containing penicillin (100 U/mL), streptomycin (100 μg/mL), and 10% FBS) was added onto the foams in a 12 well plate, and incubation continued for one week with medium being refreshed every 2 days.

2.2.4.4. Differentiation Medium

Three types of induction protocols were tested to differentiate the BMSCs to neurons. 1) BMSCs were cultured in Neurogenic Differentiation Medium (Promocell, Germany) for 7 days. 2) BMSCs were cultured for 24 h with preinduction (PI) medium containing 10 ng/mL Epidermal Growth Factor (EGF), 10 ng/mL basic Fibroblast Growth Factor (bFGF), and with 2 mM Valproic Acid (VA) in the absence of FCS. Then, culture was continued with neural induction medium supplied with 2 mM VA, 50 ng/mL Insulin-like Growth Factor 1 (IGF1), and 2% B27 in the absence of FCS for 6 days. 3) BMSCs were cultured with PI for 24 h, and then continued culturing with mesenchymal stem cell Neurogenic Differentiation Medium for 6 days. Incubation was continued for one more week with the medium being refreshed every 2 days.

2.2.4.5. Alamar Blue Cell Viability Assay

Alamar Blue is a water soluble dye in oxidized form of and is reduced in the cytosol by mitochondrial enzyme activity by accepting electrons from NADPH, FADH, and NADH (Azbill and Carlson, 1998). This redox reaction results changes in the color of the culture medium from

indigo blue (resazurin) to fluorescent pink (resorufin). The UV-Vis absorbances or fluorescence intensity is measured by an UV-Vis spectrophotometer or a fluorimeter.

Cell seeded and unseeded scaffolds were washed twice with DMEM-high glucose colorless tissue culture medium, and incubated in Alamar Blue solution (1 mL 10% in DMEM-high glucose colorless supplemented with penicillin (100 U/mL), streptomycin (100 µg/mL), amphotericin B (250 µg/mL)) at 37°C for 1 h. The supernatant (200 µL) was transferred into 96 well plates, and the absorbances at 570 and 595 nm were measured. Reductions were calculated as follows (Invitrogen Inc., USA)

$$\text{Percent Reduction (\%)} = \frac{\left((\varepsilon_{ox})_{\lambda_2} \text{x } A_{\lambda_1}\right) - \left((\varepsilon_{ox})_{\lambda_1} x\, A_{\lambda_2}\right)}{\left((\varepsilon_{red})_{\lambda_1} \text{x } A'_{\lambda_2}\right) - \left((\varepsilon_{red})_{\lambda_2} x\, A'_{\lambda_1}\right)} x\, 100$$

λ_1= 570 nm λ_2 = 595 nm

$(\varepsilon_{ox})_{\lambda_1}$ = 117.216 $(\varepsilon_{red})_{\lambda_1}$ = 155.677

$(\varepsilon_{ox})_{\lambda_1}$= 80.586 $(\varepsilon_{red})_{\lambda_2}$= 14.652 where,

A_{λ_1}= Absorbance of the test well, at λ_1= 570 nm

A_{λ_2}= Absorbance of the test well, at λ_2 = 595 nm

A'_{λ_1}= Absorbance of the negative control (blank), at λ_1= 570 nm and

A'_{λ_1}= Absorbance of the negative control, at λ_2 = 595 nm.

A calibration curve was constructed using known concentrations of cells (rBMSCs) to relate the cell numbers to the dye reduction (%).

2.2.4.6. Microscopy of the Tissue Engineered Construct

2.2.4.6.1. Fluorescence Microscopy

In order to observe the cell morphology and distribution on the scaffolds, the cytoskeletons of the cells were stained with Alexa 532-labeled phalloidin (red) and their nuclei with DAPI (blue) on days 1, 4 and 7 in the culture medium for all the three types of scaffolds. The cell seeded 3D scaffolds were washed with PBS (10 mM, pH 7.4), fixed with 4% (w/v) paraformaldehyde at room temperature for 15 min, and treated with Triton X100 (0.1% v/v in 10 mM Tris-HCl buffer) at room temperature for 5 min in order to permeabilize the cell membrane. After each step, the constructs were washed with PBS to remove any remnants of the treatment solutions. The samples were then incubated in BSA (1% w/v in PBS) at 37 °C for 30 min to prevent nonspecific binding

of the dyes. Scaffolds were kept in Alexa 532-labeled phalloidin (0.5 μg/mL in 0.1% BSA in PBS) at 37°C for 1 h, washed with 0.1 % BSA (in PBS), and incubated in DAPI (1/5000 dilution in PBS) at room temperature for 10 min. After a washing step with PBS, the constructs were studied with a fluorescence microscope (Olympus IX70, Japan).

2.2.4.6.2. SEM

Cell seeded scaffolds were removed from cell culture medium, washed twice with PBS, and then with cacodylate buffer (0.1 M sodium cacodylate, pH 7.4), and incubated in glutaraldehyde (2.5%, v/v in cacodylate buffer) at room temperature for 2 h. After washing with cacodylate buffer, the scaffolds were freeze dried for 2-3 h, and examined by SEM.

2.2.5. Differentiation Studies

2.2.5.1. Flow Cytometry Analysis

Neuronal specific markers such as anti-synaptophysin, anti-neuron specific beta III tubulin, anti-nestin, anti-thyrosine hydroxylase were checked by using flow cytometer (BD Accuri C6). First, the cells were trypsinized, and centrifuged (3000 rpm, 5 min). Pellet was washed with PBS containing 1/100 BSA and 1/1000 sodium azide, and centrifuged again. Paraformaldehyde (100 μL, 4% (w/v)) was added to provide fixation, and this cell suspension was vortexed. After 15 min incubation at room temperature, cells were centrifuged. Then, pellet was resuspended with PBS. Cell suspension was seperated into eppendorfs as 100 μL in each. Antibodies were prepared as 1 μg/mL, 2 μL of them put into eppendorfs. After 30 min incubation at room temperature, cells were washed three times with PBS, and centrifuged (3000 rpm, 5 min). Fluorochrome labeled secondary antibody (Donkey anti-Rabbit IgG H&L (DyLight®488) secondary antibody) was prepared (1 μg/mL) and then the cells were resuspended in this solution, and the samples were incubated in the dark for 30 min. After the staining was completed, cells were washed with 1 mL of PBS, and centrifuged. Then, cells were resuspended in 400 μL of PBS, examined with flow cytometer through three channels: 1) forward scatter channel (FSC), 2) size scatter channel (SSC), 3) fluorescence channel (FL1 filter, laser 488 nm). Data were analyzed with CFlow®Plus software (BD Biosciences, USA) and the forward and side scatter profiles were gated out of debris and dead cells. An isotype control was used in each experiment to calculate specific staining.

2.2.5.2. Neuron Specific Enolase (NSE) Kit

Cells were rinsed with (10 mM) PBS, homogenized in 1 mL of 1x PBS and incubated overnight at -20° C. After two freeze-thaw cycles to break the cell membranes, the homogenates were centrifuged (5000 g, 5 min, 4°C). The supernatant was used as sample. Fresh standards were prepared. Standard and sample solutions (100 μL) were added into each well. The wells were covered with the adhesive strip, and incubated for 2 h at 37°C. Then, the liquid portions of the suspension in the wells were removed. Biotin-antibody solution (1x, 100 μL) was added into each well, and the wells were covered with a new adhesive strip. The plates were incubated for 1 h at 37°C. Each well was aspirated and washed three times with wash buffer (200 μL). HRP-avidin solution (1x, 100 μL) was added into each well, and the microtiter plate was covered with a new adhesive strip and incubated for 1 h at 37°C. Wells were washed five times with wash buffer.

TMB Substrate (90 μL) was added into each well, and incubation for 15-30 minutes at 37°C was performed in the dark. Stop solution (50 μL) was added to each well, and the plate was tapped to ensure thorough mixing. Absorbances were measured using at 450 nm, 570 nm and 595 nm an Elisa plate reader (Molecular Devices, USA).

2.2.5.3. Immunohistochemistry

The scaffolds were fixed with 4% paraformaldehyde for 15 min. Then they were incubated in the blocking solution (1% BSA, 10% goat serum, 0.1% Tween 20 and 0.3 M glycine in PBS). Anti-nestin and anti-thyrosine hyroxylase antibodies (1:20 and 1:100 dilution in 0.1% PBS/BSA solution, respectively) was then added onto the specimens and incubated overnight at 4 °C. Anti-beta III tubulin and anti-synaptopysin antibodies (1:20 and 1:250 dilution in 0.1% PBS/BSA solution, respectively) was also added onto the another set of specimens and incubated overnight at 4 °C After washing with 0.1% PBS-BSA solution they were incubated in both Alexafluor 488-labelled Anti-mouse antibody produced in goat (1:100 dilution in 0.1% BSA-PBS) and Alexafluor 647-labelled Anti-rabbit antibody produced in donkey (1:100 dilution in 0.1% BSA-PBS) at 37 °C for 1 hour and then washed with 0.1% PBS-BSA solution. Samples were observed using confocal laser scanning microscope (Zeiss LSM 9100, Germany) between 495-530 nm with 488 nm Argon laser for cytoskeleton, between 540-630 nm with 532 nm Argon laser for deposited collagen, and between 645-800 nm with 647 nm Argon laser for cytoskeleton.

2.3. Statistical Analysis

Statistical analyses were performed using a Student's t-test with a minimum confidence level of 95%, p values smaller or equal to 0.05 were considered statistically significant. All values were reported as the mean ± standard deviation of the mean (s.d.m).

CHAPTER 3

RESULTS AND DISCUSSION

3.1. Characterization of the Collagen Type I

The purity of the collagen isolated from Sprague-Dawley rat tails was characterized with SDS-PAGE. The results are shown in Figure 3.1. Lane one contains isolated type I collagen (0.5%, w/v), Lane two contains isolated type I collagen (0.75%, w/v), Lane three contains commercial type I collagen (Sigma-Aldrich), and the lane four contains protein ladder (Fermentas).

Figure 3.1, two doublet bands were seen in both I and II. One was observed around 260 kDa and the other around 135 kDa, the same pattern as in commercial collagen type I. This shows that isolated collagen is also collagen type I, and since there were no other bands on the gel, the collagen is pure.

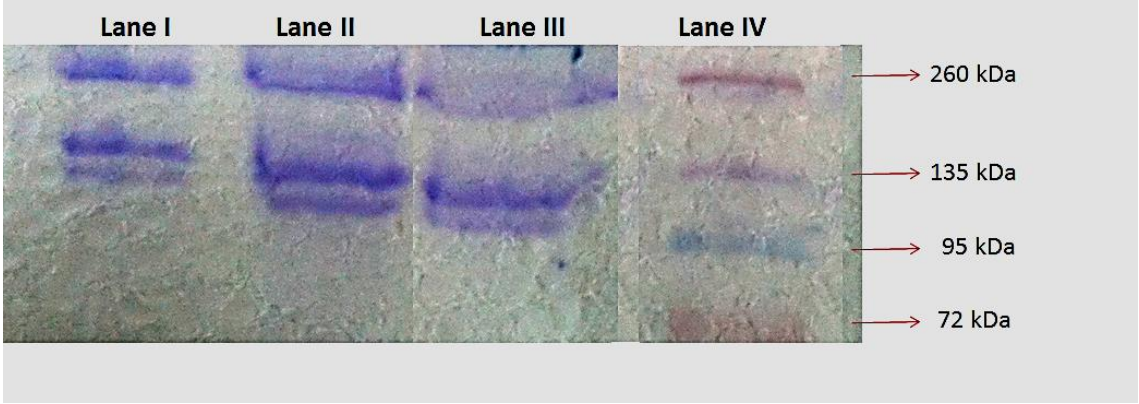

Figure 3.1. SDS-PAGE for comparison of collagen isolated from Sprague-Dawley rat tails and the commercial Type I collagen. Lanes represent: (I) isolated collagen (0.5%, w/v), (II) isolated collagen (0.75%, w/v), (III) commercial type I collagen (Sigma-Aldrich) (IV) protein ladder (Fermentas).

3.2. Characterization of Scaffolds

3.2.1 Characterization of PHBV5 Foam

The structure of the foams was examined a scanning electron microscope (SEM) (Figure 3.2.). The micrographs showed that the foams had high porosity and interconnectivity. The surface of the PHBV5 foam appeared very homogeneous in terms of pore size distribution (Figure 3.2A).

The inner structure of the foam also was homogeneous in terms of pore size distribution (Figure 3.2B). The cross section of the PHBV5 foam also showed that every part of the PHBV5 foam had homogeneous pore size, porosity, and interconnectivity (Figure 3.2C).

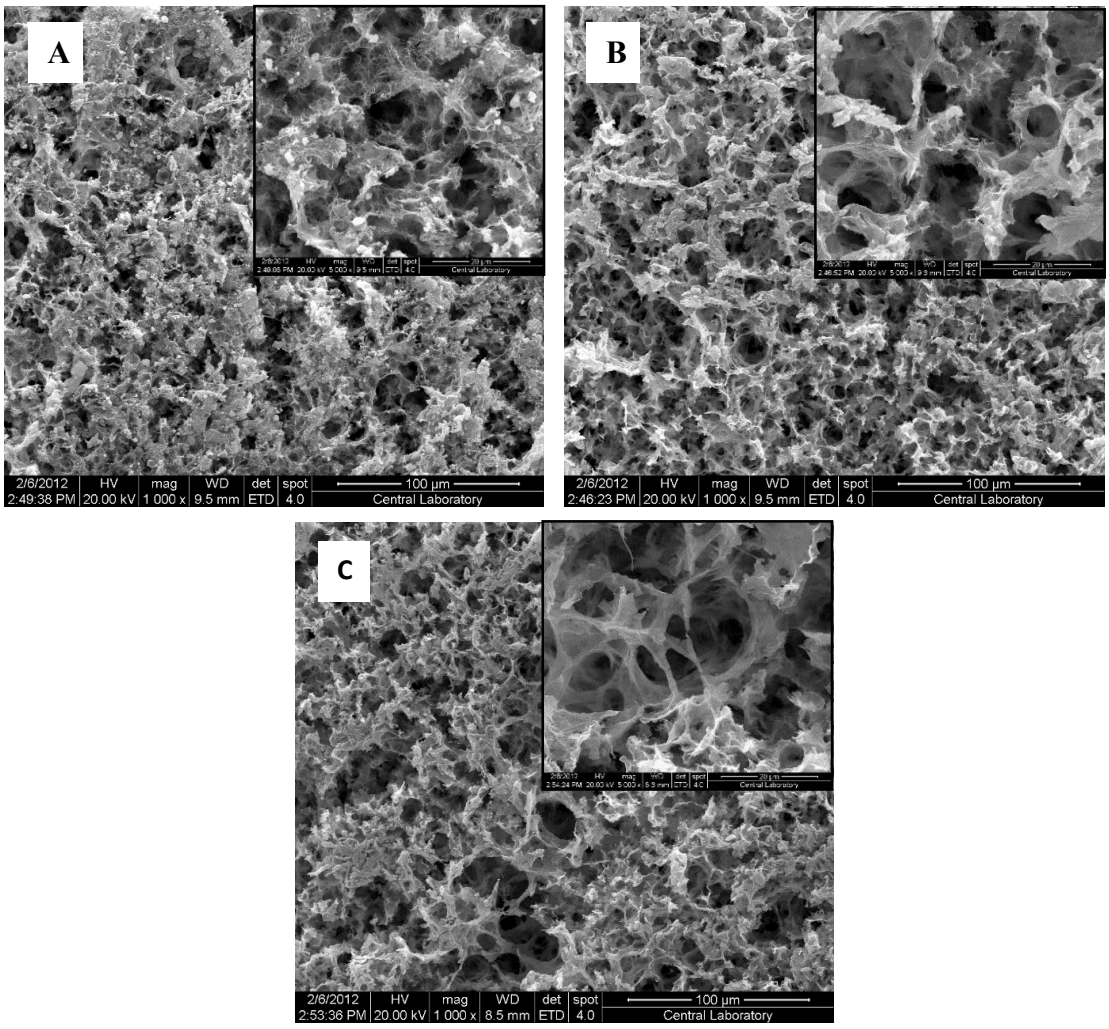

Figure 3.2. SEM of PHBV5 foam. (A) surface (x1000), (B) horizontal section (x1000), and (C) cross section (x1000). (inset: x5000 of (A), (B), and (C)).

Table 3.1. shows the pore size of the different parts of the PHBV5 foam. As seen in Figure 3.2., pore sizes of the surface, horizontal section, and the cross section of PHBV5 foam were analyzed with NIH ImageJ program. According to these results, surface of foam has the smallest pores. Horizontal section has almost the twice bigger pore sizes than the pores on the surface. Furthermore, cross section of the foam has the highest pore size.

Table 3.1. Pore size of PHBV5 foam by Image J analysis

Type	Pore Size (µm)
Surface of PHBV5 foam	18 ± 6
Horizontal section of PHBV5 foam	35 ± 8
Cross section of PHBV5 foam	43 ± 7

3.2.1.1. Porosity and Pore Size Distribution of the PHBV5 Foam

Interconnected porous structures provide a good environment for cell ingrowth, vascularization, and nutrient diffusion, which are critical for cell survival. Porosity, pore size distribution and the average pore dimension of scaffolds are very important in cell migration, nutrient penetration and waste removal. In general, scaffolds with high porosity and interconnectivity have a low polymer fraction and high surface area for cell attachment and tissue ingrowth (Griffon et al, 2006).

Porosity and pore size distribution of the PHBV5 foams was studied with mercury porosimetry which revealed that the foam had 85% porosity. Pore diameter ranged from 5 to 200 µm (Figure 3.4.) with most of the pore sizes being in the range 5-20 µm. The optimum pore size recommended for proper neovascularization is 5 µm (Dehghani et al, 2011). Cells require large pores to adhere to and populate, while they need the small pores (ca. 10-20 µm) for interconnectivity and material transport. Therefore, this pore size profile of PHBV5 foam is very suitable for nerve tissue engineering applications.

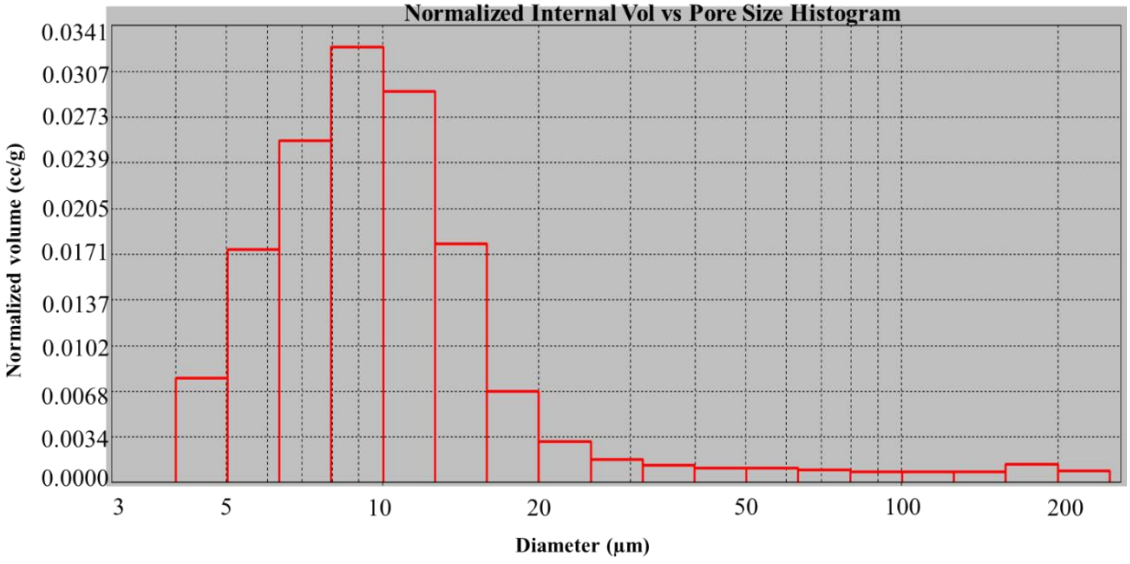

Figure 3.3. Pore size distribution of PHBV5 foam.

3.2.2. Characterization of Aligned and Random PHBV5/Collagen (2:1) Fibers

Electrospun fibers are widely used in regenerative medicine, because nanofibrous structures developed by electrospinning technology carry some of the properties of the extracellular matrix suitable for the anchorage, migration, and differentiation of cells (Shin et al, 2012). Nano and micro fibers have large surface area-to-volume ratio, high porosity, and easily processed into a variety of sizes and shapes, and their composition can be modified to match the properties and functionality of the desired tissue engineering products (Huang et al, 2003). Electrospun collagen fibers have other important properties: they transmit force, dissipate energy, prevent premature mechanical failure, have high water affinity, low antigenicity (Kolacna et al, 2007).

Figure 3.4 shows the SEM of aligned PHBV5/Collagen (2:1) fibers. Alignment of these fibers was assessed with NIH ImageJ program. The porosity of the aligned fiber mats was 65%. The fiber diameter was calculated to be in the range 200-650 nm. No beads were observed. Average deviation angle of the fibers was 46.9 ± 7.3 (mean ± s.d.m). Even though most of the fibers are aligned in the direction of the arrow, the large deviation angle is a result of the presence of some fibers that are almost perpendicular to the main axis.

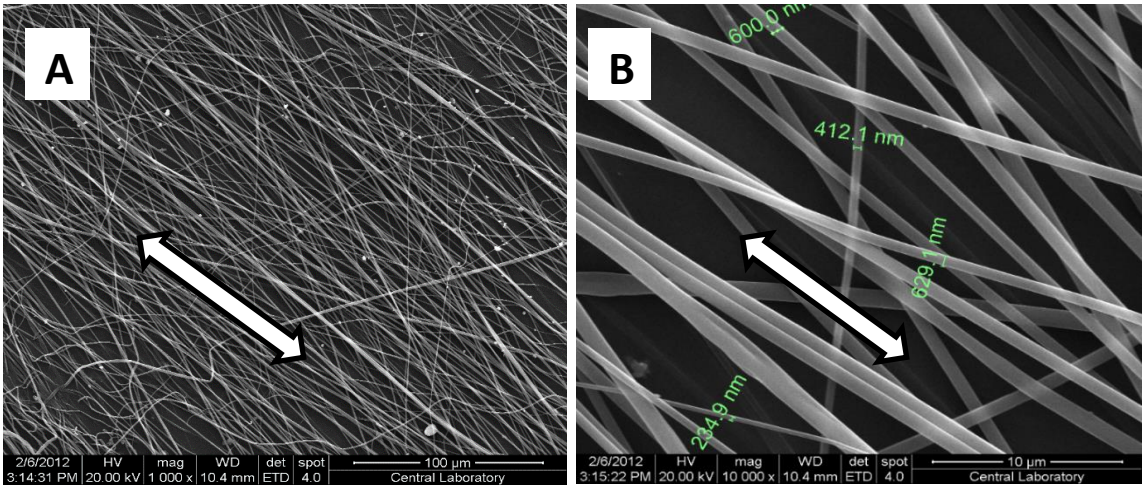

Figure 3.4. Scanning electron micrographs of aligned fibers (A) x1000, (B) x10000. Arrow shows the alignment direction.

Figure 3.5 shows the nonoriented, random PHBV5/Collagen (2:1) fibers, the porosity of which was calculated to be less than that of the aligned fibers (59.7%). This porosity is still very suitable for cell growth.

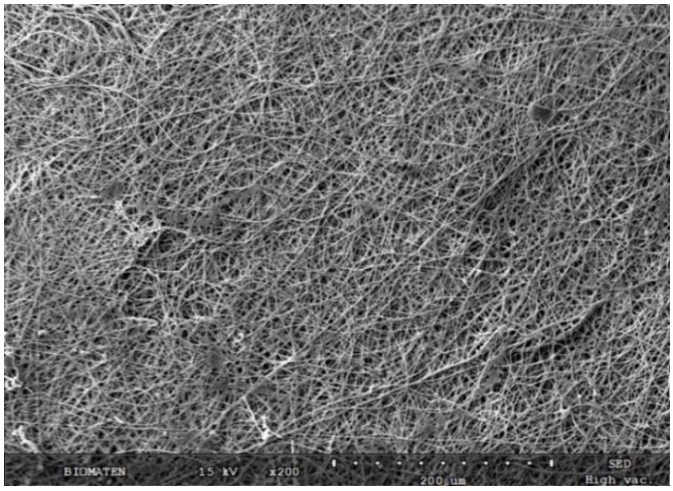

Figure 3.5. SEM of random fibers (x200).

3.2.3. Characterization of PHBV5/Collagen (2:1) Foam

The bottom part of the Fo-Fo scaffold was of PHBV5 while the upper part was composed of PHBV5/Collagen (2:1) foam. The structure of the PHBV5/Collagen (2:1) foam was examined under SEM. When these figures were examined, it can be observed that the pore size range was between 40-300 µm.

Figure 3.6A and C shows the pore sizes of PHBV5/Collagen (2:1) foam, which is between 90-300 µm. Recommended range for scaffold pore size is 100-200 µm, but amount of pores which has size of greater than 200 µm was very less in this foam. Therefore, it provided very good attachment and growth site for the cells. Interconnectivity of the pores is one of the crucial requirements of a tissue engineering construct especially for proper material transfer and cell ingrowth. Figure 3.6B shows the interconnectivity of the pores very well.

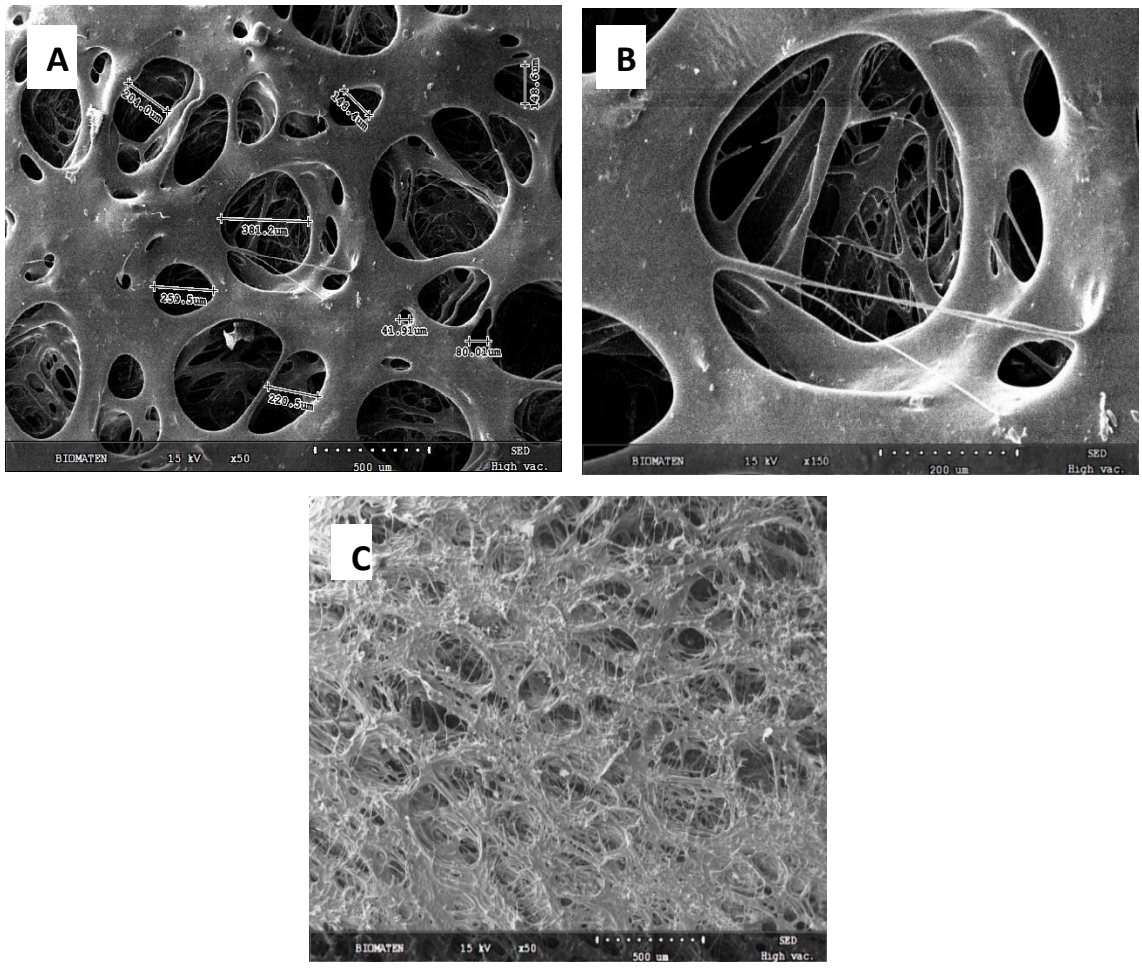

Figure 3.6. SEM of the upper part (A) x50, (B) x150, and the bottom part (C) x50 of PHBV5/Collagen (2:1) foam.

Figure 3.7 shows the schematic representation of the all three types of scaffolds. All of them have a PHBV5 foam at their bottom, but their upper layers were different from each other. In Figure 3.7A, upper layer was composed of aligned PHBV5-collagen (2:1) fibers. Second type of scaffold had a random PHBV5-collagen (2:1) fibers (Figure 3.7B). Final scaffold had PHBV5-collagen (2:1) foam on the upper layer as it was shown in Figure 3.7C.

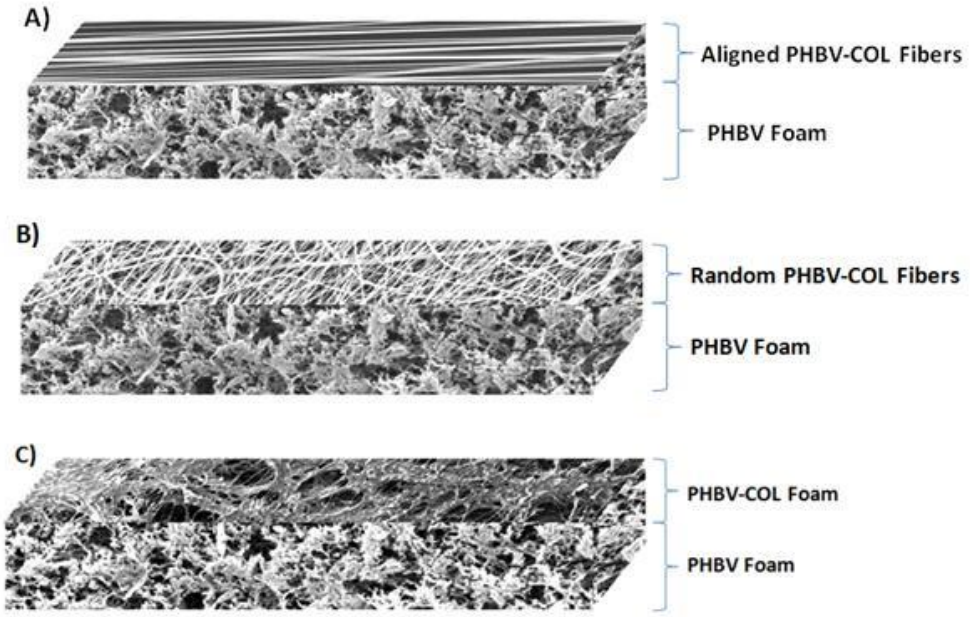

Figure 3.7. Schematic presentation of the three types of 3D scaffolds (A) Aligned PHBV5/Collagen fibers on PHBV5 foam, (B) Random PHBV5/Collagen fibers on PHBV5 foam, (C) PHBV/Collagen (2:1) over PHBV foam.

3.2.4. Examination of the 3D constructs

3.2.4.1. Thickness of Scaffolds

The Fo-Fi and Fo-Fo constructs were prepared by the procedures explained in sections 2.2.2.2 and 2.2.2.4 respectively. The thicknesses of these scaffolds were measured in both dry and wet form. Moreover, the thickness of scaffolds with and without crosslinking was recorded to observe the effect of DHT treatment on foam thickness. All thickness measurements were carried out by the method in section 2.2.3.1, and are presented in Table 3.2.

When dry and wet state of AF-Fo and RF-Fo were compared, it can be said that scaffolds did not show any swelling. Since most of their structure is composed of PHBV5 foam (Fo) layer, and PHBV is a very hydrophobic polymer, and does not absorb water, so this result was expected. For both of these scaffolds, collagen was found only in the fiber part which forms only the minor part of the scaffold. However, in Fo-Fo construct, some swelling (5%) was observed because of the collagen content of the top layer. It was also concluded from these studies that there was no effect of DHT on the thickness of Fo-Fo type of scaffolds, but a 4% and 6% decrease was recorded for AF-Fo and RF-Fo type of constructs, respectively.

Table 3.2. Thickness of Scaffolds

	Thickness of Foams (µm)		
	Before DHT (dry)	**Before DHT (wet)**	**After DHT (dry)**
AF-Fo	1703 ± 25	1708 ± 23	1630 ± 6
RF-Fo	1724 ± 20	1722 ±10	1624 ± 6
Fo-Fo	1780 ± 9	1869 ± 17	1780 ± 16

3.2.4.2. Degradation of Scaffolds

In tissue engineering, biodegradable scaffolds are preferred because in the tissue construction process first the cells are grown on porous structures, then they penetrate the structure and finally the polymer starts to degrade creating more space for cell growth within the structure. Meanwhile, cells deposit new extracellular matrix (ECM) products that occupy the space resulting from the degradation of the polymer. Eventually the scaffold completely disappears. ECM deposition rate should match the scaffold degradation rate for proper healing. Thus, the degradation time should be optimized according to the tissue studied, because the required time may differ from tissue to tissue. In this study, both PHBV, a synthetic polymer, and collagen, a natural polymer, were biodegradable. In addition, collagen was water soluble, therefore crosslinking was needed to prevent its rapid removal by dissolution and degradation. Among the crosslinking methods available, dehydrothermal (DHT) treatment was choosen, because it is a physical crosslinking method, which does not require aqueous solutions to achieve its goal (as in EDC/NHS process) nor it has the risk of leaving remnants of toxic chemicals. DHT treatment was performed as explained in section 2.2.2.5. After DHT, scaffolds were examined under SEM and observed that both fiber and foam structures did not lose their original appearance (Figure 3.8).

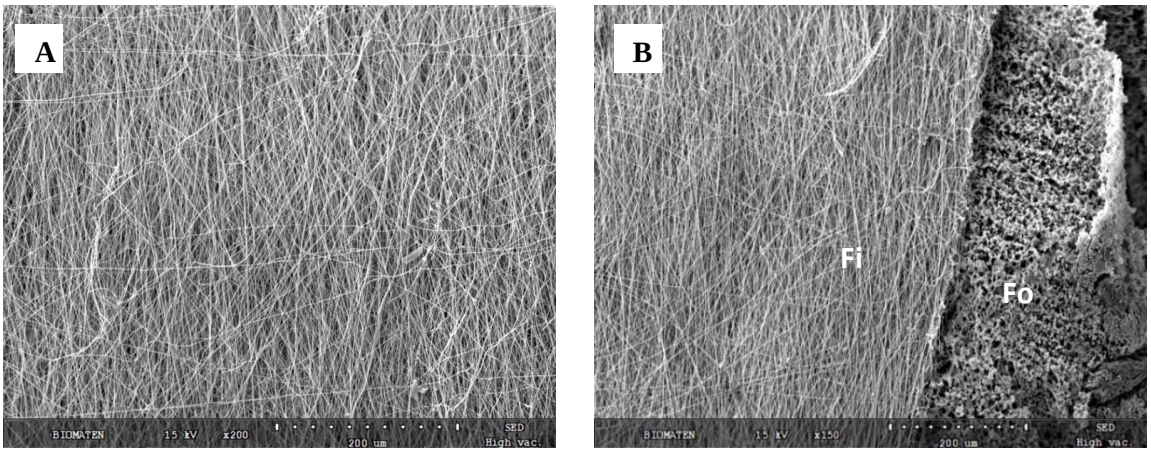

Figure 3.8. SEM of the scaffolds after dehydrothermal treatment (A) Before DHT (x200), (B) After DHT (x150).

3.2.4.2.1. Degradation with Collagenase

Collagen was used as fiber and as foam in the upper layer of the scaffolds, and therefore, its stability had to be studied before using this scaffold in tissue culture. The stability of the collagen based scaffolds was tested according to the literature (Gibson et al., 2004) by treating the samples at 37^0C with collagenase (0.1mg/mL) type II activity for 2 h. Incubation in PBS (10 mM) was used for comparison (Table 3.3). Highest weight lost with collagenase was observed in the Fo-Fo construct. This was not unexpected. Interestingly, the degradation of the crosslinked scaffold was higher. But, still the loss was not significant. The reason for this low loss is because collagen constituted only the 33% of the upper layer of the scaffolds, and also it was blended with PHBV5. Because it was in less amount in the construct and due to blending with PHBV5 low weight loss was observed. The other observation is that in equal period the loss of weight was much lower (almost negligible) in PBS. Since there was no enzymatic activity, this was an expected result.

Table 3.3. Degradation of the fibers, foams and 3D construct in collagenase type II (at 37^0C, 2 h) and in PBS (pH 7.4, 10 mM).

	Weight Loss (%)	
Scaffold Type	**Collagenase (0.1 mg/mL)**	***PBS (pH 7.4, 10 mM)**
Crosslinked PHBV5/collagen (2:1) aligned fiber on 5% PHBV5 foam (AF-Fo, DHT)	1.3 ± 0.2	0.5 ± 0.2
Uncrosslinked PHBV5/collagen (2:1) aligned fiber on 5% PHBV5 foam (AF-Fo)	1.2 ± 0.1	0.3 ± 0.1
Crosslinked PHBV5/collagen (2:1) random fiber on 5% PHBV5 foam (RF-Fo, DHT)	0.4 ± 0.1	0.2 ± 0.1
Uncrosslinked PHBV5/collagen (2:1) random fiber on 5% PHBV5 foam (RF-Fo)	0.8 ± 0.4	0.6 ± 0.3
Crosslinked PHBV5/collagen (2:1) foam on 5% PHBV5 foam (Fo-Fo, DHT)	7 ± 0.6	3 ± 0.4
Uncrosslinked PHBV5/collagen (2:1) foam on 5% PHBV5 foam (Fo-Fo)	4 ± 0.9	2 ± 0.5

*Control samples are treated with PBS (pH 7.4, 10 mM).

3.2.4.2.2. Degradation in PBS

Besides degradation test in collagenase type II and PBS in 2 h, the stability of foams was tested in PBS (pH 7.4, 10 mM) for a much longer period, 28 days. For the fiber containing (and therefore low collagen carrying) scaffolds, AF-Fo and RF-Fo, no degradation was observed in both DHT crosslinked and uncrosslinked scaffolds for 28 days. However, in the Fo-Fo constructs a total of 15.8% weight loss in four weeks was observed in uncrosslinked samples (Table 3.4). Like in the collagenase degradation results, crosslinked scaffolds (Fo-Fo, DHT) lost significantly more weight (87.2%). By day 14, most of the crosslinked scaffolds was degraded. The unexpected stability of the uncrosslinked samples, or conversely unexpected instability of the crosslinked samples led us to believe that DHT treatment procedure (150 °C for 24 h) might have caused a physical or chemical damage to the scaffold structure, and therefore, they were degraded earlier than the uncrosslinked ones. It could therefore be said that the dehydrothermal crosslinking approach was not a suitable method for these scaffolds, and therefore, it was decided that no crosslinking was needed for these scaffolds. In the rest of the study no crosslinking was done.

Table 3.4. Scaffold degradation in PBS (pH 7.4, 10 mM)

Weight Loss (%)			
	Treatment Period (days)		
Scaffold type	7	14	28
Crosslinked PHBV5/collagen (2:1) foam on 5% PHBV5 foam (Fo-Fo, DHT)	12.6 ± 1.8	81.1 ± 3.2	87.2 ± 2.7
Uncrosslinked PHBV5/collagen (2:1) foam on 5% PHBV5 foam (Fo-Fo)	5.9 ± 1.2	8.1 ± 1.6	15.8 ± 2.4

3.3. *In vitro* Studies

3.3.1. Characterization of Rat Bone Marrow Stromal Cell (rBMSC)

Characterization of the isolated cells from rat bone marrow (rBMSCs) was done with flow cytometry. Anti-CD90 antibody was used as the positive control, anti-CD45 and anti-CD11b antibodies which are cell surface markers associated with lymphohematopoietic cells were used as the negative control for rBMSCs. Both rabbit and mouse isotype controls were used.

In Figure 3.9A., fluorescence intensity of control groups (No primary Ab, Rabbit isotype, and unstained) are seen. The fluorescence intensity was low as expected and very close to each other. It means that these groups could be used as control groups. Figure 3.9B shows the fluorescence intensity of both controls and samples. As can be seen from this figure, anti-CD90 gave a significant peak with high (10^5) fluorescence intensity, and its peak can easily be

differentiated from the controls with a lower (10^3) fluorescence intensity. Anti-CD45 and anti-CD11b gave a peak as low as the controls, which shows that isolated MSCs do not contain any of the blood cell phenotype.

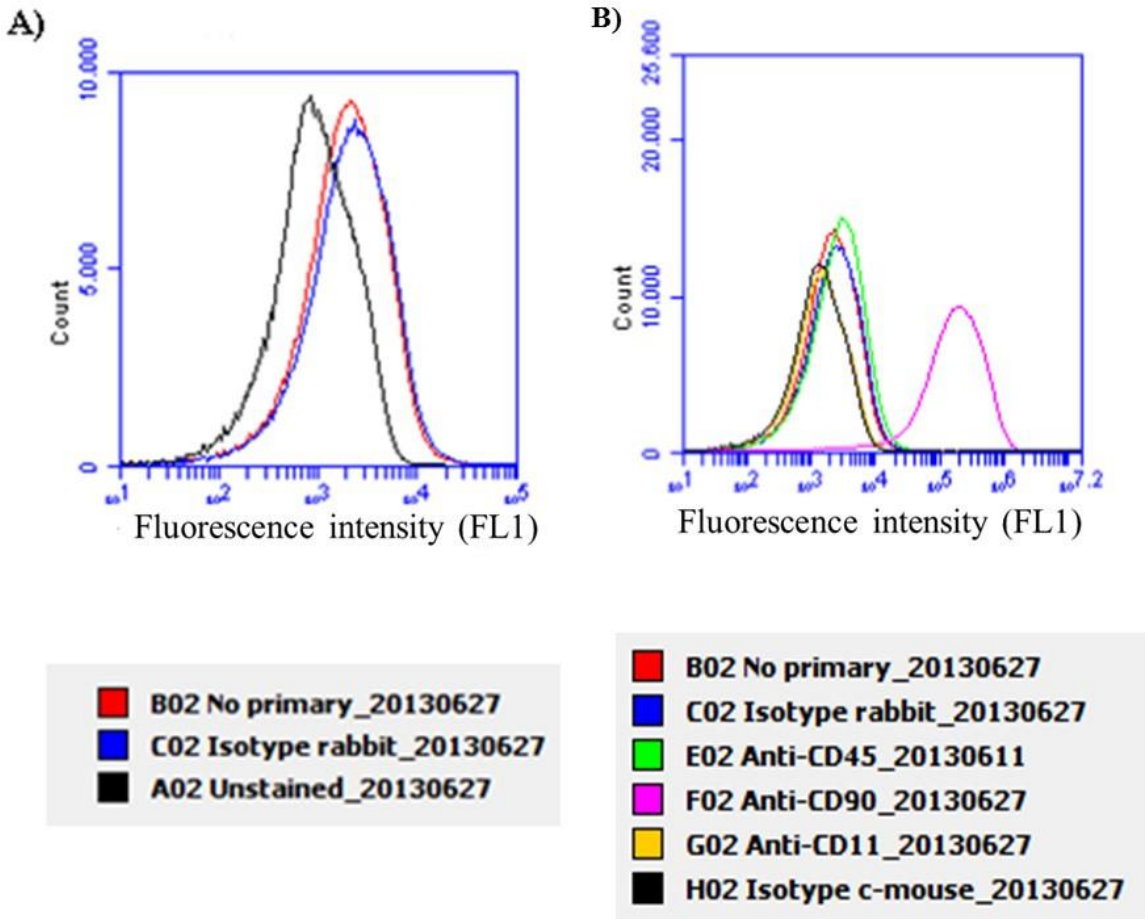

Figure 3.9. Flow cytometry analysis of rBMSC P2 after incubation in DMEM-high glucose tissue culture medium containing penicillin (100 U/mL), streptomycin (100 µg/mL). (A) Fluorescence intensity of controls, and (B) the samples, CD90, CD45, and CD11b.

Figure 3.10. shows the dot plots of different types of antibody mix. In both Anti-CD90/Anti-CD11b, and Anti-CD90/Anti-CD45 mix, there were cells in the upper left (UL) of the quadrants, which means that cells were CD90 positive (MSC marker). In these mixes, cells were negative for both CD45 and CD11b.

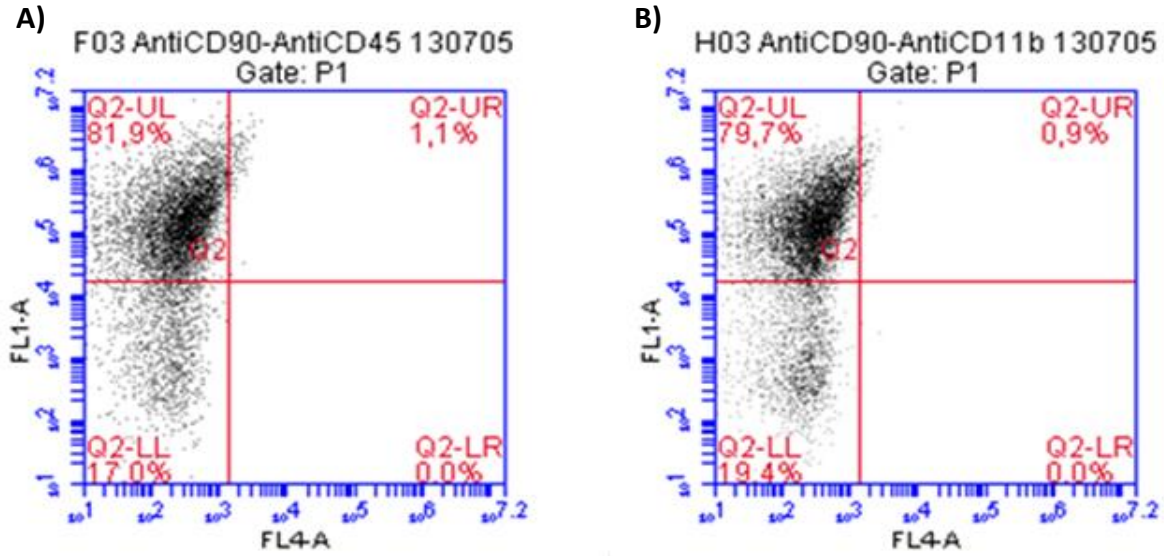

Figure 3.10. Dot plots of different types of antibodies in rBMSCs Passage 2 culture. (A) Anti-CD90/Anti-CD11b mix, (B) Anti-CD90/Anti-CD45 mix.

3.3.2. Cell Attachment and Proliferation on Scaffolds

To examine the cell attachment and proliferation, the scaffolds were seeded with rat bone marrow stromal cells (rBMSCs). Cell seeding to Fo-Fo type of scaffold was not successful due to high pore size. Therefore, cells were seeded on AF-Fo and RF-Fo scaffolds. The results at the end of 1, 4 and 7 days of culture using Alamar blue assay are presented in Figure 3.11. The calibration curve for to convert absorbances to cell numbers is presented in Figure A.1 in Appendix A. The cell number in the first day of incubation shows the cell attachment to the scaffolds. The number of rBMSCs attached to the composite scaffolds were similar to each other, and efficiency was high in both. The increase in the cell number in the next three days was not high; this is understandable because the population doubling time (PDT) of BMSCs is reported to be 4 days in the literature (Simpson et al., 2012). Still, the increase in the cell numbers was higher in the RF-Fo than AF-Fo. By day 7, the increase had continued but difference had become more apparent. Since the difference between these samples is that in AF the microfibers were aligned and in RF they were random it can be concluded that increase in cell number was higher in the random fiber structure than the aligned fiber. Ramakrishna et al. (2009) found a similar result when Schwann cells were

seeded on aligned and random polycaprolactone/gelatin (PCL/gelatin) fibers. They explained this by stating that the random fibers contained more interconnected pores, and gaps. Also rough surfaces assist adhesion and proliferation of cells and random surfaces are more irregular and thus be considered rougher (Wang et al., 2004). In another study (Shin et al., 2004), it was also found that collagen deposition by human ligament fibroblast (HLF) cells was higher on polyurethane (PU) random fibers than it was on the aligned ones. The collagen deposition was not checked in the present study, but if it were than it is highly likely that more cells would have secreted more collagen.

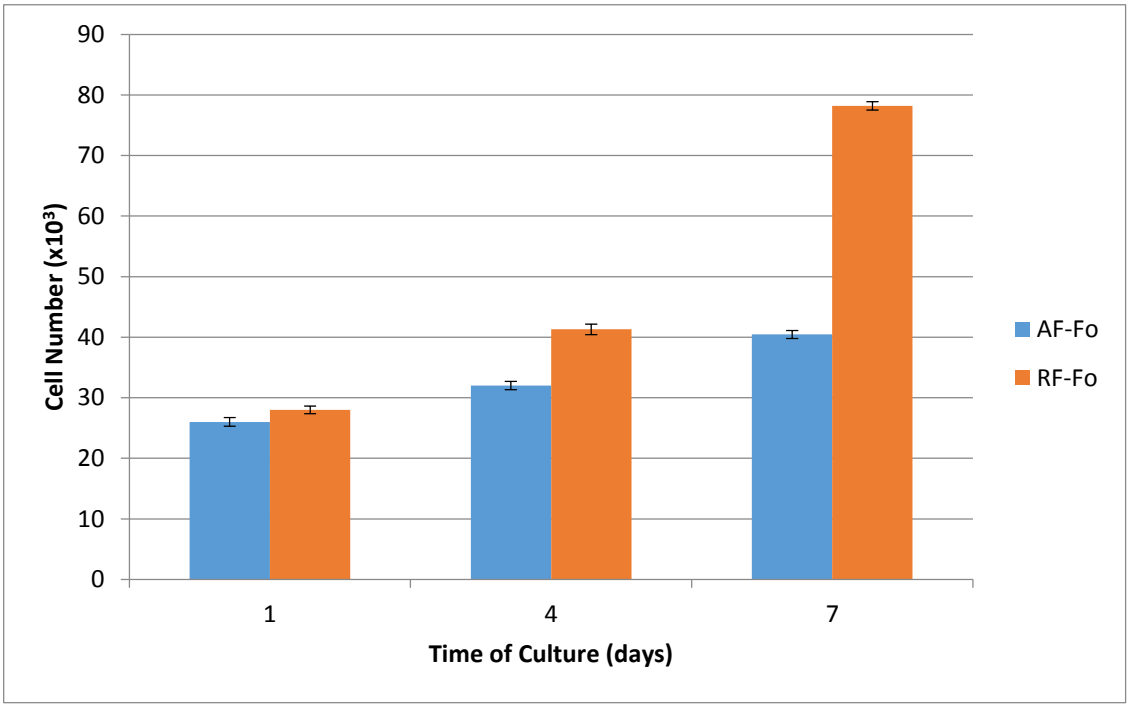

Figure 3.11. Cell proliferation profile of rat bone marrow stromal cells (rBMSCs) on bilayer AF-Fo, and RF-Fo scaffolds. Cell seeding density was $3x10^4$ in neuronal differentiation medium.

3.3.3. Microscopy of Tissue Engineered Construct

3.3.3.1. Fluorescence Microscopy

The attachment of cells to the scaffolds was determined by counting the cell numbers (Figure 3.11). It is also important to observe the cell morphology and distribution on the scaffolds before drawing a conclusion about quality of adhesion. In order to achieve that the cytoskeleton of the rBMSCs were stained with Alexa 532-labeled phalloidin (red) and their nuclei with DAPI (blue) on Days 1, 4 and 7 in the culture medium for both the aligned fiber-foam (AF-Fo) and random fiber-foam (RF-Fo) constructs (Figures 3.12-3.17).

On Day 1, the cells on AF-Fo type of construct did not seem to have attached to the scaffolds with a specific orientation; in other words there was no alignment (Figure 3.12). Some micrographs were not sharp because scaffold was not flat, therefore, it was not possible to keep the whole sample in focus. On Day 4, morphology of the cells was not different than on Day 1 (Figure 3.13). At the end of one week, morphology of the cells looked same with the day 4 staining. On the other hand, the cells on the RF-Fo construct have more elliptical cytoplasm than the cells on the AF-Fo constructs. Although the staining procedure was the same for AF-Fo and RF-Fo samples, better images were obtained with the AF-Fo type of scaffold probably due to their staying more flat.

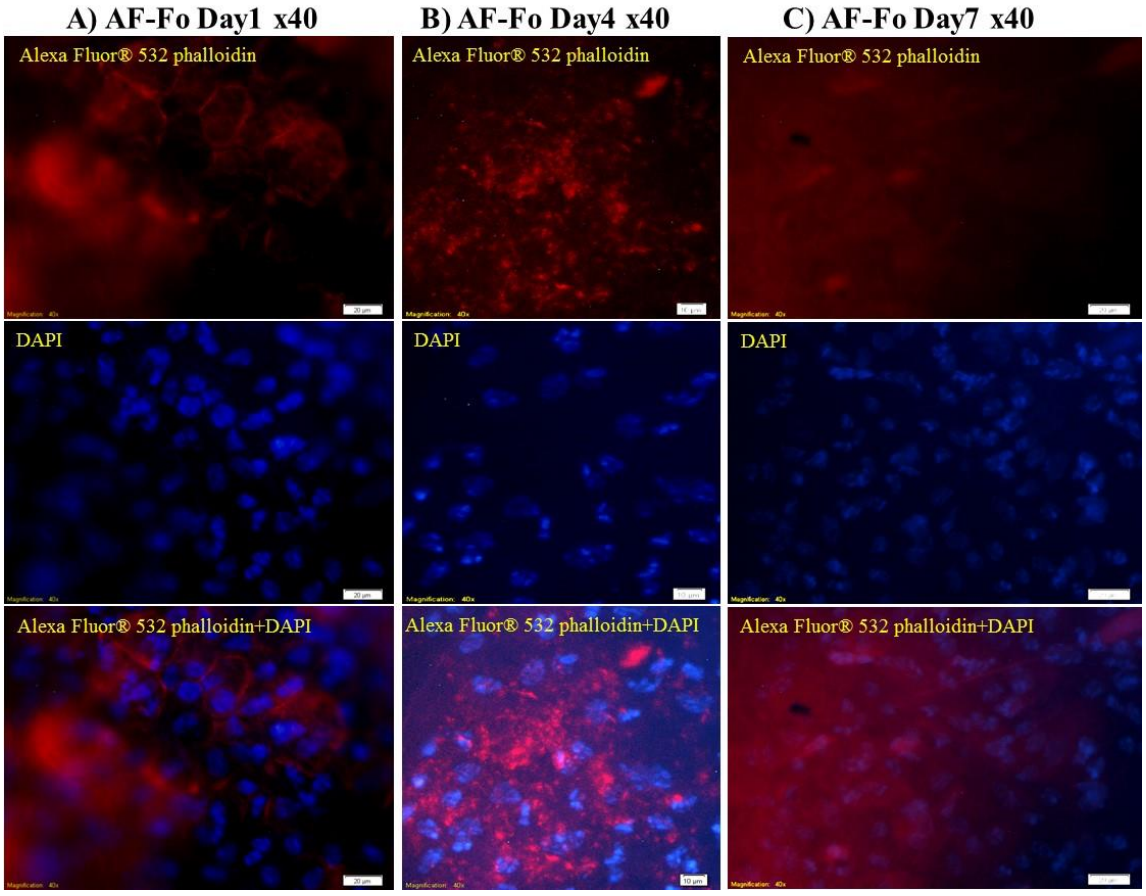

Figure 3.12. Fluorescence microscopy on aligned fiber-foam (AF-Fo) constructs of after (A) Day 1, (B) Day 4, and (C) Day 7 of cell culture, Alexa Fluor® 532-Phalloidin for cytoskeleton and DAPI for the nucleus, x40.

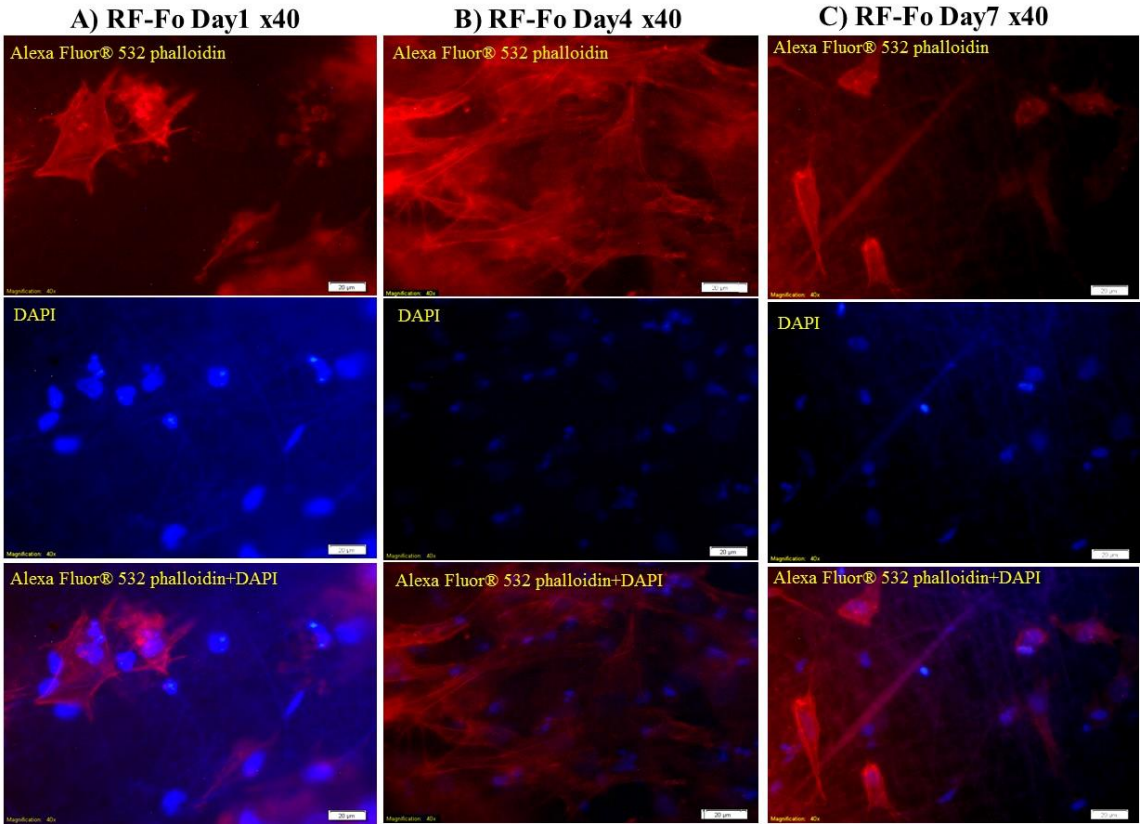

Figure 3.13. Fluorescence microscopy on random fiber-foam (RF-Fo) constructs of after (A) Day 1, (B) Day 4, and (C) Day 7 of cell culture, Alexa Fluor® 532-Phalloidin for cytoskeleton and DAPI for the nucleus, x40.

3.3.3.2. SEM

The SEM micrographs of rBMSCs seeded composite constructs were also obtained on Days 1, 4, and 7 in the culture to observe the cell attachment, migration and growth on these constructs (Figures 3.14-3.19). Figure 3.14. shows the Day 1 SEM of aligned fiber-foam construct. They were attached to the fibrous layer very well because they had cell projections all along the fibers. On Day 4, more of the fibrous layer were covered with cell and they aligned themselves along the fibers (Figure 3.15).

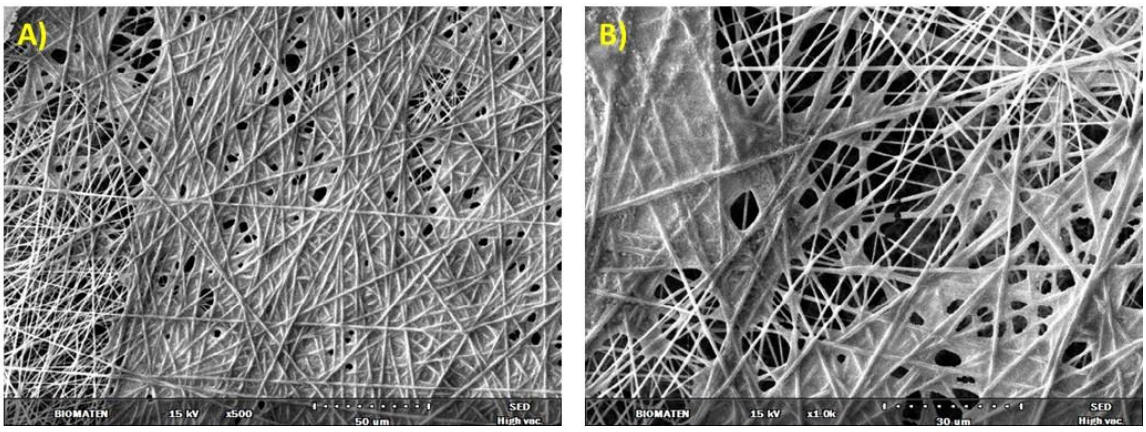

Figure 3.14. SEM of rBMSC seeded AF-Fo after Day 1 of cell culture in differentiation medium. (A) x500, (B) x1000.

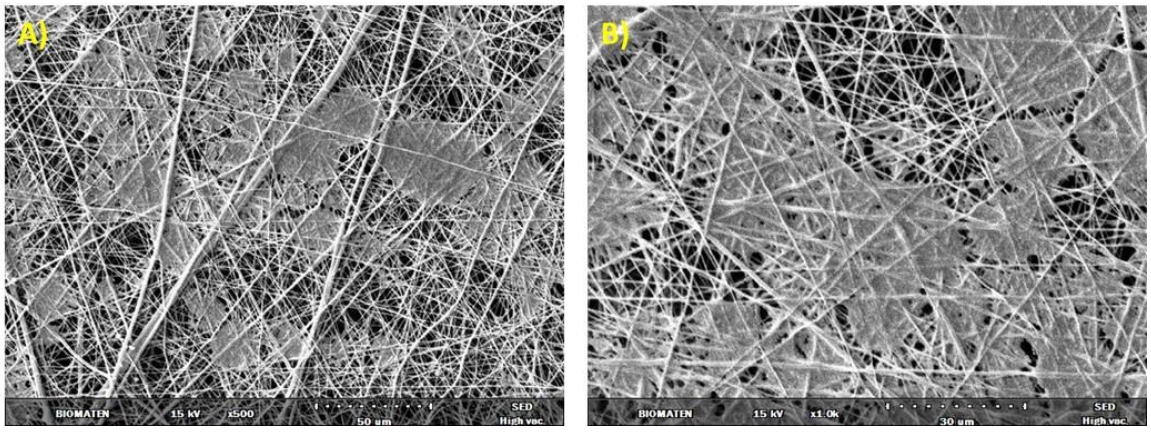

Figure 3.15. SEM of rBMSC seeded AF-Fo after day 4 of cell culture in differentiation medium. (A) x500, (B) x1000.

Figure 3.16 shows the cell behavior on AF-Fo type of bilayer constructs on Day 7. As can be seen, scaffold was very much covered with cells leaving very few voids even though the cell counts showed that AF-Fo had much lower number of cells on Day 7 compared to RF-Fo. These results were consistent with the cell viability assay results, which showed increase in cell number at the end of seven days.

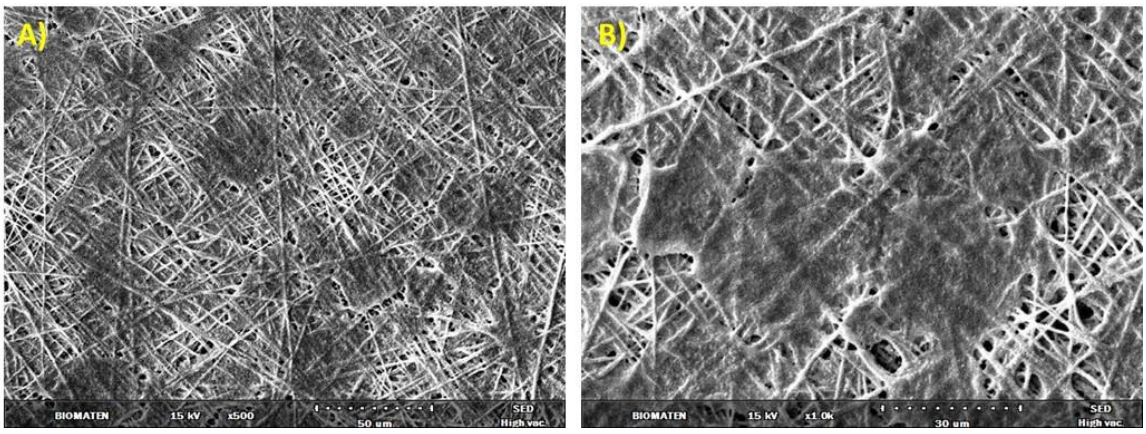

Figure 3.16. SEM of cell seeded AF-Fo after day 7 of cell culture in differentiation medium. (A) x500, (B) x1000.

Similar to AF-Fo, random fiber-foam (RF-Fo) type scaffolds had a low density of cells on Day 1 as expected (Figure 3.17). On Day 4, cells had grown very close to each other and formed clumps. Even though the fibers on RF-Fo were not oriented, the cells tended to grow on the fibers (Figure 3.18).

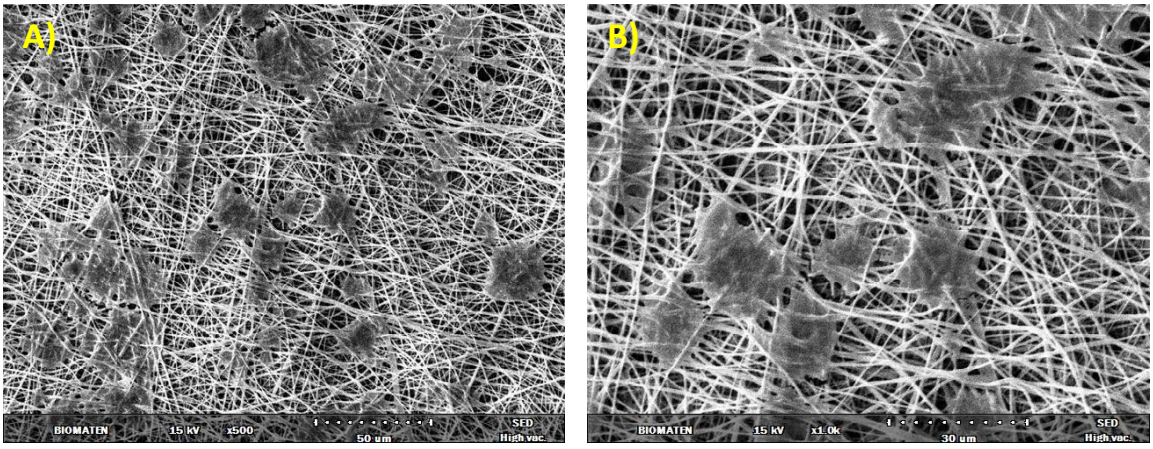

Figure 3.17. SEM of cell seeded RF-Fo after day 1 of cell culture in differentiation medium. (A) x500, (B) x1000.

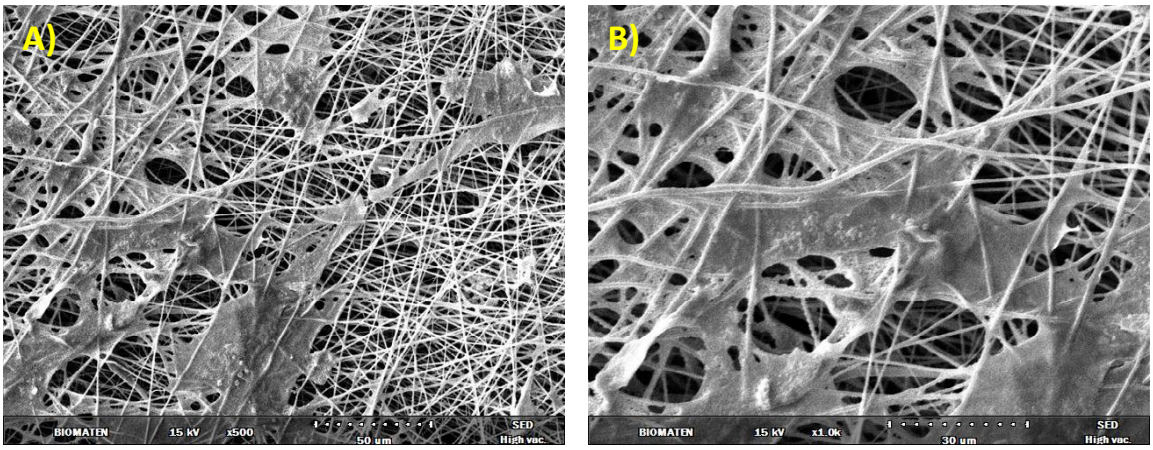

Figure 3.18. SEM of cell seeded RF-Fo after day 4 of cell culture in differentiation medium. (A) x500, (B) x1000.

Figure 3.19 shows the SEM of RF-Fo on day 7, as in RF-Fo, scaffold was covered with cells. When it is compared with day 1 and 4, cells were attached the surface very well. They almost seem to fuse with the fibers on day 7. As observed in this study, Yoshimoto et al. (2003) found that at the random PCL fibers was partially covered with multi-layers of rBMSCs at 1 week, but the surface was completely covered with cell multilayers at 4 weeks. Therefore, it can be stated that if incubation day was longer, cells would covered all of the fibrous structure.

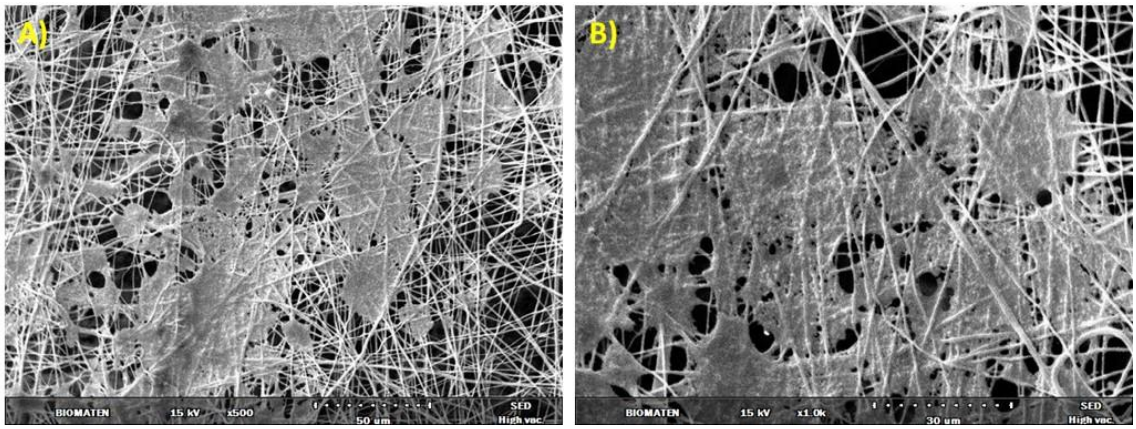

Figure 3.19. SEM of cell seeded RF-Fo after day 7 of cell culture in differentiation medium. (A) x500, (B) x1000.

When the cells were checked whether they migrate to under the fibers, no cells were observed on the foam layer (Figure 3.20). Therefore, it can be concluded that seven day cell culture might not provide the required time to migrate the rBMSCs to foam layer.

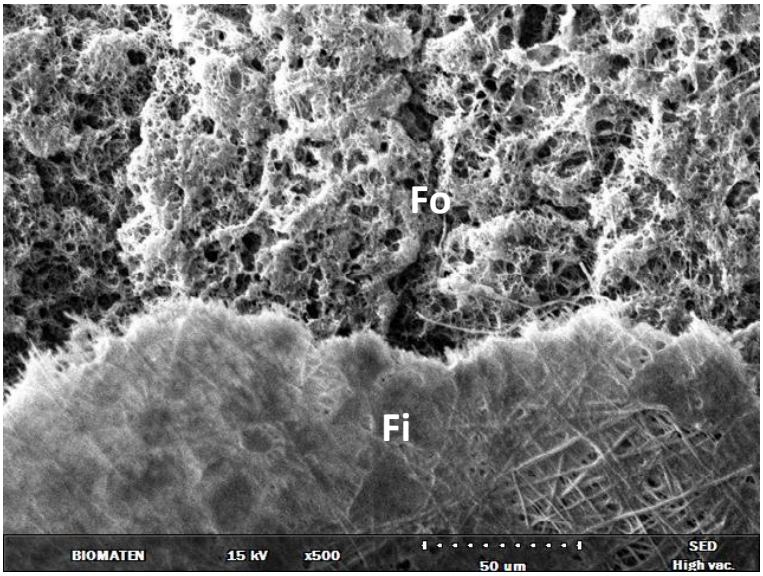

Figure 3.20. SEM of cell seeded AF-Fo after Day 7 of cell culture in differentiation medium, x500.

3.3.4. Differentiation Studies

As it was explained in Section 2.2.4.4., three different types of differentiation procedures were tested.

In the first procedure, BMSCs were cultured in Neurogenic Differentiation Medium (Promocell, Germany) for 7 days.

In the second one, BMSCs were cultured with PI for 24 h, and then continued culturing with mesenchymal stem cell Neurogenic Differentiation Medium for 6 days.

Finally, in the third approach BMSCs were cultured for 24 h with preinduction (PI) medium containing 10 ng/mL Epidermal Growth Factor (EGF), 10 ng/mL basic Fibroblast Growth Factor (bFGF), and with 2 mM Valproic Acid (VA) in the absence of FCS. Then, culture was continued with neural induction medium supplied with 2 mM VA, 50 ng/mL Insulin-like Growth Factor 1 (IGF1), and 2% B27, in the absence of FCS for 6 days.

3.3.4.1. Flow Cytometry

Success of these protocols were assessed with flow cytometry. Firstly, rBMSCs were examined before they were exposed to any differentiation medium. Figure 3.21. shows the nestin and beta III-tubulin expression in rBMSCs. As it is seen in the upper left (UL) part of the quadrant, rBMSCs have already expressed the neuronal markers nestin and beta III-tubulin 13.4% and 10%, respectively. These results were consistent with the literature. It was stated that MSCs express neuronal markers, nestin (Kania et al., 2004) and beta III-tubulin (Mörk et al., 2003). Moreover, in 2012, Miloso et al. found that expression of neuronal markers could be different depending on

the passage number of the MSCs. At the end, they stated that at the later passages, the expression of neuronal markers decreases or is absent when compared with early passages. Therefore, passages 1-3 of rBMSCs were used in this study.

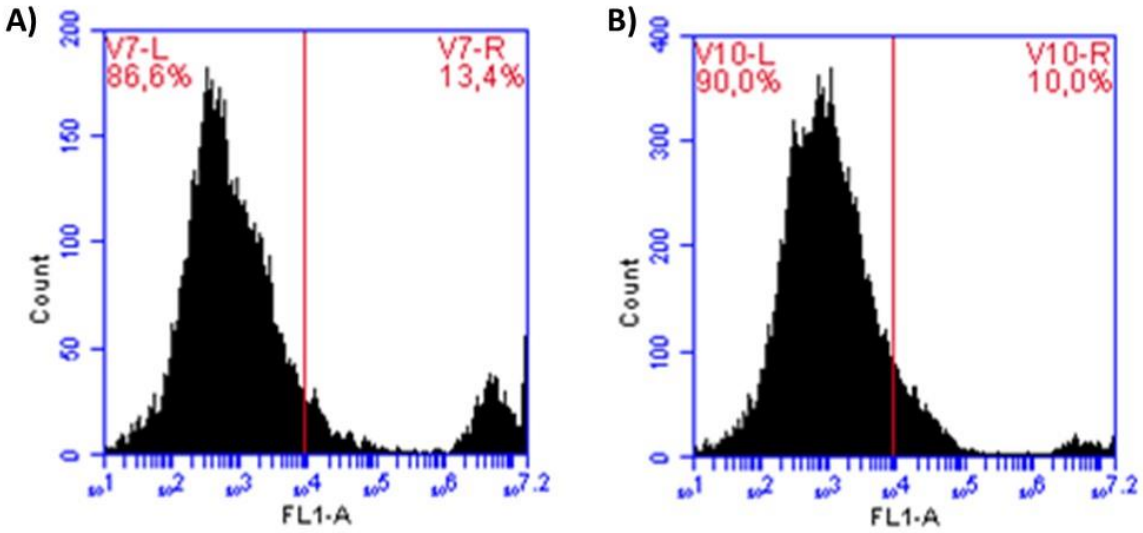

Figure 3.21. Flow cytometry results of (A) Nestin, (B) Beta III-tubulin expression of undifferentiated rBMSCs Passage 2.

Figure 3.22A shows the expression of the positive marker, CD90, and the neuronal markers nestin and beta III-tubulin. Red lines represent CD90 expression, and it was much higher than the expression of neuronal markers tubulin and nestin, respectively (blue and black lines). Nestin and beta III-tubulin expressions were also shown in Figure 3.22B with the controls, unstained cells, no primary antibody, and mouse IgG. When the neuronal marker expression were compared with all the controls, it is seen that they were a little higher than the controls. It can be stated that rBMSCs express neuronal markers in their undifferentiated state.

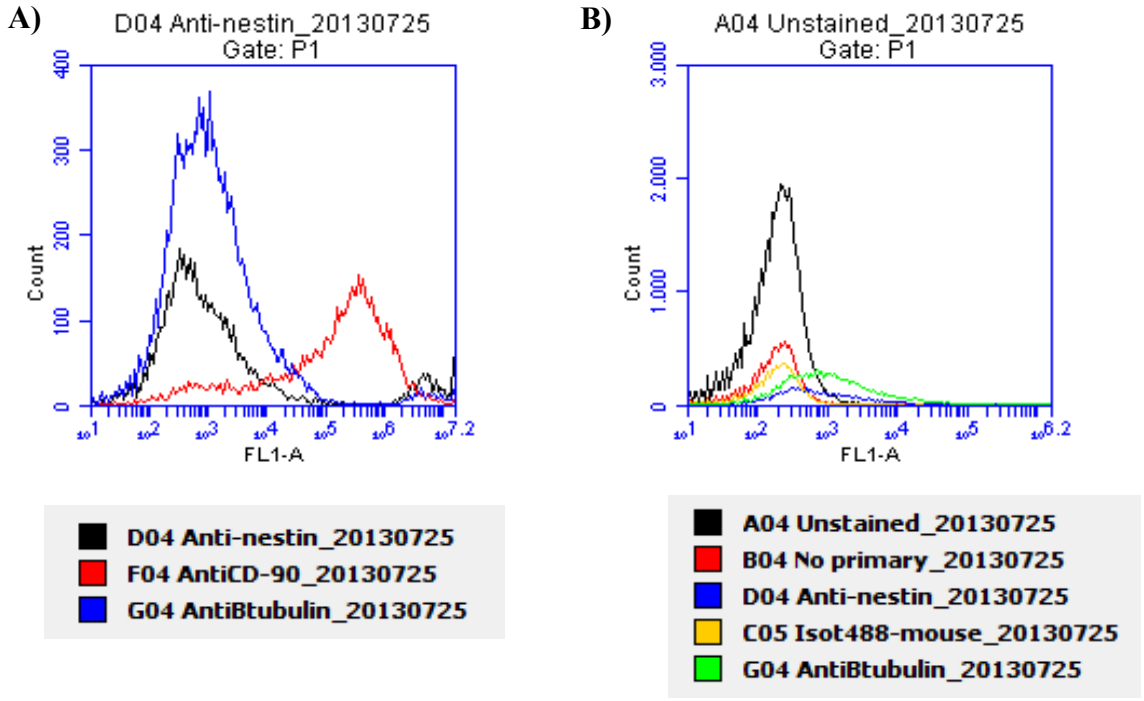

Figure 3.22. Flow cytometry results of (A) Nestin, CD-90, beta III-tubulin, (B) Controls, nestin and beta III-tubulin expression of undifferentiated rBMSCs.

After the analysis of undifferentiated rBMSCs was completed, differentiation level of these cells was also checked with flow cytometry after the differentiation procedures were completed.

First procedure only included the application of Neurogenic Differentiation Medium (Promocell, Germany) for 7 days. Results are shown in Figures 3.23. and 3.24. In Figure 3.23, increase of the neuronal markers can be seen easily. Nestin and beta III-tubulin expressions were 40.3% and 47.6%, respectively.

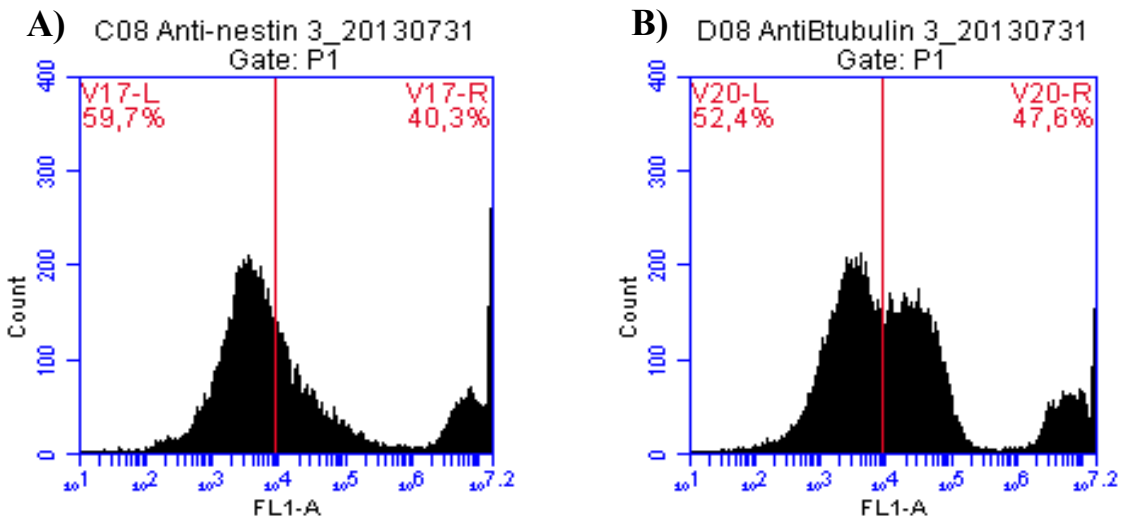

Figure 3.23. Flow cytometry results of (A) Nestin, (B) Beta III-tubulin expression of Passage 2 rBMSCs after application of Differentiation Procedure 1.

Figure 3.24. shows the comparison of the neuronal marker expression with the controls, unstained cells and mouse isotype controls. According to the figure, almost half of the cells express nestin and beta III-tubulin. Results were very good in terms of neurogenic expression because it was only a seven day long procedure. If the incubation duration were longer, expression of the neuronal markers would probably be higher. Besides, even a 30% increase in the expression of these neuronal markers shows the capacity of rBMScs to differentiate into neurons.

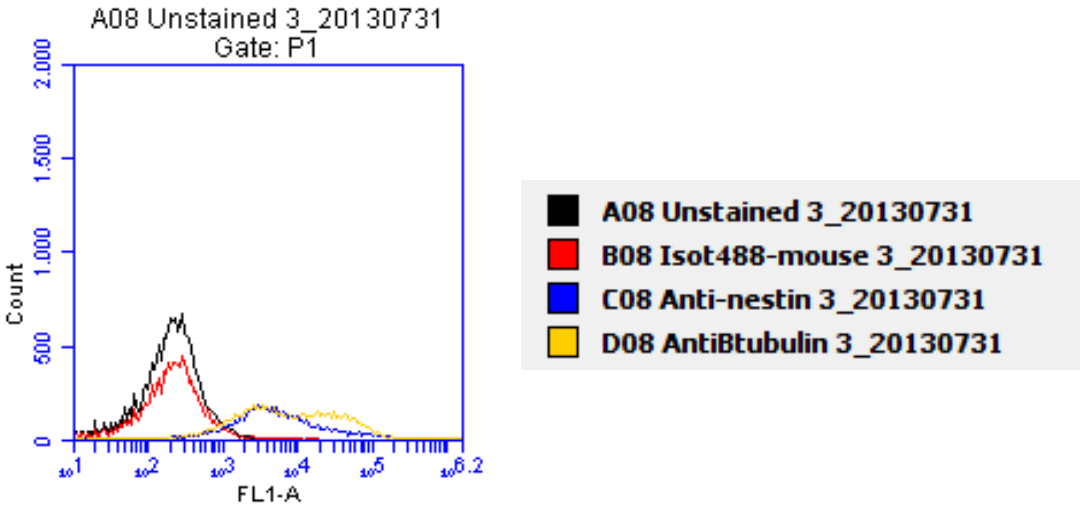

Figure 3.24. Flow cytometry results of controls, nestin and beta III-tubulin expression of Passage 2 rBMSCs after application of Differentiation Procedure 1.

In the second differentiation procedure, BMSCs were cultured in PI for 24 h, and then incubation in the mesenchymal stem cell Neurogenic Differentiation Medium for 6 days. Results are shown in Figures 3.25. and 3.26. When compared with the controls (unstained and mouse IgG), expression of nestin and beta III-tubulin was increased to a level similar to the first procedure. 38.2% of cells expressed nestin, 45% of cells expressed tubulin at the end of the differentiation procedure.

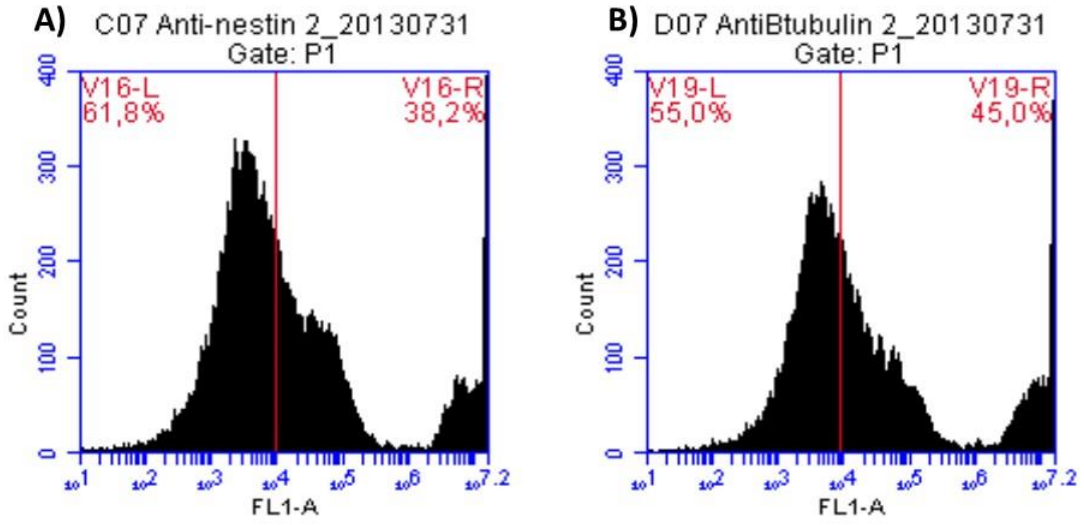

Figure 3.25. Flow cytometry results of (A) Nestin, (B) Beta III-tubulin expression of Passage 2 rBMSCs after application of Differentiation Procedure 2.

Figure 3.26. shows the comparison of expression of the neuronal markers expression with the controls (unstained cells and mouse isotype controls). Both nestin an beta III-tubulin gave peaks with much higher fluorescence intensity. It means that neurogenic expression was observed, even though complete differentiation was not achieved.

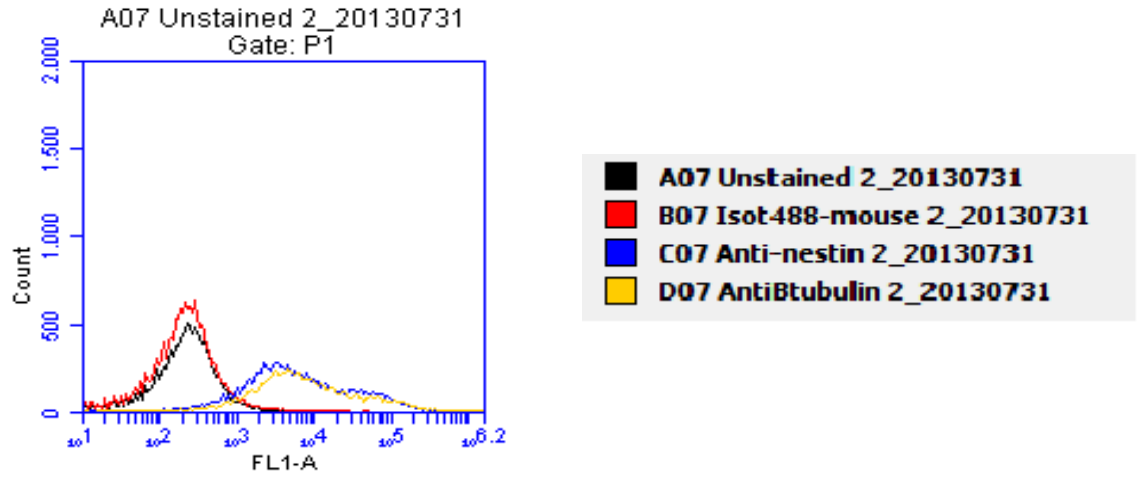

Figure 3.26. Flow cytometry results of controls, nestin and beta III-tubulin expression of Passage 2 rBMSCs after application of Differentiation Procedure 2.

Final differentiation procedure consisted of culturing the cells for 24 h with preinduction (PI) medium containing EGF, bFGF, and VA in the absence of FCS. Then, the culture was continued for 6 days with neural induction medium supplied with VA, IGF1, B27 in the absence of FCS. Results were shown in Figures 3.27. and 3.28. 31.1% of cells expressed nestin, and 28.7% of cells expressed beta III-tubulin at the end of the differention procedure. When compared with the first two procedures, this procedure appears to be less efficient one because expression of neuronal markers was the lowest, but on the otherhand it was one of the simplest of the three.

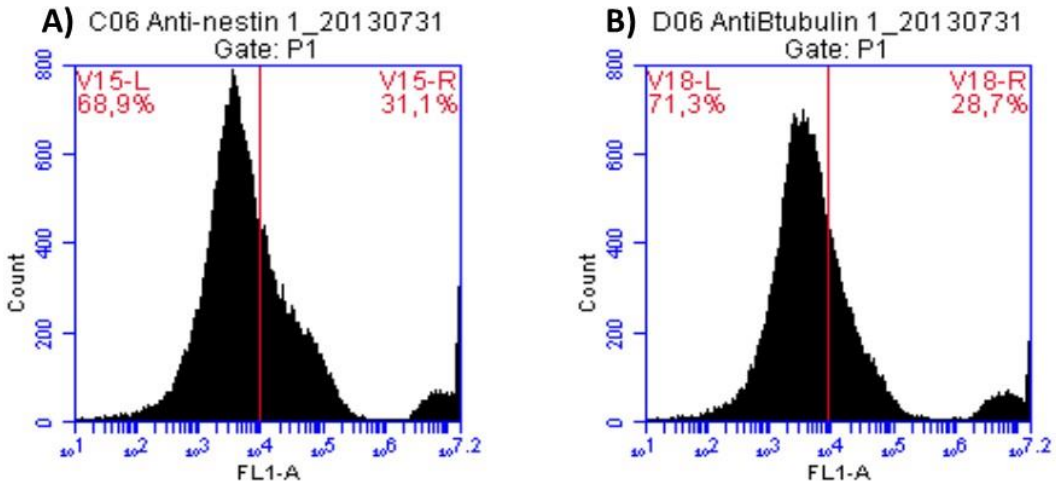

Figure 3.27. Flow cytometry results of (A) Nestin, (B) Beta III-tubulin expression of Passage 2 rBMSCs after application of Differentiation Procedure 3.

Figure 3.28. shows the plot of both the controls and the neuronal markers. Although the amount of expression was not as high as in the earlier 2 procedures, they had peaks with high fluorescence intensity implying that neuronal expression was present.

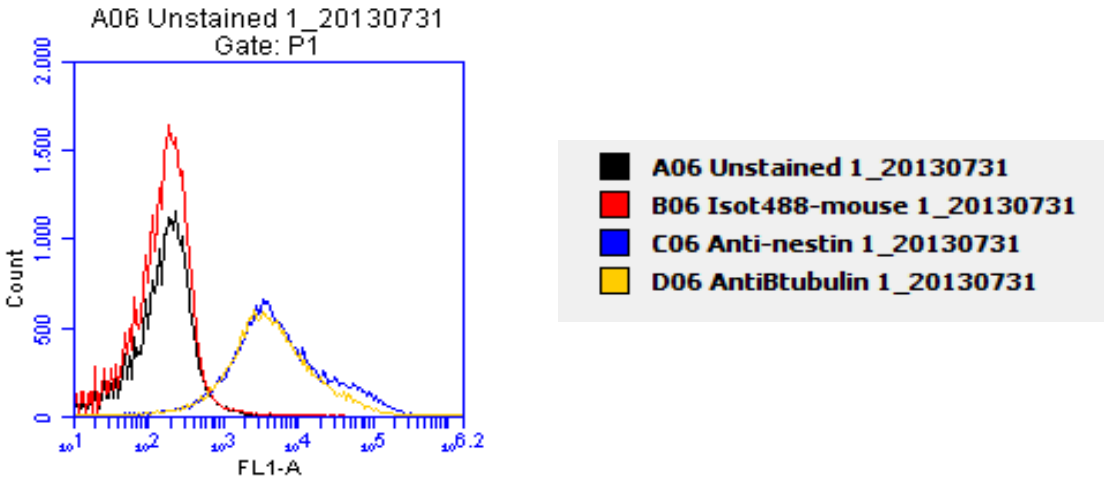

Figure 3.28. Flow cytometry results of controls, nestin and beta III-tubulin expression of Passage 2 rBMSCs after application of Differentiation Procedure 3.

Results of all of these differentiation protocols are summarized in Table 3.5. At can be seen the highest expression of neuronal markers was achived with the first procedure, and therefore, this medium was used at the final experimental set up.

Table 3.5. Expression of nestin and beta III-tubulin with different differentiation procedures and quantified with flow cytometry.

	Nestin (%)	**Beta III-tubulin (%)**
Procedure 1	40.3	47.6
Procedure 2	38.2	45
Procedure 3	31.1	28.7

3.3.4.2. Neuronal Specific Enolase ELISA

Neuron specific enolase (NSE) is localized in neurons and neuroendocrine cells (Schmechel et al., 1978). Glial cells, on the other hand, do not contain NSE and they constitute about half of the cytoplasmic volume in brain. Therefore, a very high percentage of the soluble protein in the neural cytoplasm is NSE. In some neurons NSE may account for as much as 3-4% of the total soluble protein. This very high level of NSE in the brain is a very accessible tool for studying neural cells at both the basic and clinical level (Marangos and Schmechel, 1987). In this study, levels of NSE was determined with ELISA kit in both undifferentiated and differentiated cells. Results of this test are shown in Table 3.6. It is seen that NSE levels of 1.10 and 1.21 for the

differentiated cells and substantially larger than that of 0.07 of the undifferentiated cells has increased the NSE levels in cells on both AF-Fo and RF-Fo type of scaffolds after 7 days incubation with differentiation medium (calibration curve for absorbance vs NSE level is presented in Figure B.1 in Appendix B). This level might not be very significant. According to the literature, the appearance of NSE occurs with the onset of neurogenesis and continues to increase well after the end of neurogenesis, during the period of early neuronal differentiation (Jorgensen and Centervall, 1982). Therefore, when these results were compared with the literature, it can be said that increase in the NSE level is an indication of differentiation of BMSCs to neurons on the nerve guides.

Table 3.6. NSE expression in undifferentiated and differentiated cells

Sample Type	NSE level (ng/mL)
Undifferentiated BMSCs	0.07 ± 0.01
Differentiated cells on AF-Fo bilayer	1.10 ± 0.02
Differentiated cells on RF-Fo bilayer	1.21 ± 0.04

3.3.4.3. Immunohistochemistry

Scaffolds were incubated in both normal medium (in DMEM-high glucose tissue culture medium containing penicillin (100 U/mL), streptomycin (100 µg/mL)) and in neurogenic differentiation medium for seven days. Neural markers such as anti-nestin, anti-tyrosine hydroxylase, anti-beta III tubulin, and anti-synaptophysin antibodies were used for the immunostaining of cell seeded constructs. Expression of these neuronal markers by rBMSCs was studied in both normal and differentiation media by this method on Days 4, and 7 of incubation. Figures 3.29-38 show the results.

Figure 3.29. shows the expression of nestin (green) and tyrosine hydroxylase (blue) on Day 4 with incubation in both the normal medium (Figure 3.29A) and the differentiation medium (Figure 3.29B). When these figures were compared, it can be seen that both nestin and thyrosine hydroxylase expression were higher in the differentiation medium. These results are also consistent with the flow cytometry results where higher expression of neuronal markers in the differentiation medium was observed. Figure 3.30. also shows the expression of different neuronal markers, beta III-tubulin (green) and synaptophysin (blue) in different medium types. Same with the Figure 3.29, higher expression of neuronal markers were observed.

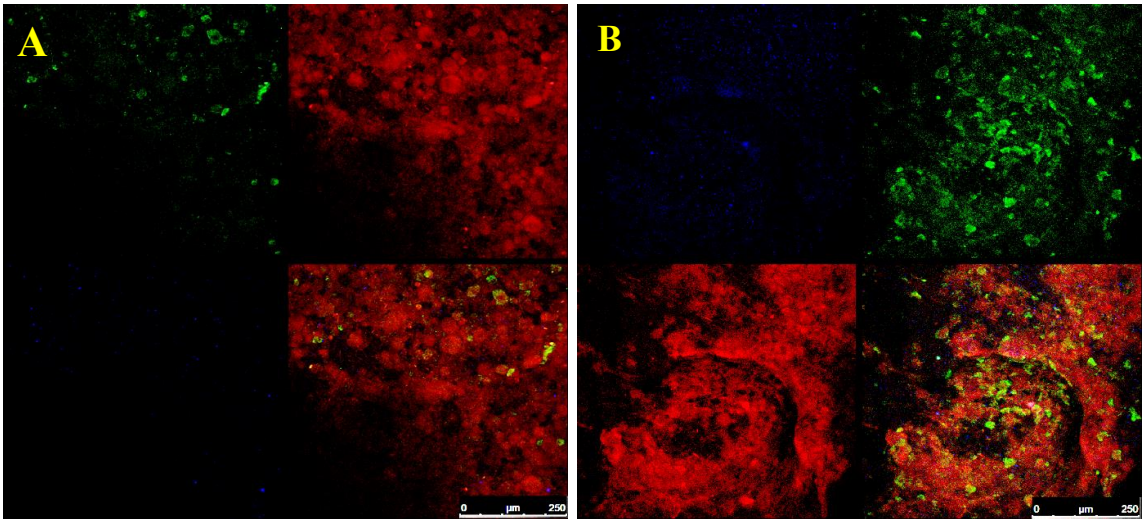

Figure 3.29. Immunohistochemistry results of AF-Fo in terms of nestin (green) and tyrosine hydroxylase (blue) expression after Day 4 of cell culture. (A) Normal medium, (B) Neurogenic Differentiation medium (Differentiation Procedure 1).

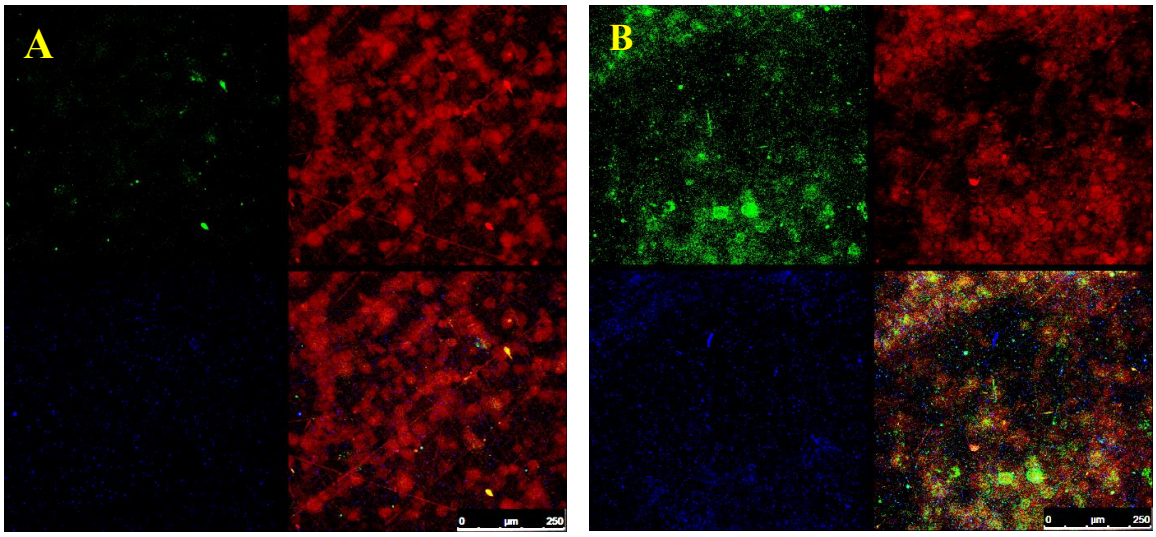

Figure 3.30. AF-Fo beta III-tubulin (green) and synaptophysin (blue) expression after Day 4 of cell culture. (A) Normal medium, (B) Neurogenic Differentiation medium (Differentiation Procedure 1).

Figure 3.31. shows the expression of nestin (green) on Day 7 with incubation in both normal and differentiation media. Figure 3.32. shows the beta III-tubulin (green) expression. When these figures are compared, it can be seen that both nestin and beta III-tubulin expression were higher when the cells were incubated in the differentiation medium. When the results of Day 4 and 7 were compared, it can be seen that expression was higher on day 7 incubation as expected.

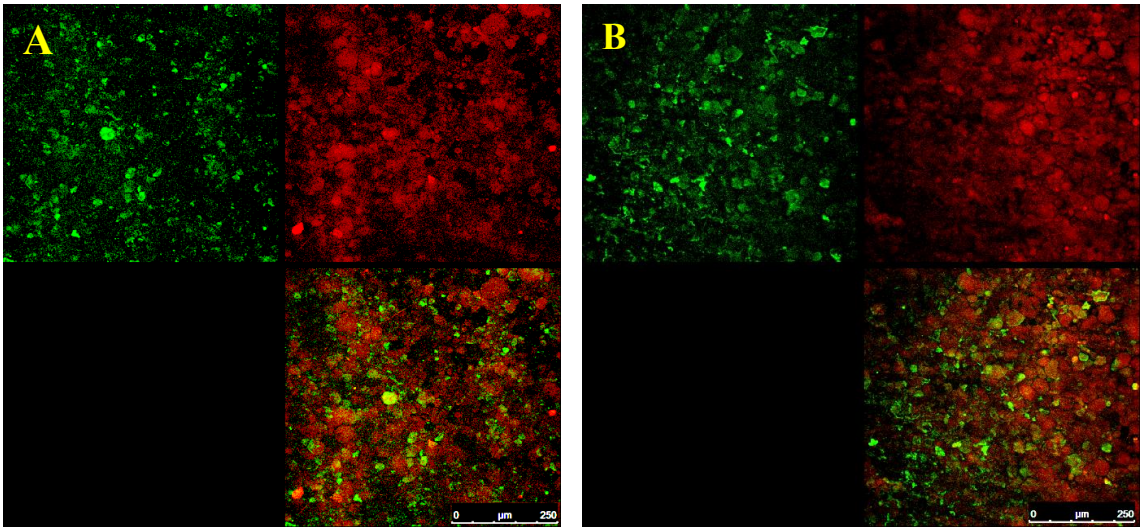

Figure 3.31. AF-Fo nestin (green) and tyrosine hyroxylase (blue) expression afer day 7 of cell culture. (A) Normal medium, (B) Neurogenic Differentiation medium (Differentiation Procedure 1).

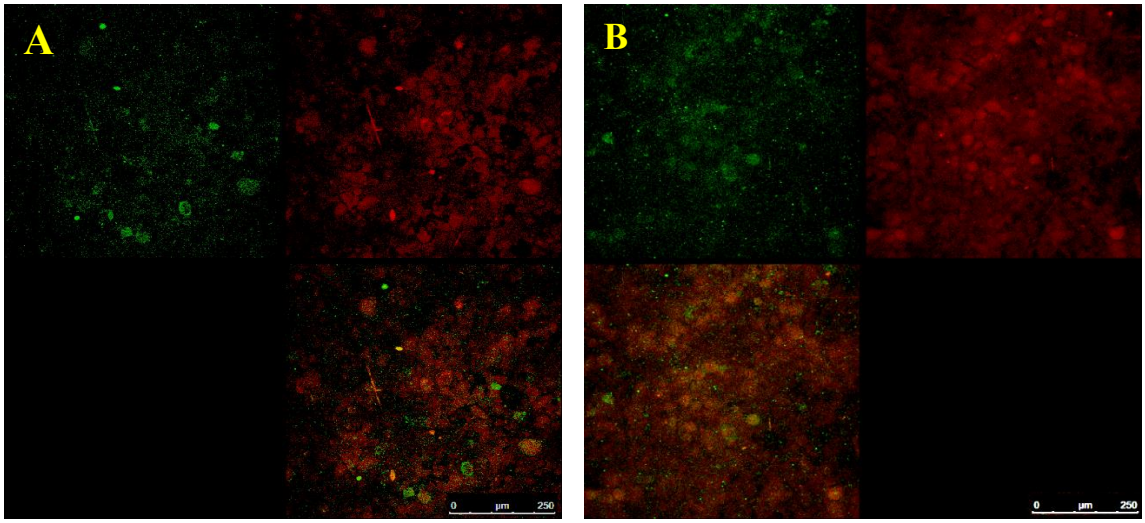

Figure 3.32. AF-Fo beta III-tubulin (green) and synaptophysin (blue) expression after day 7 of cell culture. (A) Normal medium, (B) Neurogenic Differentiation medium (Differentiation Procedure 1).

Figures 3.33. and 3.34. show the expression of the same neuronal markers with the RF-Fo type of scaffold. In Figure 3.33. the expression of nestin (green) and tyrosine hydroxylase (blue) are shown. When Figures 3.33A and B were compared, the increase in the nestin expression is obvious. However, in the normal medium, both the green and blue colors are observed because undifferentiated BMSCs also express neuronal markers to some extent (Rogister et al., 2005).

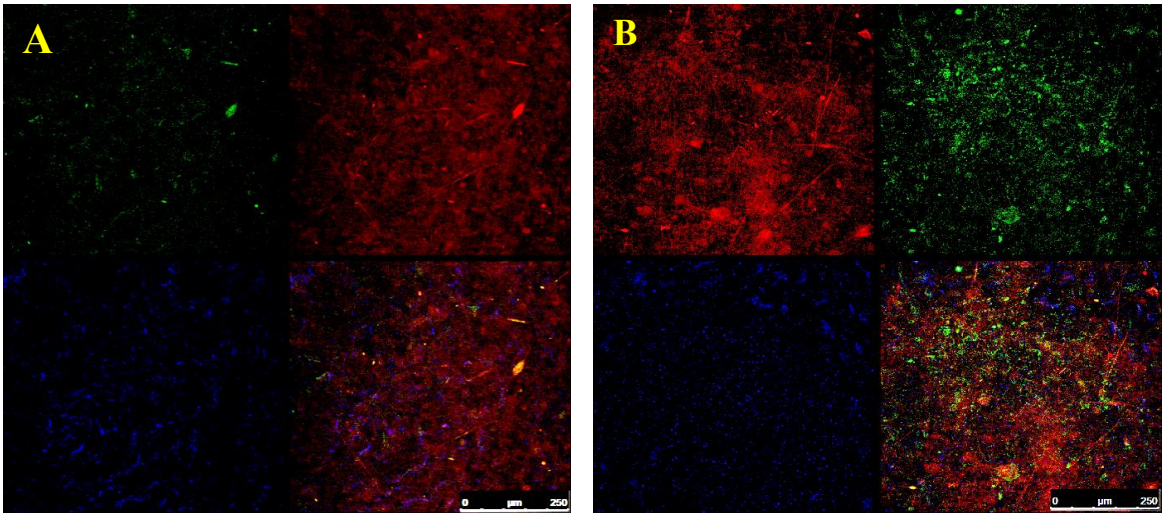

Figure 3.33. RF-Fo nestin (green) and tyrosine hyroxylase (blue) expression after Day 4 of cell culture. (A) Normal medium, (B) Neurogenic Differentiation medium (Differentiation Procedure 1).

In Figure 3.34, beta III-tubulin and synaptophysin expression in RF-Fo type of bilayer were tested with immunostaining. Results were similar to that of the AF-Fo scaffold. As expected the expression of these markers was increased in the differentiation medium. Results of immunostaining were consistent with that of flow cytometry which also showed the higher expression of neuronal markers in the differentiation medium.

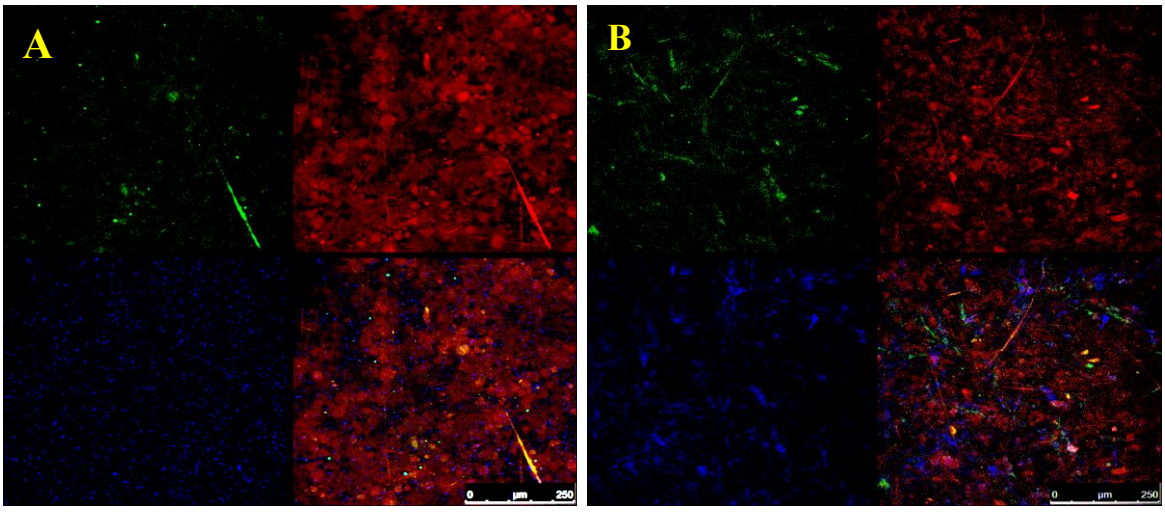

Figure 3.34. RF-Fo beta III-tubulin (green) and synaptophysin (blue) expression after Day 4 of cell culture. (A) Normal medium, (B) Neurogenic Differentiation medium (Differentiation Procedure 1).

For Figures 3.35. and 3.36. 647 nm laser was closed because no signal came from this laser showing that staining procedure was not successful for these dyes. Therefore, neurol markers are seen as only green. Figure 3.26. shows the expression of nestin (green) on Day 7 with incubation in both the normal and the differentiation media. Figure 3.36. shows the beta III-tubulin (green) expression. When these figures are compared, it can be seen that both nestin and beta III-tubulin expressions were higher upon incubation in the differentiation medium. When these figures also were compared with Day 4 of incubation, it can be seen that expression increases with time.

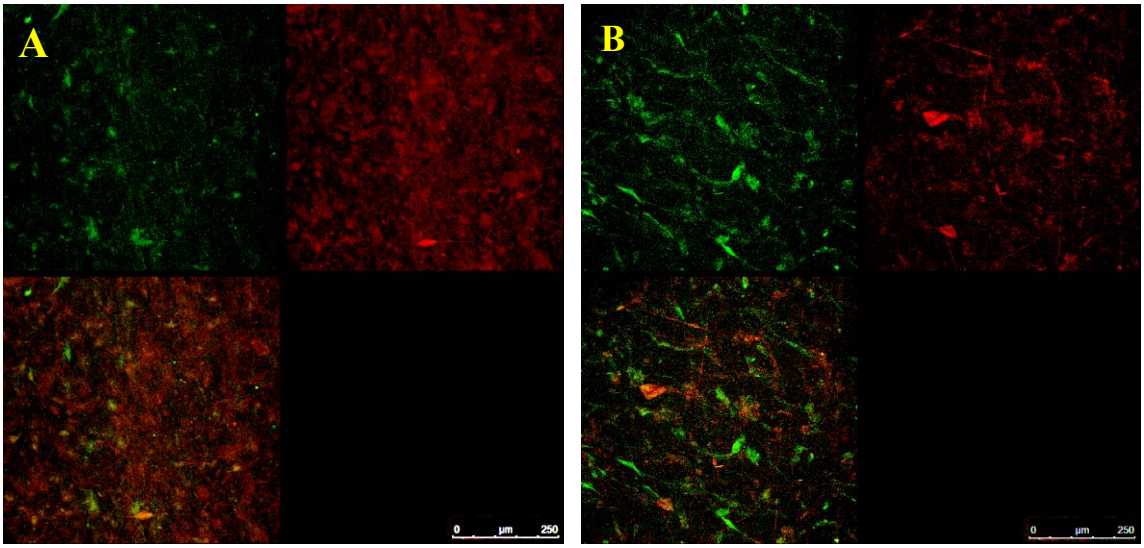

Figure 3.35. RF-Fo nestin (green) expression after Day 7 of cell culture. (A) Normal medium, (B) Neurogenic Differentiation medium (Differentiation Procedure 1).

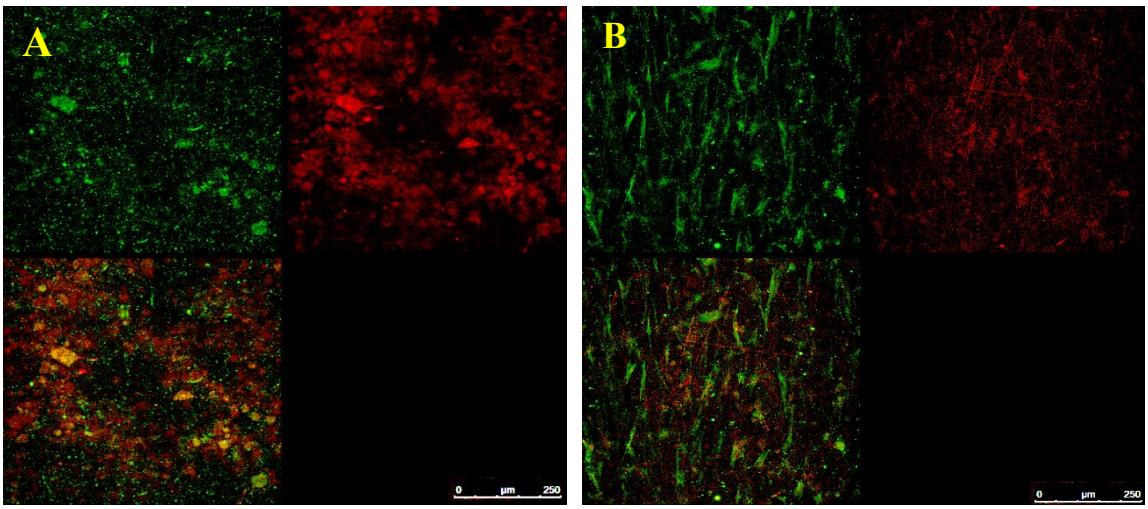

Figure 3.36. RF-Fo beta III-tubulin (green) after Day 7 of cell culture. (A) Normal medium, (B) Neurogenic Differentiation medium (Differentiation Procedure 1).

Figure 3.37. shows the negative control of the immunostaining. Only the signals that came from the scaffold (red) was seen in the figure. Therefore, it can be said that staining procedure was successful.

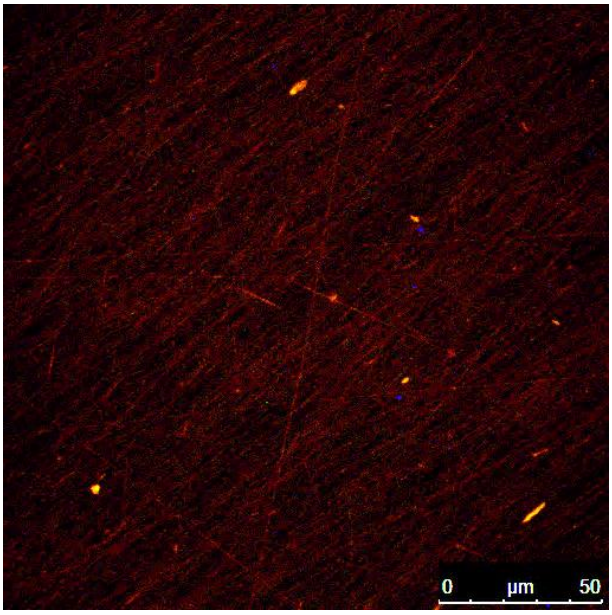

Figure 3.37. Negative control of immunostaining.

CHAPTER 4

CONCLUSION AND FUTURE STUDIES

In case of a spinal cord injury (SCI), both sensory and motor axons are distrupted which breaks down the continuity of the spinal cord. Compared with the use of peripheral nerve autografts and nerve bridges in peripheral nervous system, there is currently no reproducible and successful clinical therapy for SCI. The predominant focus of tissue engineering strategies has been a combination of cell transplantation with supportive matrices and scaffolds.

In this study, a 3D scaffold was constructed from PHBV and PHBV/Collagen in fiber and foam form in an attempt to mimic the natural structure and organization of the neural cells. An important goal was to compare the effectiveness of guidance provided in the tube but this could not be conclusively completed. Probably another design is needed in the filling of the tube and may be a change of chemicals can be considered. These scaffolds were examined in terms of cell attachment, proliferation, and differentiation.

The AF-Fo and RF-Fo constructs were shown to support cell attachment and proliferation. Differentiation level of rat bone marrow stromal cells (rBMSCs) was studied with flow cytometry, and found that expression of neural markers was increased. The constructs appeared to have the potential for use as an implant at the SCI site and their performance should be enhanced before *in vivo* studies. These enhancements could be achieved by increasing the incubation duration to reach a higher level of differentiation. If the seeded cell number is increased, the ECM secretion can be increased and shown microscopically and quantified. On the electrospun fiber mat, the degree of alignment decreases as the mat gets thicker. In the study, the degree of alignment is quite similar to the random fiber mat. One approach could be to decrease the duration of electrospinning, and another could be to use a rotating mandrel. Bioreactors could be used to achieve better culture conditions especially a thick nerve guide. These should then be tested *in vivo* on rats by using BMSCs. We still believe that the nerve guide designed can perform as good as the currently available ones in the market.

REFERENCES

Azbill RD, and Carlson SL. A rapid and sensitive assay for measuring mitochondrial metabolic activity in isolated neural tissue. Brain Research Protocols 1998; 2: 259-263.

Bahr M, and Bonhoeffer F. Perspectives on axonal regeneration in the mammalian CNS. Trends Neurosci. 1994; 17: 473–479.

Ballios BG, Baumann MD, Cooke MJ, Shoichet MS. Central Nervous System. In: Atala A, Lanza R, Nerem R, Thomson JA, editors. Principles of Regenerative Medicine, First edition, Elsevier, USA, 2008; 1025-1027.

Bray GM, Villegasperez MP, Vidalsanz M, and Aguayo AJ. The use of peripheral-nerve grafts to enhance neuronal survival, promote growth and permit terminal reconnections in the central-nervous-system of adult-rats. J. Exp. Biol. 1987; 132: 5–19.

Caplan AI. Tissue engineering strategies for the use of mesenchymal stem cell store generate skeletal tissues. In Functional Tissue Engineering, Guilak F, Butler DL, Goldstein SA, and Mooney DJ, editors. Springer-verlag, New York, 2003.

Chen YS, Hsieh CL, Tsai CC, Chen TH, Cheng WC, Hu CL, Yao CH. Peripheral nerve regeneration using silicone rubber chambers filled with collagen, laminin and fibronectin. Biomaterials 2000; 21: 1541–1547.

Clark P, Connolly P, Curtis ASG, Dow JAT, and Wilkinson CDW. Topographical control of cell behaviour: II. Multiple grooved substrata. Development 1990; 108: 635–644.

Dalton P, Harvey A, Oudega M, and Plant G. Tissue engineering of the nervous system. In: Blitterswijk C, Thomsen P, Lindahl A, Hubbell J, Williams D, Cancedda R, Bruijn J, Sohier J, editors. Tissue Engineering, First Edition, Elsevier, 2008; 612-643.

Dehghani F, Annabi N, Engineering porous scaffolds using gas-based techniques. Current Opinion in Biotechnology 2011; 22: 661–666.

Evans GRD, Brandt K, Widmer MS, Lu L, Meszlenyi RK, Gupta PK, Mikos AG, Hodges J, Williams J, and Gurlek A. In vivo evaluation of poly(-lacticacid) porous conduits for peripheral nerve regeneration. Biomaterials 1999; 20: 1109–1115.

Evans GRD. Challenges to nerve regeneration. Semin. Surg. Oncol. 2000; 19: 312–318.

Faweett JW, and Keynes RJ. Peripheral Nerve Regeneration. Annu Rev Neurosci 1990; 13: 43-60.

Foudah D, Redondo J, Caldara C, Carini F, Tredici G, and Miloso M. Expression of Neural Markers by Undifferentiated Rat Mesenchymal Stem Cells. Journal of Biomedicine and Biotechnology 2012. Article ID 820821, doi:10.1155/2012/820821

Franklin RJM, Gilson JM, Franceschini IA, and Barnett SC. Schwann cell-like myelination following transplantation of an olfactory bulb-ensheathing cell line into areas of demyelination in the adult CNS. Glia 1996; 17: 217–224.

Frerichs O, Fansa H, Schicht C, Wolf G, Schneider W, and Keilhoff G. Reconstruction of peripheral nerves using acellular nerve grafts with implanted cultured Schwann cells. Microsurgery 2002; 22: 311–315.

Griffon DJ, Sedighi MR, Schaeffer DV, Eurell JA, Johnson AL. Chitosan scaffolds: Interconnective Pore Size and Cartilage Engineering. Acta Biomater 2006; 2: 313-320.

Grill R, Murai K, Blesch A, Gage FH, and Tuszynski MH. Cellular delivery of neurotrophin-3 promotes corticospinal axonal growth and partial functional recovery after spinal cord injury. J. Neurosci. 1997; 17: 5560–5572.

Guyton AC, Hall EJ. Organization of the Nervous System, Basic Functions of Synapses, "Transmitter Substances". In: Textbook of Medical Physiology, Eleventh Edition, Elsevier Saunders, 2006; 560-562.

Hutmacher DW. Scaffolds in tissue engineering bone and cartilage. Biomaterials 2000; 21: 2529-43.

Jackson KA, Majka SM, Wang H, Pocius J, Hartley CJ, Majesky MW, Entman ML, Michael LH, Hirschi KK, and Goodell MA. Regeneration of ischemic cardiac muscle and vascular endothelium by adult stem cells. J. Clin. Invest. 2001;107, 1395–1402.

Jiang X, Lim SH, Mao H, Chew SY. Current applications and future perspectives of artificial nerve conduits. Experimental Neurology 2010; 223: 86–101.

Jorgensen OS, Centervall G. α_γ-enolase in the rat: Ontogeny and tissue distribution. J. Neurochem. 1982; 39: 537-542.

Kandel ER. Nerve cells and behavior. In: Kandel ER, Schwartz JH, Jessel TM, editors. Principles of Neural Science. McGraw-Hill Professional, 2000; 22-32.

Katsedos CD, Legido A, Perentes E, Mörk SJ. Class III β-Tubulin Isotype: A Key Cytoskeletal Protein at the Crossroads of Developmental Neurobiology and Tumor Neuropathology J Child Neurol 2003; 18: 851-866.

Kim BS, and Atala A. Periperal nerve regeneration. In: Methods of Tissue Engineering, Atala A, and Lanza R, editors. Academic Press, New York, 2002; 1135–1142.

Kinikoglu B, Rodriguez-Cabello JC, Damour O, Hasirci V. A smart bilayer scaffold of elastin-like recombinamer and collagen for soft tissue engineering. Journal of Materials Science. Materials in Medicine 2011; 22(6): 1541-1554.

Kolacna L, Bakesova J, Varga F, Kostakova E, Planka L, Necas A, Lukas D, Amler E, Pelouch V. Biochemical and biophysical aspects of collagen nanostructure in the extracellular matrix. Physiol. Res. 2007; 56: 51-60.

Lanza RP, Langer RS, Vacanti J. Biomaterials in Tissue Engineering Polymer scaffold fabrication. In: Lanza RP, Langer RS, Vacanti JP, editors. The History and Scope of Tissue Engineering. Joseph Vacanti and Charles A. Vacanti. Principles of Tissue Engineering. 3rd ed. Amsterdam; Boston: Elsevier / AcademicPress, 2007; 309-323.

Lavik E, Teng YD, Zurakowski D, Qu X, Snyder E, and Langer R. Functional recovery following spinal cord hemisection mediated by a unique polymer scaffold seeded with neural stem cells. MRS Proceedings, 2001; 62.

Lee AC, Yu VM, Lowe JB, Brenner MJ, Hunter DA, Mackinnon SE, Sakiyama-Elbert SE. Controlled release of nerve growth factor enhances sciatic nerve regeneration. ExpNeurol 2003; 184: 295-303.

Marieb EN, Hoehn K. Fundamentals of Nervous System and Nervous Tissue. In: Human Anatomy and Physiology, Seventh Edition, Pearson, Benjamin Cummings, 2006; 388-397.

Martini FM (Ed.). Neural Tissue. In: Fundamentals of Anatomy and Physiology, Seventh Edition. Pearson, Benjamin Cummings, 2006; 375-390.

Matheson CR, Carnahan J, Urich JL, Bocangel D, Zhang TJ, and Yan Q. Glial cell line-derived neurotrophic factor (GDNF) is a neurotrophic factor for sensory neurons: comparison with the effects of the neurotrophins. J. Neurobiol. 1997; 32: 22-32.

McDonald JW, and Becker D. 2008. Spinal Cord. In: Lanza RP, Langer RS, Vacanti JP, editors. Principles of Tissue Engineering. 3rd ed. Amsterdam; Boston: Elsevier / Academic Press, 2007; 942-955.

Mitalipov S, Wolf D. Totipotency, pluripotency and nuclear reprogramming. Adv. Biochem. Eng. Biotechnol. 2009; 114: 185–199.

Nakahara Y, Gage FH, Tuszynski MH. Grafts of fibroblasts genetically modified to secrete NGF, BDNF, NT-3, or basic FGF elicit differential responses in the adult spinal cord. Cell Transplant. 1996; 5: 191-204.

National Spinal Cord Injury Database, 2013.

Navarro X, Valero A, Gudino G, Fores J, Rodriguez FJ, Verdu E, Pascual R, Cuadras J, and Nieto-Sampedro M. Ensheathing glia transplants promote dorsal root regeneration and spinal reflex restitution after multiple lumbar rhizotomy, Ann. Neurol. 1999; 45: 207–215.

Pek YS, Spector M, Yannas IV, Gibson LJ. Degradation of a collagen–chondroitin-6-sulfate matrix by collagenase and by chondroitinase. Biomaterials 2004; 25: 473–482.

Ramon-Cueto A, Plant GW, Avila J, and Bunge MB. Long-distance axonal regeneration in the transected adult rat spinal cord is promoted by olfactory ensheathing glia transplants. J.Neurosci. 1998; 18: 3803–3815.

Recknor JB, Mallapragada SK. Nerve Regeneration: Tissue Engineering Strategies. In Francis JP, Mikos AG, Bronzino DJ, editors. Tissue engineering. London: CRC; Taylor & Francis, 2007; 301-314.

Recknor JB, Recknor JC, Sakaguchi DS, and Mallapragada SK. Oriented astroglial cell growth on micropatterned polystyrene substrates. Biomaterials 2004; 25: 2753–2767.

Schafer M, Fruttiger M, Montag D, Schachner M, and Martini R. Disruption of the Gene for the Myelin-Associated Glycoprotein Improves Axonal Regrowth along Myelin in C57BL/Wlds Mice Neuron 1996; 16: 1107-1113.

Scherer SS, and Salzer JL. In: Glial Cell Development. Jessen KR and Richardson WD, editors. Oxford, Oxford University Press, 2nd Edition, 2001; 299-330.

Schmechel DE, Brightman MW, Barker JL. Localization of neuron specific enolase in mouse spinal cord neurons grown in tissue culture. Brain Res. 1980; 181: 391-400.

Schmechel DE, Marangos PJ. Neuron Specific Enolase, A Clinically Useful Marker for Neurons and Neuroendocrine Cells. Ann. Rev. Neurosci. 1987; 10: 269-295.

Schöler, HR. The Potential of Stem Cells: An Inventory. In: Knoepffler N, Schipanski D, and Sorgner SL. Human biotechnology as Social Challenge. Ashgate Publishing, Ltd., 2007; 28.

Sendtner M, Kreutzberg GW, and Thoenen H. Ciliary neurotrophic factor prevents the degeneration of motor neurons after axotomy. Nature 1990; 345; 440-441.

Sharp I, Frame I, Siegenthaler M, Nistor G, Keirstead HS. Human embryonic stem cell-derived oligodendrocyte progenitor cell transplants improve recovery after cervical spinal cord injury. Stem Cells 2010; 28: 152-163.

Shen YJ, DeBellard ME, Salzer JL, Roder J, and Filbin MT. Myelin-Associated Glycoprotein in Myelin and Expressed by Schwann Cells Inhibits Axonal Regeneration and Branching. Molecular and Cellular Neuroscience 1998; 12: 79-91.

Shi S, and Gronthos S. Pervascular niche of postnatal mesenchymal stem cells in human bone marrow dental pulp. J. Bone Mineral Res. 2003; 18: 696–704.

Shier D, Butler J, Lewis R. (Ed.). In Nervous System I. Human Anatomy and Physiology. McGraw-Hill Professional, 2010; 354-365.

Shin S, Purevdorj O, Castano O, Planell JA, and Kim HW. A short review: Recent advances in electrospinning for bone tissue regeneration. Journal of Tissue Engineering 2012; 3(1).

Silver J, and Miller JH. Regeneration beyond the glial scar. Nat. Rev. Neurosci. 2004; 5: 146-156.

Singhvi R, Kumar A, Lopez G, Stephanopoulous G, Wang DIC, Whitesides G, and Ingber D. Engineering cell shape and function. Science 1994; 264: 696–698.

Sundback C, Hadlock T, Cheney M, and Vacanti J. Manufacture of porous polymer nerve conduits by a novel low-pressure injection molding process. Biomaterials 2003; 24: 819–830.

Tatagiba M, Brosamle C, and Schwab ME. Regeneration of injured axons in the adult mammalian central nervous system. Neurosurgery 1997; 40: 541–546.

Tawonsawatruk T, Spadaccino A, Murray IR, Peault B, Simpson HA. Growth kinetics of rat mesenchymal stem cells from 3 potential sources: bone marrow, periosteum and adipose tissue. J Med Assoc Thai. 2012;10: 189-197.

Temple S. The development of neural stem cells. Nature 2001; 414: 112–117.

Teng YD, Lavik EB, Qu X, Park KI, Ourednik J, Zurakowski D, Langer R, and Snyder EY. Functional recovery following traumatic spinal cord injury mediated by a unique polymer scaffold seeded with neural stem cells. Proc. Natl Acad. Sci. USA 2002; 99: 3024–3029.

Ulloa-Montoya F, Verfaillie CM, Hu WS. Culture systems for pluripotent stem cells. J Biosci Bioeng. 2005; 100 (1): 12–27.

Urdzíková L, Jendelová P, Glogarová KR, Burian M, Hájek M, and Syková E. Transplantation of Bone Marrow Stem Cells as well as Mobilization by Granulocyte-Colony Stimulating Factor Promotes Recovery after Spinal Cord Injury in Rats. Journal of Neurotrauma. 2006; 23(9): 1379-1391.

Vacanti J, and Vacanti CA. The History and Scope of Tissue Engineering. In: Lanza RP, Langer RS, Vacanti JP, editors. Principles of Tissue Engineering. 3rd ed. Amsterdam; Boston: Elsevier / Academic Press, 2007; 3-6.

Valentini RF. Nerve guidance channels. In: Bronzino JD, editor. The Biomedical Engineering Handbook, 2nd ed. CRC Press, Boca Raton, FL, 2000; 1-12.

Verdu E, Navarro X, Gudino-Cabrera G, Rodriguez FJ, Ceballos D, Valero A, and Nieto-Sampedro M. Olfactory bulb ensheathing cells enhance peripheral nerve regeneration. Neuroreport 1999; 10: 1097–1101.

Web site of Dr. Tal Dvir. Illustration retrieved from http://www.tau.ac.il/lifesci/departments/biotech/members/dvir/dvir.html.

Wiese C, Rolletschek A, Kania G, Blyszczuk P, Tarasov KV, Tarasova Y, Wersto RP, Boheler KR, Wobus AM, Nestin expression- a property of multi-lineage progenitor cells? Cell Mol. Life Sci. 2004; 61: 2510–2522.

Wislet-Gendebien S, Wautier F, Leprince P, Rogister B. Astrocytic and neuronal fate of mesenchymal stem cells expressing nestin. Brain Research Bulletin 2005; 68: 95–102.

Xu XM, Chen A, Guernard V, Kleitman N, Bunge MB. Bridging Schwann cell transplants promote axonal regeneration from both the rostral and caudal stumps of transected adult rat spinal cord. J Neurocytol 1997; 26: 1–16.

Yang F, Murugan R, Ramakrishna S, Wang X, Ma YX, Wang S. Fabrication of nano-structured porous PLLA scaffold intended for nerve tissue engineering. Biomaterials 2004; 25: 1891–1900.

Yiu G, He Z. Glial inhibition of CNS axon regeneration. Nature Reviews Neuroscience 2006; 7: 617-627.

Yoshimoto H, Shin YM, Terai H, Vacanti JP. A biodegradable nanofiber scaffold by electrospinning and its potential for bone tissue engineering. Biomaterials 2003; 24: 2077–2082.

Yucel D, Kose GT, Hasirci V. Polyester based nerve guidance conduit design. Biomaterials 2010; 31: 1596-1603.

Zhang N, Yan H, Wen X. Tissue-engineering approaches for axonal guidance. Brain Research Reviews 2005; 49: 48–64.

Zhang YZ, Su B, Venugopal J, Ramakrishna S, and Lim CT. Biomimetic and bioactive nanofibrous scaffolds from electrospun composite nanofibers. Int J Nanomedicine 2007; 2(4): 623–638.

APPENDIX A

ALAMAR BLUE CALIBRATION CURVE

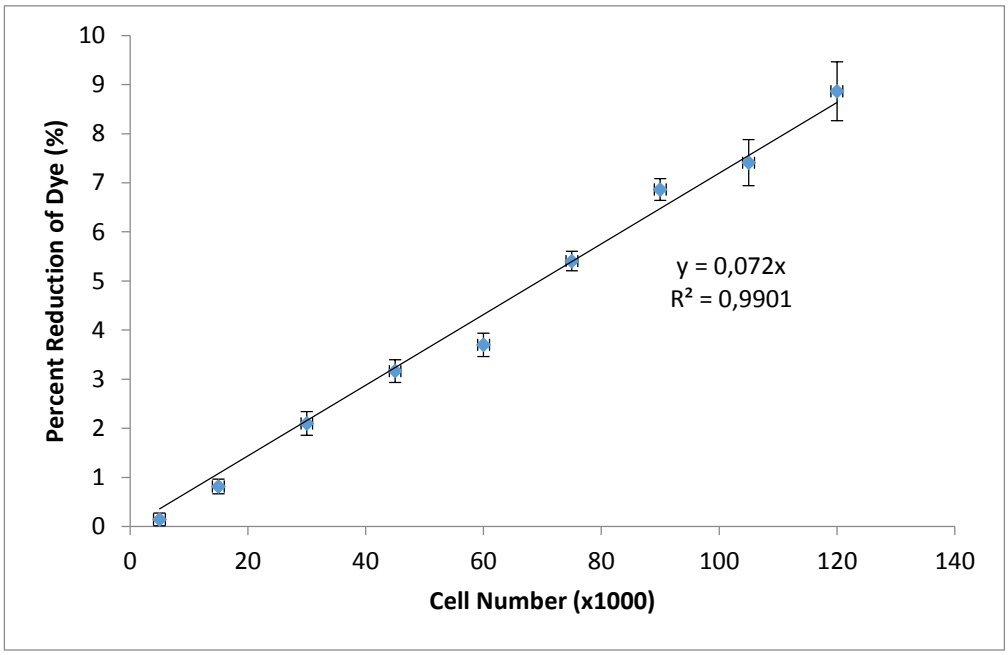

Figure A.1: Alamar blue assay calibration curve for rat bone marrow stromal cells.

APPENDIX B

NEURON-SPECIFIC ENOLASE (NSE) CALIBRATION CURVE

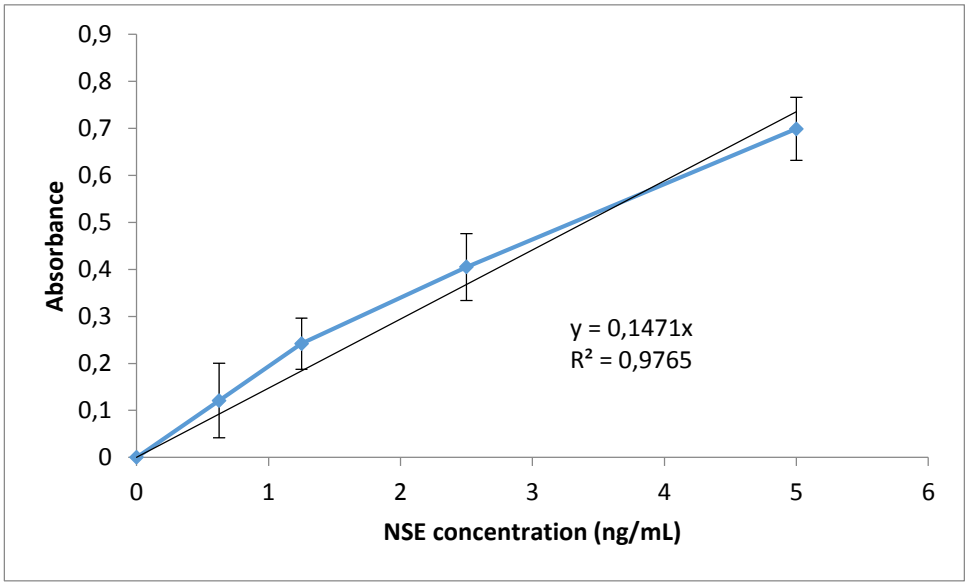

Figure B.1: NSE concentration vs absorbance calibration curve.